Frequency Translation Loops for RF Filtering

Theory and Design

Shadi Youssef

Frequency Translation Loops for RF Filtering

Theory and Design

Shadi Youssef

Committee:

Chairman:	
prof. dr. ir. A.J. Mouthaan	Universiteit Twente
Promotor:	
prof. dr. ir. B. Nauta	Universiteit Twente
Assistant promotor:	
dr. ir. R.A.R. van der Zee	Universiteit Twente
Members:	
prof. dr. ir. F.E. van Vliet	Universiteit Twente
prof. ir. A.J.M. van Tuijl	Universiteit Twente
prof. dr. ir. C.H. Slump	Universiteit Twente
prof. dr. ir. P.G.M. Baltus	Technische Universiteit Eindhoven

This research was financially supported by the
Dutch Technology Foundation STW (10055).

Centre for Telematics and Information Technology
P.O. Box 217, 7500 AE
Enschede, The Netherlands

ISSN: 1381-3617 (CTIT Ph.D. Thesis Series No. 13-249)
ISBN: 978-90-365-1468-2
DOI: http://dx.doi.org/10.3990/1.9789036514682

Typeset with LaTeX.
This thesis was printed by Gildeprint Drukkerijen, The Netherlands.

Frequency Translation Loops for RF Filtering

Theory and Design

Dissertation

to obtain
The degree of doctor at the University of Twente,
on the authority of the rector magnificus,
prof. dr. H. Brinksma,
on account of the decision of the graduation committee
to be publicly defended
on Wednesday 29 May 2013 at 16:45

by

Shadi Shawky Tawfik Youssef
born on 9 October 1977
in Cairo, Egypt

This dissertation is approved by:

promoter prof. dr. ir. B. Nauta

assistant-promoter dr. ir. R.A.R. van der Zee

To Maggie and my parents

Abstract

Modern wireless transceivers are required to operate over a wide range of frequencies in order to support the multitude of currently available wireless standards. Wideband operation also enables future systems that aim for better utilization of the available spectrum through dynamic allocation. As such, co-existence problems like harmonic mixing and phase noise become a main concern. In particular, dealing with interference scenarios is crucial since they directly translate to higher linearity requirements in a receiver.

With CMOS driving the consumer electronics market due to low cost and high level of integration demands, the continued increase in speed, mainly intended for digital applications, offers new possibilities for RF design to improve the linearity of front-end receivers. Furthermore, the readily available switches in CMOS have proven to be a viable alternative to traditional active mixers for frequency translation due to their high linearity, low flicker noise, and, most recently recognized, their impedance transformation properties.

In this thesis, frequency translation feedback loops employing passive mixers are explored as a means to relax the linearity requirements in a front-end receiver by providing channel selectivity as early as possible in the receiver chain. The proposed receiver architecture employing such loop addresses some of the most common problems of integrated RF filters, while maintaining their inherent tunability.

Through a simplified and intuitive analysis, the operation of the receiver is first examined and the design parameters affecting the filter characteristics, such as bandwidth and stop-band rejection, are determined. A systematic procedure for analyzing the linearity of the receiver reveals the possibility of LNA distortion canceling, which decouples the trade-off between noise, linearity and harmonic radiation.

Next, a detailed analysis of frequency translation loops using passive mixers is developed. Only highly simplified analysis of such loops is commonly available in literature. The analysis is based on an iterative procedure to address the complexity introduced by the presence of LO harmonics in the loop and the lack of reverse isolation in the mixers, and results in highly accurate expressions for the harmonic and noise transfer functions of the system. Compared to the alternative of applying

general LPTV theory, the procedure developed offers more intuition into the operation of the system and only requires the knowledge of basic Fourier analysis. The solution is shown to be capable of predicting trade-offs arising due to harmonic mixing and loop stability requirements, and is therefore useful for both system design and optimization.

Finally, as a proof of concept, a chip prototype is designed in a standard 65nm CMOS process. The design occupies $< 0.06\text{mm}^2$ of active area and utilizes an RF channel-select filter with a 1-to-2.5GHz tunable center frequency to achieve 48dB of stop-band rejection and a wideband IIP3 $> +12$dBm.

As such, the work presented in this thesis aims to provide a highly-integrated means for programmable RF channel selection in wideband receivers. The topic offers several possibilities for further research, either in terms of extending the viability of the system, for example by providing higher order filtering, or by improving performance, such as noise.

Samenvatting

Moderne draadloze zendontvangers werken over een groot frequentiebereik waarin ze een veelheid aan draadloze standaarden moeten ondersteunen. Een groot frequentiebereik maakt het ook mogelijk zuiniger met het beschikbare spectrum om te gaan door dynamische toewijzing. Echter, door het mixen van hogere harmonischen en door faseruis worden coxistentieproblemen een belangrijke zorg. Met name het omgaan met interferentie wordt cruciaal, omdat interferentie zich direct vertaalt in hogere lineariteitseisen aan de ontvanger.

CMOS technologie is leider in de consumentenmarkt door zijn lage kosten en hoge mate van integratie. De toenemende snelheid, vooral bedoeld voor digitale elektronica, biedt ook mogelijkheden voor RF elektronica om de linearitеit van ontvangers te verbeteren. Verder hebben de overvloedig beschikbare schakelaars in CMOS bewezen dat ze een goed alternatief zijn voor traditionele actieve mixers omdat ze zeer lineair zijn, lage $1/f$ ruis hebben en geschikt zijn voor impedantie transformatie.

In dit proefschrift worden frequentietranslatie-lussen verkend die gebaseerd zijn op passieve mixers met als doel de lineariteitseisen in ontvangers te versoepelen door zo vroeg mogelijk in de ontvangstketen frequentieselectiviteit aan te brengen. Een ontvangerarchitectuur die een dergelijke lus gebruikt kan bijdragen aan de oplossing van de meest voorkomende problemen van gentegreerde RF filters.

Allereerst wordt de werking van de voorgestelde ontvanger geanalyseerd met behulp van een simpele, intutieve analyse waaruit de filterkarakteristieken zoals bandbreedte en stopband onderdrukking worden bepaald. Via een systematisch procedure om de lineariteit van de ontvanger te analyseren blijkt dat het mogelijk is vervormingscompensatie toe te passen, waardoor de afweging tussen ruis, lineariteit en harmonische straling eenvoudiger wordt.

Vervolgens wordt een gedetailleerde analyse gemaakt van frequentietranslatielussen met passieve mixers. In de literatuur zijn alleen zeer eenvoudige analyses van zulke lussen beschikbaar. De analyse is gebaseerd op een iteratieve procedure welke overweg kan met de harmonischen in de lus en het gebrek aan isolatie in de mixers, en resulteert in zeer nauwkeurige uitdrukkingen voor de overdracht en de ruis in het systeem. Vergeleken met een analyse gebaseerd op lineaire periodiek tijd-

variante systemen, is de analyse bovendien meer intutitief en vereist slechts kennis van Fourier transformaties. De uitkomsten laten zien dat er afwegingen bestaan die worden veroorzaakt door het mixen van hogere harmonischen in de lus en door stabiliteitseisen; deze kunnen worden gebruikt voor het ontwerp en de optimalisatie van een dergelijk systeem.

Ten slotte, om de theorie te verifiren, wordt een chip gefabriceerd in een standaard 65nm CMOS proces. Het ontwerp past in minder dan $< 0.06\text{mm}^2$ en bestaat uit een RF kanaalfilter met een frequentie die regelbaar is van 1-tot-2.5GHz, 48dB maximal stopband onderdrukking heeft en een IIP3 van meer dan $> +12$dBm buiten de doorlaatband.

Het werk dat in dit proefschrift wordt gepresenteerd helpt het mogelijk te maken programmeerbare RF kanaalselectie filters voor breedbandige ontvangers te integreren op chip. Het onderwerp biedt verschillende mogelijkheden voor nader onderzoek, bijvoorbeeld naar hogere orde filters of naar mogelijkheden om de ruis te verlagen.

Contents

List of Abbreviations

ADC	Analog-to-Digital Converter
AGC	Automatic Gain Control
AM	Amplitude Modulation
BER	Bit Error Rate
DB	Double Balanced
DR	Dynamic Range
HD	Harmonic Distortion
HPF	High Pass Filter
IF	Intermediate Frequency
IIP3	Third order Input Intercept Point
IM3	Third order InterModulation
IMD3	Third order InterModulation Distortion ratio
NF	Noise Figure
LO	Local Oscillator
LNA	Low Noise Amplifier
LP	Low Power
LPF	Low Pass Filter
LPTV	Linear Periodically Time Varying
P–1dB	1–dB Compression Point
PCB	Printed Circuit Board
RF	Radio Frequency
SB	Single Balanced
SBR	Stop-Band Rejection
SFDR	Spurious Free Dynamic Range
SNR	Signal-to-Noise Ratio

Chapter 1

Introduction

The early success of cellular telephony in parallel with the phenomenal expansion of the internet created new potential, in both business and personal environments, for wireless communication to provide digital interactive and multimedia services. Because first generation cellular systems were mainly designed for voice communication, the high data rates necessary for providing these additional services were obviously beyond their capabilities and a vast number of wireless standards have since been developed to provide the necessary bandwidth.

Today, a look at the increasingly crowded (and consequently valuable) radio spectrum shows the variety of standards that enable wireless connectivity (Fig. 1.1). Using cell phones to make personal or business calls on the go, navigating city streets via GPS, or having the online content of news and social media outlets permanently available at our finger tips have all become standard, and often taken for granted, features of everyday life. With such a multitude of pervasive and ubiquitous digital services, it is estimated that in over 1.8 petabytes of internet data flow daily across the globe [1], and the trend is only foreseen to continue to result in double that number by 2016.

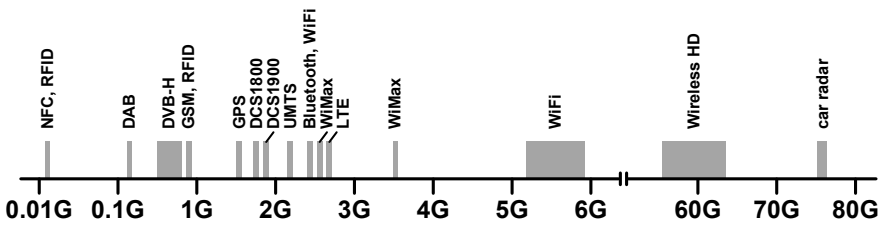

Figure 1.1: Frequency allocation of different wireless standards (frequency axis only for demonstration; not to scale).

The bulk of the vast infrastructure required to handle such stupendous volumes of data traffic remains mostly wired in the form of high speed optic fiber cables [2]. In contrast, the wireless part can be thought of as one interface (among many) to these data super highways and comprises a variety of networks that provide different services to users. Nevertheless, whether it is a cellular network spanning several tens of kilometers, or a WiFi access point serving a single home, the radio design of a mobile wireless network poses a unique set of challenges that mainly stem from the fact that wireless communication occurs over a shared and varying medium. Issues like cellular handover, near-far reception, and multi-path fading [3], to name a few, are essential problems to consider at all levels of radio design.

1.1 Radio Design

To enable wireless communication, radio design involves three main, and naturally interlinked, levels as shown in Fig. 1.2: (1) radio planning, (2) air interface definition, and (3) transceiver design.

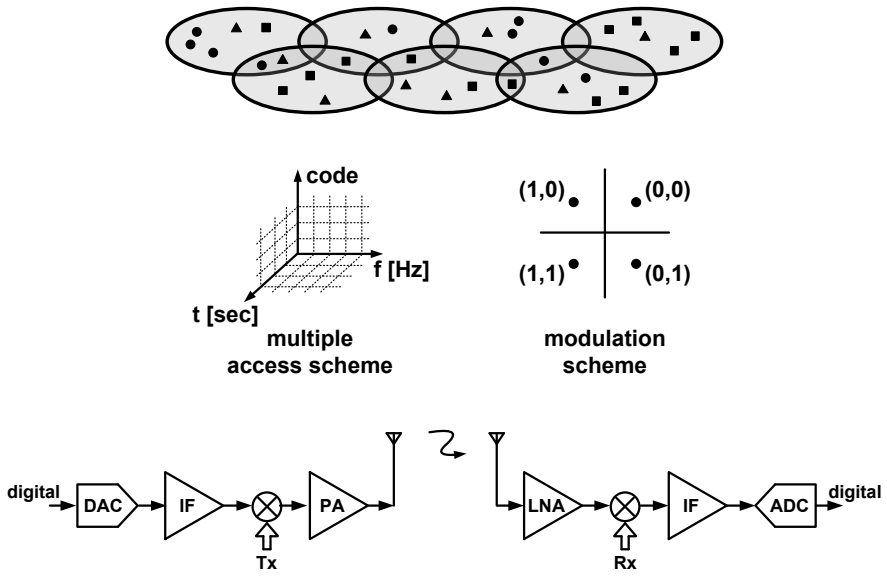

Figure 1.2: Radio design: radio planning (top), air interface (middle), transceiver design (bottom).

The limited radio spectrum available and the demand for higher data rates requires radio planning for frequency re-use. By controlling transmission power levels, geographically non-overlapping areas cells can be defined, in which the full set of available radio frequencies can be re-used without disturbance from neighboring cells.

In practice however, cells do overlap, but with careful planning, interference from adjacent cells is kept below a power level that is manageable by the radio transceivers.

In addition, an air interface is needed to essentially define the protocol by which radio transceivers communicate; it manages the sharing of available radio spectrum among simultaneous users (multiple access scheme), and how information is encoded onto transmitted/received Radio Frequency (RF) signals (modulation scheme).

Finally, because propagating signals are ultimately analog, a wireless transceiver will inevitably contain an RF front-end portion for interfacing with the digital back-end. As such, a transceiver is required to operate within the set of parameters defined by the first two levels of radio design (i.e. frequencies, power levels, type of modulation .. etc.) to ensure proper transmission and reception of data. At the receiver side of a mobile device, which is the main focus of this thesis, the fundamental limitation is the achievable Dynamic Range (DR) within a given power budget. The dynamic range defines the range of signal power levels that can be detected for successful decoding of information. A signal too weak would be buried in the noise inevitably present in the system, while a signal too large would create excessive distortion, and ultimately, cannot be accommodated within the limited power supply of the receiver. Thus, for a given range of coverage, the Noise Figure (NF) and the Third order Input Intercept Point (IIP3) of a front-end receiver determine its Spurious Free Dynamic Range (SFDR) [4].

1.2 Co-existence Problems in Wideband Receivers

With such an ever increasing demand for higher data rates and the accompanied explosive growth in available wireless standards, next generation wireless transceivers are required to have multi-mode capabilities (i.e. multiple standards operation) in order to meet cost, size and time-to-market demands. Furthermore, newly emerging concepts like cognitive radio aim for better utilization of the available radio spectrum through smart sensing and sharing of frequency channels between multiple users [5]. In both cases, a wireless transceiver requires the flexibility of operating within a wide range of frequencies, while simultaneously being able to deal with co-existence problems where, for instance, a receiver tries to detect a weak signal in the vicinity of at least one active transmitter. As a result, high linearity requirements, with IIP3 values as high as 30-to-40dBm [6], are needed to prevent desensitization of the receiver. Strictly speaking, the problems associated with multi-mode operation are also present in narrowband dedicated transceivers. However, it is the wideband nature of a multi-mode transceiver that causes several of these problems to be much more pronounced.

From a radio receiver's perspective, three main problems are exacerbated in wide-

band operation, namely: distortion, harmonic mixing, and phase noise. As will be seen from the subsequent discussion, these problems all dictate a higher linearity requirement for the receiver. Theoretically, a brick-wall noiseless channel select filter that would extract the desired signal right at the antenna would provide an ultimate solution to these problems.

1.2.1 Noise

With the inevitable presence of noise, the sensitivity of a receiver is the minimum signal power received that allows for successful detection of information carried by that signal. Eventually, this sensitivity level should be above the noise floor of the receiver by a minimum Signal-to-Noise ratio (SNR) requirement at the input of the Analog-to-Digital Converter (ADC). For a given modulation scheme, providing that minimum SNR, in turn, allows for achieving the required Bit Error Rate (BER) during data detection in the digital back-end. Consequently, NF is an important metric of a receiver, since it quantifies the degradation of SNR as the signal propagates down the front-end chain.

In a wideband receiver, such a general problem is exacerbated by several factors. Since noise is a wideband stochastic process [4], the most obvious problem is the fact that higher data rate, and the correspondingly wider signal bandwidth, results in higher integrated noise power within that bandwidth. For a given sensitivity level, this means it becomes more difficult to meet the necessary SNR. In addition, the presence of interferers at the input of a wideband receiver can significantly degrade the NF by reducing the gain of the desired signal (blocking) and through other indirect mechanisms like reciprocal mixing (Section 1.2.4). Furthermore, noise folding due to highly non-linear operations like mixing cause further degradation in a receiver's NF.

1.2.2 Distortion

Active devices required for amplification and switching are generally non-linear. For analog/RF signals, the effect of non-linearity is the introduction of distortion. That is, an amplifier, for instance, will not reproduce a faithfully up-scaled version of the input signal. In the frequency domain, such deviations from a perfectly amplified replica are equivalent to introducing new frequency components at the output that were not present in the signal input to the amplifier. The effect of these distortion components on the overall performance of the system depends on the application. In audio systems, distortion components manifest themselves as poor sound quality, while in data applications, distortion in the analog/RF front end directly results in data errors (a transmitted '1' is detected as a '0' upon reception or vice versa).

For an RF front-end receiver, the relevant distortion products can be demonstrated

with the aid of a simple generic model of non-linearity. Assuming a memoryless [1] and weakly non-linear receiver [2], it is well known that its transfer function in the time domain can be written as a Taylor series expansion

$$x_o(t) = \alpha_1 x_i(t) + \alpha_2 x_i^2(t) + \alpha_3 x_i^3(t) + ... \tag{1.1}$$

where $x_i(t)$ and $x_o(t)$ are the input and output signals, respectively, and α_1 is the linear gain of the receiver and α_2 and α_3 are the second and third order non-linearity coefficients (i.e. for a perfectly linear receiver, $\alpha_2 = \alpha_3 = 0$).

For the sake of demonstration, the expansion in (1.1) can be truncated to a third order polynomial, and the response of the receiver due to different combinations of single tone sinusoids can be examined. Although signals present at the antenna (both desired and interferers) are usually modulated carriers, the conclusions derived from simplified single or two tone excitation remain valid because the spectrum of a modulated signal is essentially a group of sinusoidal tones. In the context of a front-end receiver, several cases are relevant:

1. **Harmonic distortion:** Assuming only the desired signal is present at the antenna, it can be shown that Harmonic Distortion (HD) products are available at the output of the receiver. With a desired sinusoidal tone input at frequency ω_d, even and odd order harmonics appear at the output at frequencies $2\omega_{\text{in}}$ (due to α_2) and $3\omega_{\text{in}}$ (due to α_3), respectively. For narrow-band receivers, harmonic distortion products are usually not a concern, because they fall out of the application band of interest. However, for a wideband receiver that aims to digitize a wide range of frequencies for further signal processing, harmonic distortion products become relevant.

2. **Intermodulation distortion:** With two single tone interferes present at the antenna at frequencies ω_1 and ω_2 and equal amplitude A, it can be shown that Third order InterModulation (IM3) products are generated at $2\omega_1 - \omega_2$ and $2\omega_2 - \omega_1$, both of amplitude $3\alpha_3 A^3/4$ [4]. Typically, this type of distortion is the most problematic, since in a wireless environment, the situation constantly arises where other users in the vicinity are transmitting and receiving at frequencies that, even though are away from the desired frequency, would still cause the IM3 products to fall on top of the desired signal.

   The most common metric to characterize the strength of IM3 products is IIP3. By defining IM3 Distortion ratio (IMD3) as the ratio of the IM3 component to

[1] although a memoryless system is, strictly speaking, not a valid representation for a wideband receiver, the main conclusions remain unchanged.

[2] in a weakly non-linear system, the limited power supply and the associated signal clipping are not considered.

the first order (linear) component, and equating it to unity, IIP3 can be found as

$$\text{IMD3} = \frac{3}{4}\frac{\alpha_3}{\alpha_1}A_{\text{IIP3}}^2 = 1 \rightarrow \text{IIP3} = A_{\text{IIP3}} = \sqrt{\frac{4}{3}\frac{\alpha_1}{\alpha_3}} \tag{1.2}$$

Graphically, IIP3 can be represented by constructing a logarithmic plot of the first and IM3 responses versus the input signal amplitude as shown in Fig. 1.3. The difference in slopes of the two responses makes it possible to extrapolate the curves to find the IIP3 as the input signal amplitude at which the two curves intersect (IMD3 = 1). Note that IIP3 is an usually an extrapolated, and not a physically attainable, value. This is because for higher signal amplitudes, higher order non-linearity terms dominate and the curves deviate from the ideal 1 and 3 slopes by either clipping or expanding. Nevertheless, IIP3 serves as a useful metric for link budget calculations and benchmarking of wireless transceivers.

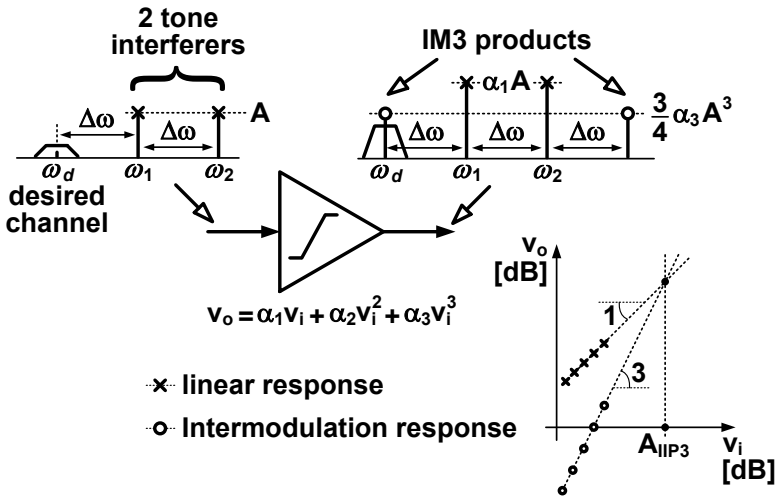

Figure 1.3: Third order Intermodulation (IM3) and Third order Input Intercept Point (IIP3) as a characterization metric.

3. **Cross modulation:** Third order non-linearity also causes a modulated interferer to transfer its modulation on top of the desired signal. This is relevant because interferers are usually modulated carriers of other users in the vicinity. Using the simple non-linearity model in (1.1), it can be shown that an Amplitude Modulated (AM) interferer of amplitude A_i and a modulation index m received alongside a desired signal of amplitude A_d would result in the modulation of the desired signal with a modulation index equal to $3m\alpha_3 A_i^2$ (Fig. 1.4). Obviously, such a cross modulation component is problematic because it always falls on top of the desired signal.

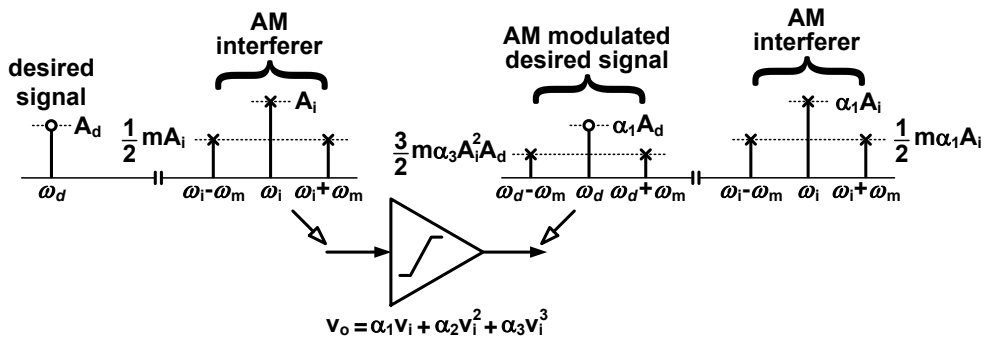

Figure 1.4: Cross modulation causes AM variation of an interferer to appear on top of a desired signal.

One way of quantifying cross modulation into a metric useful for system level calculations is an equivalent IIP3 [6]. However, as explained above, the cross modulation term, unlike an IM3 product, is proportional to the desired signal A_d. Since the desired signal is usually weak, the equivalent IIP3 value of cross modulation is often significantly lower than that resulting from IM3. Thus, in many cases, intermodulation distortion remains the dominant factor in determining the overall IIP3 requirement of the receiver.

From a circuit level perspective, each of the non-linearity coefficients in (1.1) captures several sources of non-linearity in a transistor. For a single MOS transistor, the drain source current i_{ds} in response to its terminal voltages can be expressed as

$$\begin{aligned} i_{ds} = {} & g_{m1}v_{gs} + g_{m2}v_{gs}^2 + g_{m3}v_{gs}^3 + ... \\ & + g_{o1}v_{ds} + g_{o2}v_{ds}^2 + g_{o3}v_{ds}^3 + ... \\ & + g_{m1d1}v_{gs}v_{ds} + g_{m2d1}v_{gs}^2v_{ds} + g_{m1d2}v_{gs}v_{ds}^2 + ... \end{aligned} \tag{1.3}$$

where v_{gs} and v_{ds} are the gate-source and drain-source voltages, respectively. The coefficients g_{m1} and g_{o1} are the transistor's transconductance and output conductance, respectively. The terms g_{m2}, g_{m3}, .. etc. represent the transconductance (or the V-to-I conversion) non-linearity of the transistor, while the terms g_{o2}, g_{o3}, .. etc. account for the output resistance non-linearity. The cross terms g_{m1d1}, g_{m2d1}, g_{m1d2} represent distortion due to simultaneous variation in v_{gs} and v_{ds}. To obtain any of the n-th order coefficients in (1.3), the relevant I-V curve of the device is differentiated n times with respect to the appropriate voltage(s) [7]. For instance, g_{m2} is the second derivative of the $I_{DS} - V_{GS}$ with respect to V_{GS} evaluated at the given V_{GS} and V_{DS} bias voltages, while g_{o3} is the third derivative of the $I_{DS} - V_{DS}$ curve with respect to V_{DS}, again for the given V_{GS} and V_{DS} bias voltages, where in both cases, the uppercase notation denotes the DC characteristic curves of the device. Thus, all

the non-linearity coefficients in (1.3), just like the transistors transconductance and output resistance, exhibit a strong bias dependence.

The above description consequently means that the overall linearity performance of an active device depends on its operation in the circuit. A common source MOS transistor used as a transconductor with low ohmic termination will experience low voltage swing at its drain, and thus, its linearity performance will most likely be dominated by the g_m coefficients. On the other hand, the linearity of the same common source MOS (i.e. same scaling and bias conditions) used as a voltage amplifier will usually be dominated by its g_o coefficients due to the high voltage swing resulting at the output.

As will be shown in Chapter 2, the combination of the different n-th order coefficients in (1.3) result in an equivalent n-th order coefficient that can be used in (1.1).

1.2.3 Harmonic Mixing

In a typical front-end receiver, a mixer frequency translates (down-converts) the received RF signal to a lower Intermediate Frequency (IF) specified by the difference between the input frequency and the frequency of the Local Oscillator (LO) signal signal driving the mixer. The received RF carrier is usually a bandpass signal which, depending on the architecture of the receiver, is either down-converted to an IF bandpass signal (in case of a superheterodyne [4] or a low IF architecture [8]), or an IF baseband signal (in case of a direct conversion receiver [9]). By tuning the LO frequency for reception, any of the available RF frequency channels are down-converted to the same IF frequency. With such an arrangement, only the RF circuits (the ones preceding, and including, the mixer) are required to operate at gigahertz frequencies, which in general results in lower overall power consumption of the receiver. For the IF part, this also enables employing low frequency analog techniques such as feedback, which allows for higher linearity and accurate Automatic Gain Control (AGC) required for signal digitization.

In a modern front-end receiver, the mixer is considered to be a Linear Periodically Time Varying (LPTV) system that periodically switches the input signal ON and OFF in time according to a large driving LO signal. Thus, whether active [10] or passive [11], the action of the mixer is to essentially multiply the signal with a square wave. By examining the process in the frequency domain, the multiplication process results in a convolution of the input spectrum with that of the LO. By considering the fundamental LO frequency ω_{LO}, the mixer produces a replica of the RF signal ω_{in} at both the sum and difference frequencies $\omega_{\mathrm{in}} \pm \omega_{\mathrm{LO}}$. Since only the down-converted signal is of interest, the replica at $\omega_{\mathrm{in}} + \omega_{\mathrm{LO}}$ is usually filtered out after down-conversion.

However, even in a perfectly linear mixer, the convolution process described above also occurs for all LO harmonics, which are not of negligible magnitude due to the square nature of the LO signal. Thus, multiple replicas of the input signal similarly appear at the sum and difference frequencies due to all LO harmonics, i.e. at $\omega_{\text{in}} \pm m\omega_{\text{LO}}$ for $m = 0, 1, 2, 3...$ For a receiver with a wideband input, such "harmonic mixing" is problematic; interferer(s) with the right frequency spacing from one or more of the LO harmonics can be down-converted on top of the desired signal (Fig. 1.5). Although the mixer conversion (i.e. RF-to-IF) gain due to harmonics is lower than that due to the LO fundamental, interferer power is usually much larger than that of the desired signal due to near-far effects. Consequently, the resulting harmonic mixing products can dominate over the desired signal and prevent successful detection of information if not enough filtering or some other measure is implemented to get interferer power down to manageable levels.

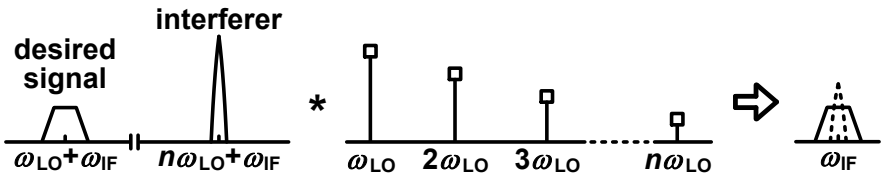

Figure 1.5: Harmonic mixing due to LO harmonics. An interferer at the right spacing from one of the LO harmonics would be down-converted on top of the desired signal. The * operator denotes the convolution operation.

1.2.4 Reciprocal Mixing

Having a purely sinusoidal LO simply down-converts the received signals, without any overlap between the desired signal and any interferer that may be present at the input of the mixer. In practice, however, an LO signal always contains phase noise, which appears as a "skirt" in the LO spectrum as shown in Fig. 1.6. As such, the frequency domain convolution associated with the mixing process between the received signals and the LO causes the down-converted versions of both the desired signal and the interferer to exhibit overlapping skirts. The overlap between the two down-converted spectra causes the desired signal to suffer from significant noise increase due to the skirt of the interferer. With near-far effects, a weak desired signal can be completely drowned in the phase noise skirt of a large interferer. Because ultimately, SNR is the performance metric of interest, phase noise is usually characterized relative to the strength of the fundamental LO frequency (in dBc), specified, due to the roll-off in the skirt, at different frequency offsets from LO (usually in the range of hundreds of kHz to a few MHz). Therefore, by minimizing this phase noise specification, filter-

ing requirements in the receiver are relaxed, or equivalently, wider band operation becomes feasible.

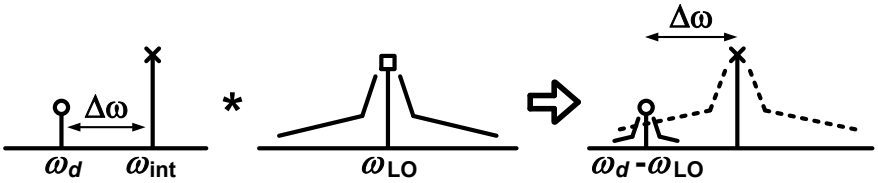

Figure 1.6: Reciprocal mixing due to phase noise of the LO. The resulting phase noise skirts of a down-converted interferer can significantly increase the noise floor in the band of interest.

1.3 State-of-the-Art

Extensive efforts have been made in recent years to improve the performance of front-end receivers to mitigate co-existence issues. This is evident from the variety of approaches reported in literature, which, as shown in this section, range from re-discovered concepts to novel receiver architectures.

1.3.1 Negative Feedback

It is well known that negative feedback improves linearity [12]. This is because, in general, it reduces the signal swing across active devices in the circuit, which reduces distortion, ideally, without a noise penalty. Even if noise is not an issue, feedback can offer higher linearity improvement compared to simply attenuating the signal at the input of the amplifier because the generated distortion components are further suppressed by the available loop gain. For instance, assuming a loop gain of T_o at all frequencies of interest, it can be shown that the IIP3 of a closed loop amplifier is improved by a factor equal to $(1 + T_o)^{\frac{3}{2}}$ compared to its open loop counterpart [13]. In contrast, attenuating the signal by an amount equal to T_o at the input of the open loop amplifier only improves IIP3 by a factor of $1 + T_o$.

One of the main advantages of negative feedback is making the performance of the closed loop amplifier insensitive to process spread. That is, once enough loop gain is provided, both the gain accuracy of the amplifier and its IIP3 are guaranteed to remain higher than a desired minimum value. Unfortunately, however, such an advantage is limited in RF circuits. This is because a high loop gain usually requires mutlti-stage amplifiers, which in turn limits their loop bandwidth due to stability requirements. Thus, negative feedback has been successfully employed in RF circuits mainly where a low loop gain is required. One such example is employing resistive shunt feedback to design compact Low Noise Amplifiers (LNAs) which provide a

wideband 50Ω match at the input of multi-standard receivers [13, 14]. In such cases, the matching conditions dictate a loop gain of about unity, which corresponds to a modest improvement in IIP3 (roughly 4.5 dB).

1.3.2 Derivative Superposition

The detailed examination of non-linearity coefficients briefly mentioned in Section 1.2.2 reveals the possibility of canceling some of the distortion products in an amplifier. More specifically, considering the V-to-I non-linearity of a MOS transistor in common source configuration shown in Fig. 1.7, its g_{m3} coefficient (third derivative of input I-V characteristics) is found to exhibit a sign reversal, typically occurring in the transition region between weak and strong inversion regimes of the transistor [15]. In other words, the transistor sinks or sources third order distortion current depending on its region of operation, while the fundamental current maintains the same direction for all values of bias voltage (an NMOS sinks current and a PMOS sources current). This offers the possibility of exploiting the change in g_{m3} polarity to cancel distortion products in the output current while maintaining the desired signal.

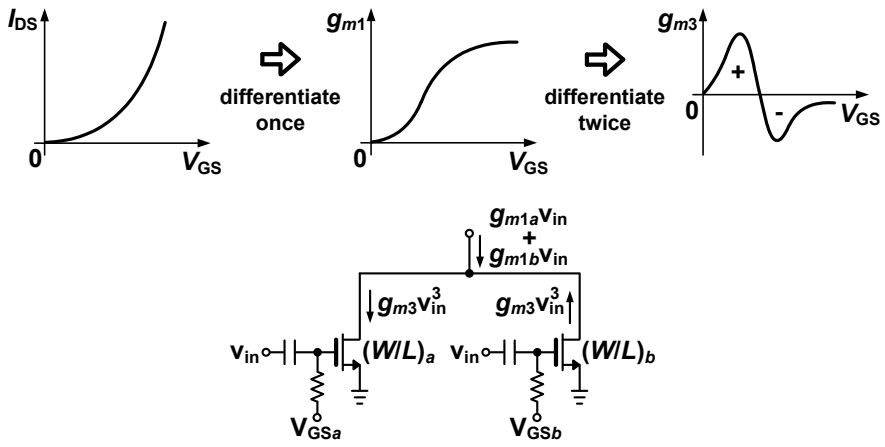

Figure 1.7: Principle of derivative superposition for g_{m3} cancellation. The idea relies on summing the output currents of a main and auxilliary device biased in strong and weak inversion, respectively.

Fig. 1.7 also demonstrates one such arrangement for an NMOS amplifying stage [16]. By connecting the output of two NMOS devices, properly biased and scaled according to their second derivatives, the output current is the superposition of currents from the individual devices, and is, consequently, more linear in response to the input signal. That is, the composite amplifier, ideally, has $g_{m3} = 0$. Since the auxiliary device added for g_{m3} cancellation operates in weak inversion and amplifies the signal to the output, its noise contribution is minor.

It is obvious, however, that such a technique is only suitable for canceling g_m non-linearity due to g_{m3} and not simultaneously to higher order coefficients (g_{m5}, g_{m7} ... etc.). In addition, it does not apply for output conductance non-linearity. Thus, for an amplifying to have a useful amount of voltage gain, the swing of the amplified signal at the output will remain the determining factor for the linearity of the amplifier.

Furthermore, the derivative superposition technique is essentially a feedforward technique, thus, unlike feedback, it is highly sensitive to process spread and mismatch, and attempts have been made to provide an adaptive bias scheme to overcome such problem [17]. Previous work have also demonstrated diminishing IIP3 improvement at high frequencies due to bondwires and a modified derivative superposition method has been reported to mitigate this effect [18], but the resulting improvement remains limited.

1.3.3 Feedforward Cancellation

Interference cancellation relies on a two-path receiver architecture [19]. As shown in Fig. 1.8, the LNA in the main path amplifies both the desired signal and the present interferer. Simultaneously in the additional path, both signals are first down-converted and the desired signal, now centered at DC, is then filtered out using a High Pass Filter (HPF). By up-converting the remaining interferer once again to the same RF frequency and subtracting the outputs of the two paths, only the desired signal remains at the output. The transfer function of the auxiliary path is basically equivalent to a high-Q notch filter centered at the frequency of the desired signal, and, consequently, the complete the two-path receiver implements a high-Q bandpass filter centered around the same frequency.

The fact that interference cancellation is carried out in a feedforward fashion means that careful gain and phase matching between the two paths is necessary. In addition, the linearity of auxiliary path is required to be high since it handles large interferers. This can be relatively easily achieved by employing passive mixers, which are significantly more linear than their active counterparts, together with passive high pass filtering. However, even with a perfectly linear auxiliary path, the fact that the interferer is canceled at the output of the LNA means that g_m non-linearities of the LNA remain a bottleneck.

1.3.4 Mixer-First Receivers

Because, in general, IF stages can employ negative feedback to achieve high linearity, RF sages comprising the LNA and mixer are usually the main linearity bottle neck blocks in a front-end receiver. As shown in Fig. 1.9, a mixer first receiver architecture

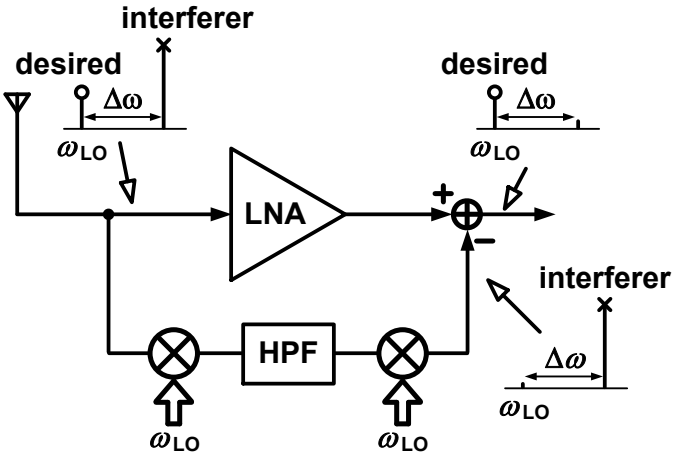

Figure 1.8: Interference cancellation by utilizing a two-path feedforward receiver architecture.

aims to overcome this limitation by eliminating the LNA altogether and employing passive mixers, which are significantly more linear than their active counterparts, connected directly to the antenna [20]. As such, mixer first receivers are capable of achieving significantly high in-band IIP3[3] values ranging from 12 [21] to 27dBm [22]. In addition, such an LNA-less architecture can further exploit the passive nature of the mixer to provide a low-noise 50Ohm match at the antenna interface via synthesizing an impedance on the IF side of the mixer [22].

The most obvious disadvantage of a mixer first receiver is the noise penalty associated with the absence of the LNA and placing a passive mixer with less than 0dB conversion gain as the first block of the receiver chain. Demonstrations of such an architecture show a NF in the range of 4-to-6dB [21, 22], which is acceptable in some applications. Moreover, the lack of reverse isolation between the mixer and the antenna and the strong harmonics of the LO signal make harmonic radiation an issue.

1.3.5 Harmonic Rejection Mixers

It is well known that a double balanced mixer configuration suppresses even harmonics of the LO [4]. This, in turn, eliminates the possible harmonic mixing components

[3]In a conventional receiver with an RF bandpass filter, in-band IIP3 traditionally refers to intermodulation distortion due to interferers in the same application band, while out-of-band IIP3 refers to distortion caused by all other signals. For a receiver that incorporates some means of RF channel selection, this definition needs revision into the more appropriate distinction of in-channel and out-of-channel IIP3, where in-channel IIP3 quantifies intermodulation distortion caused in-channel by the different frequency components of the modulated signal being received itself, and out-of-channel IIP3 quantifies intermodulation distortion due to all other signals, whether in the same application band or not.

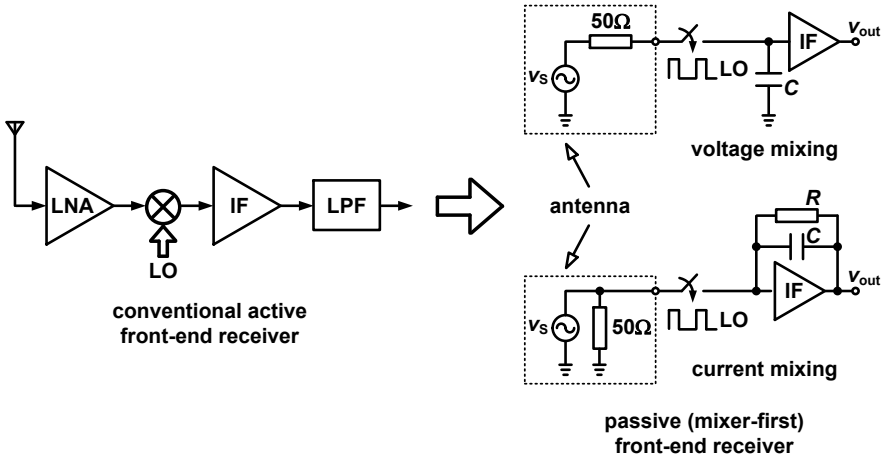

Figure 1.9: Passive (mixer-first) receiver is derived from a conventional active topology by eliminating the LNA and employing switches for down-conversion.

associated with these harmonics, but the odd LO harmonics remain problematic.

A harmonic rejection mixer aims to eliminate some of the odd LO harmonics by using multi-phase square waves. As shown in Fig. 1.10, three square waves with 45° phase shifts relative to each other are used to drive three mixers and their outputs are scaled in the ratio $1 : \sqrt{2} : 1$ before being summed together. In practice, the scaling and summation operations are most easily done in the current domain. It can then be shown that such an arrangement is equivalent to a switching mixer driven by an LO signal with no third and fifth LO harmonics [23]. Thus, implemented in a double balanced configuration (8 phase LO), a harmonic rejection mixer has the seventh LO harmonic as the first non-suppressed harmonic that causes harmonic mixing, which significantly reduces the amount of filtering required early in the receiver chain, or equivalently allows for wider band operation. Theoretically, with a multi-phase LO signal of infinite number of phases, the operation of a harmonic rejection mixer can be extended to emulate a purely sinusoidal LO signal that contains no harmonics. Obviously, practical limitations such as gain and phase mismatch set an upper limit on the number of LO phases that can be used.

Towards reducing its sensitivity to gain errors, a two-stage harmonic rejection operation has been proposed [24] in which the total relative gain error between the different paths becomes the product of individual stage errors, which increases harmonic rejection by 20dB, a significant improvement over single stage architectures.

The sensitivity to phase errors also adds a limitation on the maximum frequency of operation of such mixers. Furthermore, for passive mixer implementations, non-overlapping clocks are usually required to avoid noise and linearity degradation in the

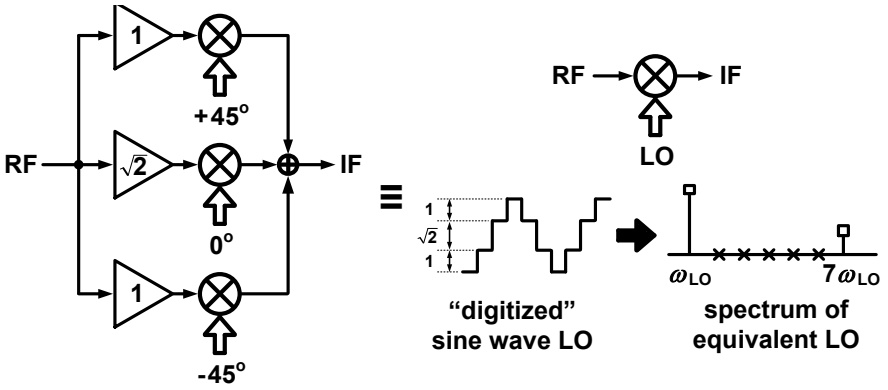

Figure 1.10: Harmonic rejection mixer concept. By emulating a sine wave, LO harmonics up to the 7-th are canceled.

receiver [25]. This, as well, sets an upper limit on the maximum frequency of operation if frequency dividers are to be used for generating the multi-phase LO signal while ensuring an acceptable phase noise performance.

1.3.6 Passive Mixer Filters

A simplified block diagram of a passive mixer band-pass filter is shown in Fig. 1.11. Since there is no isolation between the two sides of the mixer, the Low Pass Filter (LPF) connected to the mixer is transformed at the RF input into a high-Q band-pass filter centered around the LO frequency driving the mixer (ω_{LO}) [25, 26]. The square wave LO signal needed for driving the switch also means that scaled versions of the band-pass filter appear around the harmonics of LO ($2\omega_{\mathrm{LO}}$, $3\omega_{\mathrm{LO}}$, .. etc.).

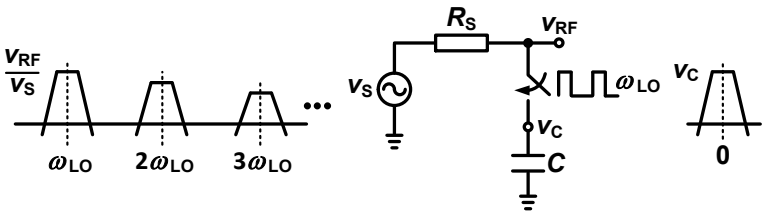

Figure 1.11: Concept of integrated RF filtering via the impedance transformation property of a passive mixer.

The aforementioned form of passive mixer filter can be considered as one specific implementation of the more generic concept of N-path filters [27]. The main advantage of these types of filters is breaking the trade-off that exists between Q and power consumption in traditional filters, which enables practical implementations of high-Q

bandpass filters at RF [28]. In addition, the noise folding due to the switching action involved in these filters only occurs starting at N-1 harmonics. Thus, the higher the number of paths, the less folding achieved, which comes at the expense of reduced LO speeds for reliable switching of the mixers.

One problem of these structures relates to the typical requirements of a front-end receiver in terms of input matching and noise. Generally speaking, both requirements lead to low resistance levels at the RF side of a receiver chain. Therefore, the RC product required for RF channel filtering results in large capacitors, and, consequently, a large die area that does not scale very well with technology. Typical capacitance values required in integrated filter designs are in the range of hundreds of picofarads to, even, one nanofarad [28–30].

In addition, the maximum achievable filter rejection is limited by the on-resistance of the switches of the passive mixer. As shown in Fig. 1.12, for frequency offsets much larger than the LO frequency, the capacitor acts as a short circuit and maximum stop-band rejection at the RF side is limited by the voltage divider formed between the source resistance and the switch resistance. This problem is further exacerbated by the low value of source resistance available at RF as previously explained. To mitigate this issue, one can step-up the source resistance using an off-chip RF transformer [28]. However, the use of such bulky components contradicts the aim of achieving integrated high-Q RF filtering. Even with the use of an RF transformer, large switches are typically needed to achieve moderate rejection values (5Ω switches for 16dB rejection [28]). This directly translates to more parasitic capacitance in the switches and higher power consumption in the LO buffers. Alternative implementations like the ones presented in [29, 30] overcome the limited rejection issue, but at the expense of large on-chip capacitance (up to one nanofarad), and consequently large die area.

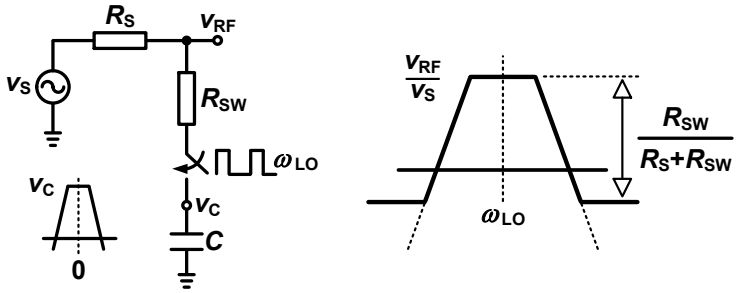

Figure 1.12: Limitation on maximum stop-band rejection that can be achieved in integrated RF filters.

Furthermore, the position of the filter along the RF part of the receiver chain entails a basic trade-off. Filtering prior to the LNA [31] or eliminating it altogether [22] improves linearity at the expense of noise and switching harmonics being injected

directly at the antenna node. Conversely, an LNA first architecture offers an opposite trade-off.

Finally, because the filter that is now supposed to suppress interferers input to the receiver heavily relies on the LO signal driving the switches, phase noise requirements of the LO are expected to be more stringent in order to keep reciprocal mixing products at the same level as in a receiver that uses conventional filters.

1.4 Research Motivation

The evident need for wideband/multi-standard operation in front-end receivers can be addressed through one of three main architectural choices:

1. A receiver possesses a bandwidth high enough to cover all possible frequency bands. This requirement would have to be met across every receiver block starting from the antenna all the way to the digital back-end. Consequently, the linearity, or equivalently DR, required for the RF/analog front-end part would be significantly high, which, even if practically possible, would result in unacceptably high power consumption, which is a main concern for battery lifetime in a mobile device.

2. A receiver in fact comprises several receivers in parallel connected to one or more antennas, and each receiver would then be dedicated, and in turn optimized, for one or more of the frequency bands of interest. In addition to consuming significantly more chip area, the fact that several corresponding transmitter paths would also exist on the same chip or Printed Circuit Board (PCB) means that interference and distortion issues, similar to the ones present between multiple users, would now be present between a transmitter and a receiver path that are simultaneously ON in the same mobile device.

3. Alternatively, a single programmable receiver chain would be tunable in such a way as to cover the necessary range of frequencies. Since, as discussed in Section 1.2, all co-existence issues can ultimately be met through ideal filtering to only receive the desired signal while rejecting all others, the tunability of such a programmable receiver essentially corresponds to high-Q RF channel selection at the antenna. Such "narrow-band flexibility", if feasible, would be an ultimate solution for distortion caused by interferers.

   Traditionally, high-Q filtering has been implemented by using off-chip components such as SAW filters [4]. In addition to being bulky and expensive, SAW filters are only suitable for selecting a fixed range of frequencies due to their lack of tunability. Therefore, they can only be used for selecting a complete application band at RF and/or IF channel selection where the desired channel

is always down-converted to the same frequency. More recent implementations based on N-path filters offer the necessary tunability at the expense of large on-chip capacitance (and consequently die-area), as well as potential problems with harmonic radiation due to the lack of isolation between the switching mixers and the antenna.

In this work, RF channel selection based on an active feedback frequency translation loop is investigated. The proposed receiver architecture aims to provide channel selectivity as early as possible in the receiver chain to reduce distortion due to interferers, or equivalently, relax (or possibly eliminate) the receiver filtering requirements for a given application. As such, the work presented in this thesis targets one of the key co-existence problems in radio receiver design.

A CMOS implementation aims to address the low cost and high level of integration demands that drive the consumer electronics market. In addition, the versatility of CMOS switches for frequency translation is exploited in the loop. High linearity [32] and low flicker noise [33] are among the characteristics that make CMOS switches viable alternatives to traditional active mixers.

The receiver is shown to result in a highly compact and tunable design that mitigates the performance limitations of integrated RF filters discussed above [34], namely: large capacitance/die area, limited stop-band rejection and the trade-off between noise, linearity and harmonic radiation. In the context of co-existence, other issues that have been described in Section 1.2 are equally important. However, since the proposed architecture poses no specific requirements in relation to these issues, they are viewed as orthogonal problems. That is, techniques available for addressing harmonic mixing or phase noise can be employed equally well in an active feedback receiver, and are therefore outside the scope of this work.

1.5 Thesis Outline

The remainder of the thesis is organized as follows:

Chapter 2 explores active feedback as a means of relaxing linearity requirements in the receiver chain. Through a simplified and intuitive analysis, the operation of the receiver is examined and the design parameters affecting the filter characteristics, such as bandwidth and stop-band rejection, are determined. In addition, a general systematic procedure for linearity analysis is developed and applied to the active feedback receiver. The analysis reveals the possibility of LNA distortion canceling, which decouples the trade-off that usually exists between noise, linearity and harmonic radiation.

In Chapter 3, a generalized and detailed analysis of frequency translation loops employing passive mixers is developed. Although open loop configurations of both

current and voltage passive switching mixers have been thoroughly analyzed in literature, no similarly detailed analysis is available for closed loop systems employing passive mixers. The developed analysis overcomes the difficulty associated with analyzing frequency translation loops by adopting an iterative procedure for solving the frequency domain equations of the system to obtain accurate closed form expressions that describe the filtering behavior of the loop. The analysis holds for a generic N-path frequency translation loop in negative or positive feedback arrangements, as well as single and double balanced configurations. The solution obtained for the RF/IF filtering provided by the loop is shown to accurately predict the simulated performance over the span of several LO harmonics, and thus is able predicts main performance parameters of the system such as stop-band rejection, in-band loss and loop stability.

Chapter 4 presents the prototype of the active feedback receiver designed in a standard 65nm CMOS process. The design occupies $< 0.06\text{mm}^2$ and utilizes an RF channel-select filter with a 1-to-2.5GHz tunable center frequency to achieve 48dB of stop-band rejection and a wideband IIP3 $> +12$dBm.

Chapter 5 presents a summary of the main contributions and conclusions of this thesis, as well as suggestions for future work.

Finally, the appendices provide a number of important detailed analyses and tests. Appendix A presents the details of the systematic method for linearity analysis and applies it to the proposed receiver architecture. Appendix B investigates the observed distortion canceling in simulation and the possible explanations for these observations. Appendix C sets the basis for the iterative procedure used for detailed analysis of frequency translation loops. The iterative procedure is then applied in Appendix D to obtain the harmonic transfer functions of a generic N-path loop, and in Appendix E to find the noise transfer functions for the different noise sources in the loop.

Chapter 2

Active Feedback Receiver

As discussed in Chapter 1, co-existence problems in a mobile terminal environment pose strict requirements on the linearity of a front-end receiver. This chapter explores active feedback as a means of relaxing such requirements by providing channel selectivity as early as possible in the receiver chain. The proposed receiver architecture addresses some of the most common problems of integrated RF filters discussed in Section 1.3.6, while maintaining their inherent tunability. Through a simplified and intuitive analysis, the operation of the receiver is examined and the design parameters affecting the filter characteristics, such as bandwidth and stop-band rejection, are determined. A systematic procedure for analyzing the linearity of the receiver reveals the possibility of LNA distortion canceling, which decouples the trade-off between noise, linearity and harmonic radiation.

Section 2.1 introduces the active feedback receiver architecture to address these issues. In section 2.2, simplified expressions for the receiver gain and the filter transfer function are derived. Section 2.3 discusses the noise behavior of the proposed architecture, and 2.4 discusses its linearity performance and a robust mechanism for distortion canceling is introduced. Finally, section 2.5 concludes this chapter.

2.1 Active Feedback Filtering Concept

The operation principle of an active feedback receiver can be developed as shown in Fig. 2.1. Conceptually starting with the simple case of a shunt feedback amplifier with high loop gain, the amplifier boosts signals from the input to the output with a voltage gain roughly equal to $-R_2/R_1$ for all input frequencies (assuming infinite loop bandwidth for simplicity at the moment).

If resistors R_1 and R_2 are now replaced with transconductors g_{m1} and g_{m2}, respectively, and a HPF is inserted in the feedback path, the loop gain becomes frequency

selective. In this case, frequencies much lower than the corner frequency of the HPF are rejected along the feedback path, causing input signals at those frequencies to experience little or no feedback action. Consequently, low frequency inputs are amplified to the output with a high gain as determined by the open loop amplifier. On the other hand, frequencies beyond the corner frequency of the HPF do experience high loop gain (because the HPF is nearly a short circuit), and their gain to the output is roughly $-g_{m1}/g_{m2}$, similar to the simple resistive feedback case. By choosing $g_{m2} > g_{m1}$, the gain of high frequencies can even be made less than unity. This difference in gain between low and high frequencies effectively creates a LPF at the feedback point, where the bandwidth of the LPF is determined by the corner frequency of the HPF and the available loop gain [34]. Thus, a HPF is transformed into a LPF.

By further inserting mixers in the loop (down-conversion in the forward path and up-conversion in the feedback path), the aforementioned operation basically remains unchanged, and the baseband HPF is now transformed into a band-pass filter centered around the driving frequency of the mixers. With g_{m1} serving as an LNA and the high frequency (RF) input being down-converted to a low frequency output (IF), the circuit becomes a direct conversion receiver with an RF pass-band filter centered around LO to provide channel selectivity. As a result, the transfer function from the LNA input to the IF output provides gain for the desired signal and suppression for interferers.

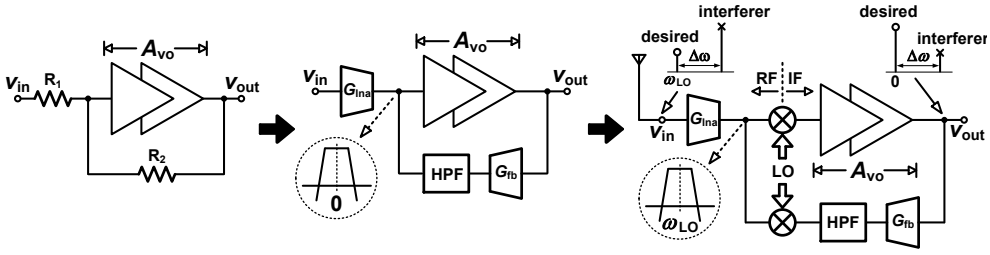

Figure 2.1: Concept of a frequency translation loop in an active feedback receiver.

Since filtering is chosen to be performed after the LNA, filter noise and harmonic radiation are not a major concern as explained in Section 1.3.6. However, the LNA now needs to handle interferers prior to suppression, thus determining the overall linearity of the receiver chain. A robust way to cancel LNA distortion is examined in section 2.4.

To demonstrate the properties and benefits of such an architecture, the gain and filter transfer function are first derived in the following section.

2.2 Analysis of Active Feedback Receiver

2.2.1 RF-to-IF Gain

A more detailed block diagram that captures the essential characteristics of the proposed architecture is shown in Fig. 2.2. In the forward path, the LNA is a transconductor G_{lna} that drives a passive mixer followed by a transimpedance amplifier to improve in-band linearity [24]. The feedback loop is implemented in a shunt-shunt fashion, where the IF output voltage is sensed, filtered and an RF current is fed back through a passive mixer driven by the feedback transconductor G_{fb}. The HPF is a first order filter with a corner frequency ω_{hpf}. Whether the loop rejects the desired signal prior to or after V-to-I conversion in G_{fb} does not change the resulting filter transfer function, but has a crucial effect on noise and distortion as will be shown in Sections 2.3 and 2.4. Including the output impedance of both transconductors would significantly complicate the analysis, but since both down- and up-conversion operations are performed via current commutating mixers, the driving impedance at one side of the mixer is typically much higher than the load impedance at the other side of the mixer. Consequently, neglecting one or both driving impedances has a negligible effect on the operation of the circuit. The choice to only include the LNA output impedance $Z_o(\omega)$ will be motivated in section 2.2.2.

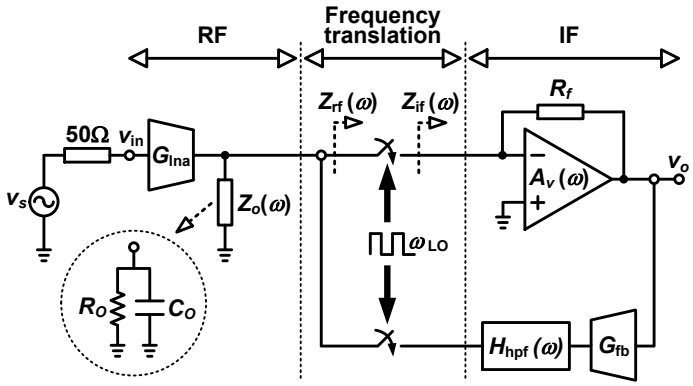

Figure 2.2: A detailed block diagram of the active feedback receiver for transfer function derivation.

The RF-to-IF gain of the receiver can be written as

$$A_{\text{RF-IF}}(\omega) = \frac{v_o(\Delta\omega)}{v_{\text{in}}(\omega)} = -G_{\text{lna}} Z_{\text{CL}}(\omega) A_{\text{mix}} A_v(\Delta\omega) \tag{2.1}$$

where $\Delta\omega$ is the frequency offset from LO, A_{mix} is the current conversion gain of the mixer and is assumed to be equal for both up- and down-conversion mixers, and

$Z_{\mathrm{CL}}(\omega)$ can be defined as an effective RF impedance seen at the output of the LNA in closed loop operation, and is given by

$$Z_{\mathrm{CL}}(\omega) = Z_{\mathrm{OL}}(\omega)\frac{1}{1+T(\omega)} = \frac{Z_o(\omega)Z_{\mathrm{if}}(\Delta\omega)}{Z_o(\omega)+Z_{\mathrm{rf}}(\omega)}\frac{1}{1+T(\omega)} \tag{2.2}$$

where $Z_{\mathrm{rf}}(\omega)$ is the RF impedance seen through the down-conversion mixer [25]

$$Z_{\mathrm{rf}}(\omega) = R_{\mathrm{SW}} + A_{\mathrm{mix}}^2 Z_{\mathrm{if}}(\Delta\omega) = R_{\mathrm{SW}} + A_{\mathrm{mix}}^2\frac{R_f}{1+A_v(\Delta\omega)} \tag{2.3}$$

and $T(\omega)$ is the active feedback loop gain and is equal to

$$T(\omega) = G_{\mathrm{fb}}\frac{Z_o(\omega)Z_{\mathrm{if}}(\Delta\omega)}{Z_o(\omega)+Z_{\mathrm{rf}}(\omega)}A_{\mathrm{mix}}^2 A_v(\Delta\omega)H_{\mathrm{hpf}}(\Delta\omega) \tag{2.4}$$

Note that the expressions in (2.3) and (2.4) are obtained by considering only the down-/up-converted gain due to the fundamental component of the LO, and assuming that the version of the signal up-converted by the down-conversion mixer is filtered out by the loop before being down-converted by the up-conversion mixer.

For the desired signal, the following assumptions apply:

1. $\Delta\omega \leq \mathrm{BW_{ch}}/2 \rightarrow H_{\mathrm{hpf}}(\Delta\omega) \approx 0 \rightarrow T(\omega) \approx 0$;
2. $A_v(\Delta\omega) \approx A_{vo}$ = IF amplifier DC voltage gain;
3. $A_{vo} \gg 1 \rightarrow Z_o(\omega) \gg Z_{\mathrm{rf}}(\omega)$.

Then the in-channel RF-to-IF gain can be simplified as

$$A_{\text{RF-IF}}(\omega_{\mathrm{IN}}) = -G_{\mathrm{lna}}R_f A_{\mathrm{mix}} \tag{2.5}$$

On the other hand, the following assumptions can be made for out-of-channel interferers:

1. $\Delta\omega \gg \mathrm{BW_{ch}}/2 \rightarrow H_{\mathrm{hpf}}(\Delta\omega) \approx 1$;
2. Large loop bandwidth $\rightarrow A_v(\Delta\omega) \gg 1 \rightarrow T(\Delta\omega) \gg 1$.

As a result, the RF-to-IF gain for out-of-channel interferers is

$$A_{\text{RF-IF}}(\omega_{\mathrm{OUT}}) = -\frac{G_{\mathrm{lna}}}{G_{\mathrm{fb}}}\frac{1}{A_{\mathrm{mix}}} \tag{2.6}$$

The ratio of (2.5) and (2.6) defines the maximum relative suppression of interferers due to the active feedback loop

$$S_{\max} = \frac{A_{\text{RF-}to\text{-IF}}(\omega_{\mathrm{OUT}})}{A_{\text{RF-}to\text{-IF}}(\omega_{\mathrm{IN}})} = \frac{1}{G_{\mathrm{fb}}R_f}\frac{1}{A_{\mathrm{mix}}^2} \tag{2.7}$$

That is, to increase the relative suppression, one has to increase R_f thereby increasing the gain of the desired signal relative to that of the interferer, and/or increase G_{fb} to reduce the gain of the interferer relative to that of the signal.

2.2.2 RF Filter Transfer Function

The relative suppression of interferers given by (2.7) is essentially the stop-band rejection of an RF channel-select filter created by the active feedback loop at the output of the LNA. Examining the filter transfer function is an alternative approach that gives further insight into the operation of the circuit.

The transfer function of the filter can be described as the normalized impedance at the output of the LNA. From (2.2)

$$H_{\rm ch}(\omega) = \frac{Z_{\rm CL}(\omega)}{Z_{\rm OL}(\omega)} = \frac{1}{1+T(\omega)} \tag{2.8}$$

The resulting filter transfer function can then be written as

$$H_{\rm ch}(\omega) = H_{\rm if}(\Delta\omega) \cdot H_{\rm rf}(\omega) \tag{2.9}$$

where

$$H_{\rm if}(\Delta\omega) = \frac{1}{1+T_{\rm if}(\Delta\omega)} \tag{2.10}$$

$$H_{\rm rf}(\omega) = \frac{1 + j\frac{\omega}{\omega_p}\frac{Z_{\rm rf}(\omega)}{R_o+Z_{\rm rf}(\omega)}}{1 + j\frac{\omega}{\omega_p}\frac{Z_{\rm rf}(\omega)}{R_o+Z_{\rm rf}(\omega)}\frac{1}{1+T_{\rm if}(\Delta\omega)}} \tag{2.11}$$

with $\omega_p = 1/(R_oC_o)$ being the pole due to the output impedance of the LNA, and $T_{\rm if}(\Delta\omega)$ is the low frequency part of the loop gain in (2.4), and is given by

$$T_{\rm if}(\Delta\omega) = G_{\rm fb}\frac{R_oZ_{\rm if}(\Delta\omega)}{R_o+Z_{\rm rf}(\omega)}A_{\rm mix}^2A_v(\Delta\omega)H_{\rm hpf}(\Delta\omega) \tag{2.12}$$

Thus, according to (2.9), the filter transfer function can be written as the product of two terms. The first term, $H_{\rm if}(\Delta\omega)$, is the contribution of the IF part of the receiver chain up-converted around $\omega_{\rm LO}$ as evident from (2.3) and (2.12). The second term, $H_{\rm rf}(\omega)$, represents the effect of the "*RF pole*" ω_p on the filter transfer function. Note that $H_{\rm ch}(\omega)$ approaches $H_{\rm if}(\omega)$ as $\omega_p \to \infty$. In fact, the dependence of $H_{\rm ch}(\omega)$ on ω_p is a parasitic effect that should be minimized as will be shown by the end of this section.

To gain further insight into the operation of the feedback loop and the resulting filtering effect, we start with two simplifying assumptions:

1. $\omega_p \gg \omega_{\rm LO} \to H_{\rm ch}(\omega) \approx H_{\rm if}(\Delta\omega)$
2. $A_v(\Delta\omega) = A_{vo} \gg 1 \to R_o \gg Z_{\rm rf}(\omega)$

The above assumptions leave the HPF as the only block determining the frequency dependence of the loop gain, mainly at small frequency offsets. Under these assumptions, substituting with (2.12) in (2.10) results in

$$H_{\rm ch}(\omega) \approx H_{\rm if}(\Delta\omega) = \frac{1+j(\frac{\Delta\omega}{\omega_{\rm hpf}})}{1+j(\frac{\Delta\omega}{\omega_{\rm hpf}/(1+T_o)})} \tag{2.13}$$

where $T_o = G_{\rm fb} R_f A_{\rm mix}^2 A_{vo}$ is the loop gain at $\Delta\omega = 0$.

By plotting $Z_{\rm CL}(\omega)$ versus frequency, the effect of the feedback loop on shaping the impedance at the output of the LNA, and consequently the gain of the receiver, can be examined. The plot in Fig. 2.3 provides an idealized plot of $Z_{\rm CL}(\omega)$ and reveals one of the key aspects of the active feedback receiver, in which the action of the loop in shaping the transfer function from the input to the output of the receiver is to introduce a pole and a zero separated by a factor of $(1+T_o)$. That is, the channel bandwidth is determined by the corner frequency of the HPF divided by the $(1+T_o)$. Thus, for a fixed resistance value of the HPF, the capacitance needed to achieve a given channel bandwidth is reduced by a factor proportional to the available loop gain. Since the major part of the loop is at IF, it is relatively easy to achieve a high loop gain and, therefore, significantly reduce the amount of capacitance/die area required. This offers a significant advantage over passive mixer filters since the capacitance values usually needed for channel selection at RF are quite large (hundreds of picofarads) as explained in section 1.3.6.

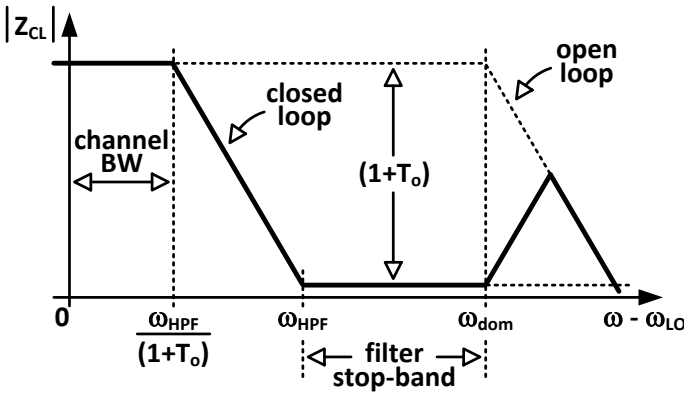

Figure 2.3: Simplified plot of the magnitude of the impedance at the output of the LNA $Z_{\rm CL}(\omega)$ in open loop and closed loop

To address the stability of the loop and its effect on filter characteristics, the above simplifying assumptions need to be re-examined. Towards this end, the loop can be conceptually divided into three parts based on the frequency of operation as shown in Fig. 2.2: an RF part $H_{\rm rf}(\omega)$ represented by the pole ω_p, a frequency translation interface provided by the mixers, and an IF part $H_{\rm if}(\Delta\omega)$ representing all IF blocks.

By first examining the frequency translation interface and the IF part, one can notice that since the mixers are driven by the same LO signal, the process of down-conversion and subsequent up-conversion ideally introduces no phase shift around the loop. In other words, provided that the two mixers and their driving networks are properly matched, the phase shift around the loop is primarily relative to the

frequency offset $\Delta\omega$ due to IF blocks rather than absolute frequency ω due to the mixers. Consequently, the frequency dependence of the loop gain due to both the frequency translation interface and the IF part can be introduced by adding a dominant pole ω_{dom} to the voltage gain in the transimpedance amplifier $A_v(\Delta\omega)$ in (2.4). This sets an upper limit on the loop bandwidth, or equivalently, the stop-band of the channel select filter (Fig. 2.4). Such a filtering loop is therefore suitable for implementation in a modern high speed process and its bandwidth is expected to improve with technology scaling.

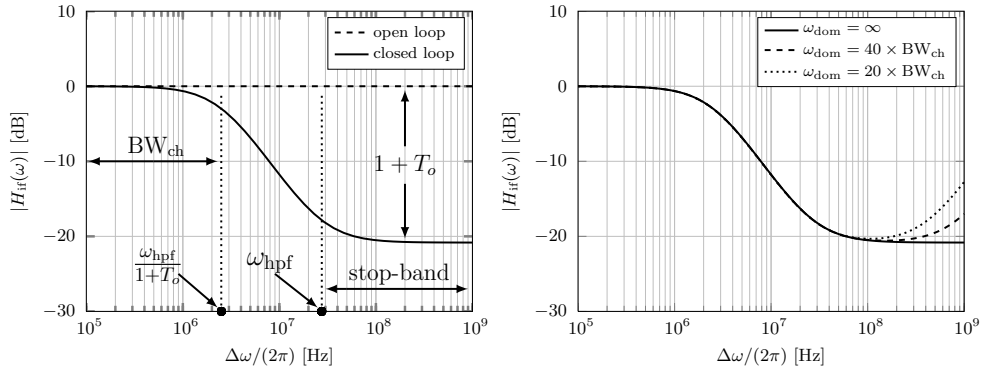

Figure 2.4: Effect of IF part of the loop on the filter transfer function as given by (2.9) for $\omega_p \gg \omega_{\text{LO}}$, $\text{BW}_{\text{ch}} = 5\text{MHz}$ ($2 \times 2.5\text{MHz}$) and $T_o = 20\text{dB}$. (a) With infinite loop bandwidth. (b) With limited loop bandwidth determined by a dominant pole ω_{dom}.

Conversely, the RF part of the loop introduces a phase shift relative to absolute frequency. As expected from (2.9), Fig. 2.5(a) shows that the asymmetric response of the RF part introduces some asymmetry in the filter shape. Furthermore, a slower RF part also results in the undesirable effect of shifting the center frequency of the filter (Fig. 2.5(b)). However, the IF part remains to be the dominating factor in determining the filter shape, thus, the center frequency of the filter retains programmability through changing the LO frequency.

2.2.3 Design Example

The results of section 2.2.1 can be used as a preliminary design guide. As an example, consider the following requirements:

1. Channel BW = 5MHz

2. Desired signal gain = 30dB

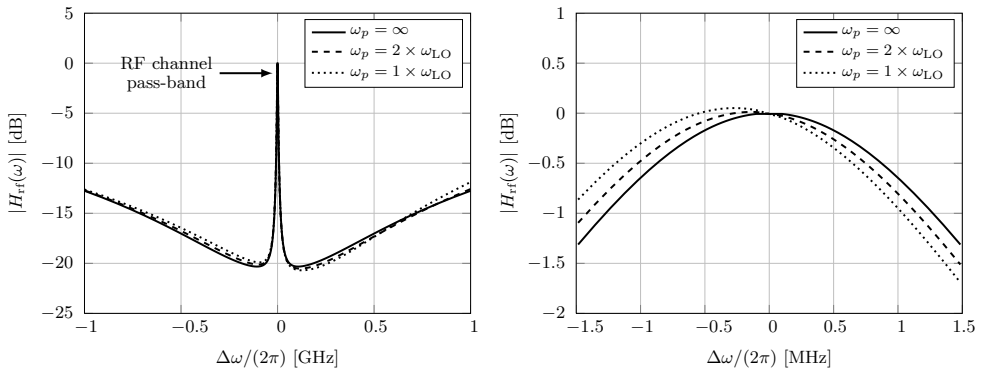

(a) (b)

Figure 2.5: Effect of RF part of the loop on the filter transfer function as given by (2.9) for $\omega_{\rm dom} = 20 \times {\rm BW}_{\rm ch}$, ${\rm BW}_{\rm ch} = 5$MHz (2×2.5MHz) and $T_o = 20$dB. (a) Complete filter characteristics. (b) Zoomed-in pass-band.

3. Interference suppression > 20dB

To design an active feedback receiver that meets the above specifications, we basically need to find five design parameters: $G_{\rm lna}$, $G_{\rm fb}$, R_f, $\omega_{\rm hpf}$ and $\omega_{\rm dom}$. Towards this end, we use the following values:

1. $A_{vo} = 20$dB
2. $A_{\rm mix} = \sqrt{2}/\pi$ (4-phase 25% duty cycle LO)
3. $R_{\rm SW} = 25\Omega$
4. $R_o = 10 \times R_{\rm SW}$
5. $\omega_p = 1 \times \omega_{\rm LO}$

Since the required channel bandwidth is determined by the corner frequency of the HPF divided by the available loop gain (Eq. (2.13) and Fig. 2.4(a)), the corner frequency of the HPF can first be found by noting that we need a loop gain that is, at least, as large as the desired interference suppression. The design then proceeds by utilizing (2.5) and (2.6) to find the ratio of $G_{\rm fb}/G_{\rm lna}$[1]. Given this ratio, the actual values of $G_{\rm lna}$, $G_{\rm fb}$ and R_f are eventually determined by the the noise requirements of the system. Finally, from (2.4), the stability of the loop can be guaranteed by setting the value of $\omega_{\rm dom}$.

[1]In case of distortion canceling (section 2.4), the ratio $G_{\rm fb}/G_{\rm lna}$ is fixed to unity, which couples the signal gain and interference suppression requirements. This effectively creates a trade-off between in-channel and out-of-channel linearity.

Based on the above procedure, Fig. 2.6 shows the RF-to-IF gain of the designed system and the corresponding loop gain. The desired performance parameters are met with a phase margin of approximately 50°.

It should be noted that the value of the switch is resistance used in the above example is about 5 times higher than what is typically seen in implementations like mixer-first receivers [21] and some N-path filter architectures [26] (More on that in Section 2.4). This directly translates to lower power consumption in the LO buffers driving the switches. This is also confirmed in the chip prototype presented in Chapter 4.

2.3 Noise Performance

In this section, the noise performance of the receiver is intuitively examined by considering the noise contributions of the forward and feedback paths separately. The discussion presented here is extended into detailed expressions of the noise folding functions (Appendix E) based on the iterative analysis method developed in Chapter 3.

The forward path is basically similar to traditional front-end receivers that have been extensively analyzed in part or as a whole in literature [20, 25]. The noise contribution of the forward path can be reduced by increasing the transconductance of the LNA and by ensuring that the switches operate with non-overlapping clocks. However, in the context of an active feedback receiver, two main issues are of specific concern; namely noise/speed requirements of the IF part of the receiver and impedance matching at the antenna interface.

In a typical receiver, the IF part, by definition, needs only to handle the down-converted channel. Thus, when considering the fundamental trade-off between noise and bandwidth, noise requirements usually take precedence. It is therefore common, even in high speed applications, to design IF blocks that operate in weak inversion to exploit the intrinsically higher transconductance efficiency (g_m/I) of a MOS device [24]. On the other hand, in our closed loop receiver, the bandwidth of the IF part determines the loop bandwidth, and, consequently, the stop-band of the RF filter. This suggests that the noise-speed trade-off is more pronounced in such a closed loop system. However, with the advances in CMOS scaling, weak inversion operation provides increasingly higher unity gain frequencies, well into the gigahertz range, while maintaining high g_m/I values [35, 36]. Thus, a noise-speed trade-off is still possible, and the trade-off is expected to relax with continued technology scaling.

In addition, providing the necessary impedance match at the input of the receiver has a significant impact on its NF. Inductor based techniques such as inductive degeneration are widely used to achieve low noise 50Ω matching [37–39]. However, when

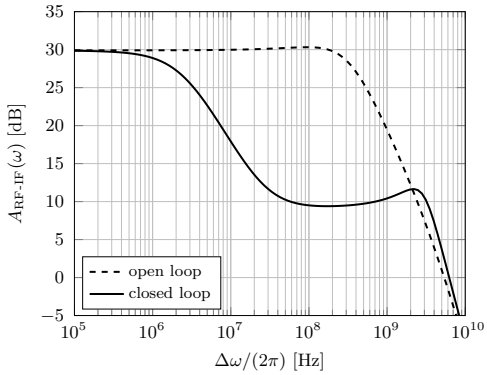

(a)

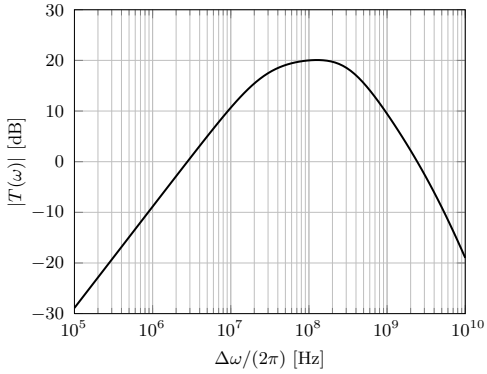

(b)

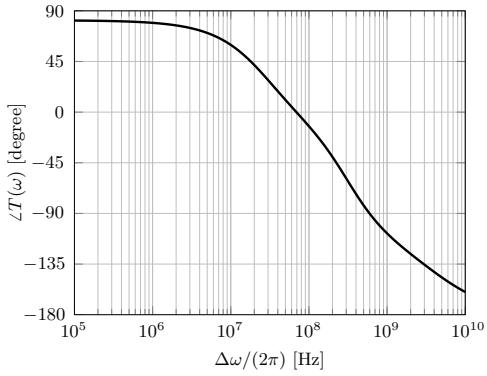

(c)

Figure 2.6: Calculated design example based on the expressions in (2.5), (2.6) and (2.13). Design parameters: $G_{\text{lna}} = 90.7\text{mS}$, $G_{\text{fb}} = 63.7\text{mS}$, $R_f = 1\text{k}\Omega$, $\omega_{\text{hpf}} = 2\pi \times 27.5 \times 10^6$ and $\omega_{\text{dom}} = 2\pi \times 50 \times 10^6$

aiming for a wide tuning range and a compact design, the use of such techniques is undesirable due to their inherent narrowband nature and the large die area required for on-chip inductors. As such, techniques like resistive matching [13, 14] or noise canceling [40, 41] present a better alternative.

In the feedback path, two cases are considered as shown in Fig. 2.7. In case 1, the feedback transconductor is placed at IF followed by the HPF. This is a favorable arrangement since the noise of the feedback transconductor is now filtered out (together with the desired signal) before being up-converted by the mixer to the filter pass-band. This way, the active feedback loop suppresses out-of-channel interferers without introducing noise in the desired channel.

In case 2, the feedback transconductor is placed at RF which introduces one extra "*RF pole*" inside the loop and changes the up-conversion mixer into a voltage mixer. Since now the feedback transconductor adds only thermal noise to the channel band, its contribution to the total NF of the receiver can still be adequately suppressed by the LNA.

A possible third arrangement in the feedback path is similar to case 2, except with the feedback transconductor placed at IF (between the HPF and the upconversion mixer). Although having an IF transconductor preceded by the HPF offers better distortion canceling as will be explained in the following section, simulations show that the NF of the receiver can degrade by as much as 10dB due to the up-conversion of transconductor flicker noise to the pass-band of the filter.

2.4 Distortion Analysis

In a conventional feedback system with high loop gain, the closed loop gain is primarily determined by the feedback ratio. Therefore, non-linearities in the feedback path are critical in determining the overall linearity of the system [12]. Thus, for a wide-band front-end receiver, utilizing a conventional feedback approach prohibits the use of active feedback components. Even if such a receiver is feasible, perfectly linear amplification of interferers would still pose strict linearity requirements on later stages in the receiver chain.

However, when employing active feedback to provide channel selection, only the desired channel appears amplified at the output while out-of-channel interferers are suppressed. Thus, although the feedback path contains non-linear elements, in principle it only needs to handle the desired signal which is typically small in amplitude. Furthermore, the linearity of later stages is now less of a concern due to suppressing interferers.

To quantitatively examine the overall linearity of the active feedback receiver, the different sources of distortion are considered as shown in Fig. 2.7 for the same two

feedback cases examined in section 2.3. The circuit is then solved according to the procedure outlined in Appendix A. In its most general form, the procedure is based on obtaining the n-th order non-linear response of the circuit based on all $n-1$ lower order responses. However, since the receiver provides a narrow-band response for channel selection, we only focus here on IM3 products which always fall in-channel. By applying the same simplifications for in-channel and out-of-channel signals used

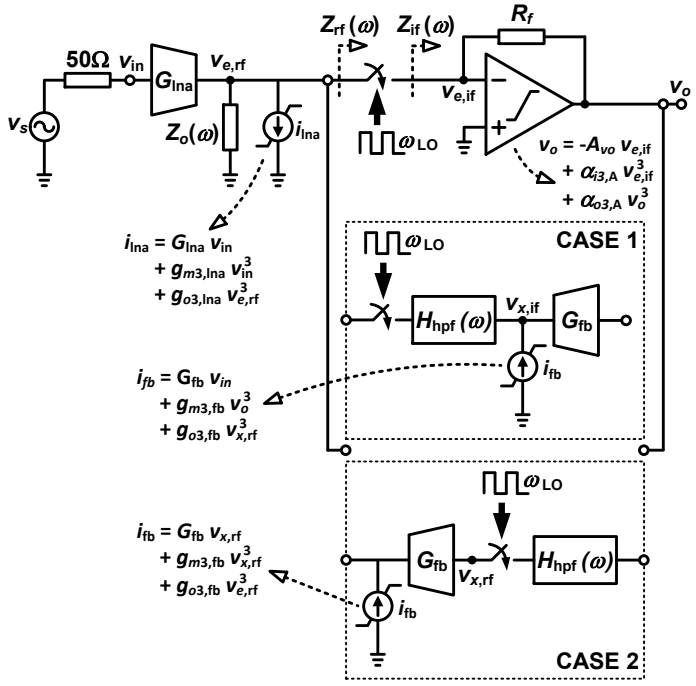

Figure 2.7: Third order non-linear contributions in the active feedback receiver.

in section 2.2.1 to the results in Appendix A, the different IM3 contributions at the output of the receiver can be summarized as shown in Tables 2.1 and 2.2.

As a first observation, one can clearly see that the RF filtering provided by the active feedback loop reduces the distortion caused by out-of-channel interferers in the IF part of the receiver ($\alpha_{i3,\mathrm{A}}$ and $\alpha_{o3,\mathrm{A}}$).

Furthermore, the distortion caused by in-channel interferers due to the output linearity of the LNA ($g_{o3,\mathrm{lna}}$) is reduced by the low input impedance of the transimpedance amplifier, but the reduction is limited by the switch resistance of the down-conversion mixer. This is expected since the switch resistance appears in series with the input of the transimpedance amplifier as given by (2.3), thus limiting the reduction in voltage swing at the output of the LNA. On the other hand, reducing the distortion of $g_{o3,\mathrm{lna}}$ due to out-of-channel interferers faces no such limitation.

This is because, as long as the output impedance of the feedback transconductor is significantly higher than the switch resistance, providing more loop gain causes the feedback loop to sink more current independently of the switch resistance. That is, unlike passive mixer filters, filter rejection at the RF side is practically not limited by the on-resistance of the mixer switches. This has a twofold benefit. First, it enables the use of smaller switches, which directly translates to smaller switch capacitances and lower power consumption in the driving LO buffers. Second, in a modern CMOS process where output non-linearity is a major contributor to the total distortion of an active device [42], the distortion of the LNA due to out-of-channel interferers can be significantly reduced. It should be noted, however, that since the loop gain is ultimately limited by stability requirements, the stop-band rejection of the filter cannot be arbitrarily high.

The most interesting observation though can be made by examining case 2 for out-of-channel interferers. One can see that the distortion products due to the V-to-I non-linearity of the LNA and feedback transconductors ($g_{m3,\mathrm{lna}}$ and $g_{m3,\mathrm{fb}}$, respectively) have opposite polarities. Such a direct consequence of the feedback action suggests that some form of distortion canceling is possible. This can be examined by considering only these two distortion components and expressing the change in IM3 distortion due to closed loop operation as

$$\Delta\mathrm{IM3} = \frac{\mathrm{IM3}_{gm3,\mathrm{lna}} + \mathrm{IM3}_{gm3,\mathrm{fb}}}{\mathrm{IM3}_{gm3,\mathrm{lna}}} = \frac{g_{m3,\mathrm{lna}} - g_{m3,\mathrm{fb}}(G_{\mathrm{lna}}/G_{\mathrm{fb}})^3}{g_{m3,\mathrm{lna}}} \tag{2.14}$$

Since $G_{\mathrm{fb}}/G_{\mathrm{lna}} = g_{m3,\mathrm{fb}}/g_{m3,\mathrm{lna}}$, denoting this ratio as m and re-arranging (2.14) yields the simple relation

$$\Delta\mathrm{IM3} = 1 - \frac{1}{m^2} \tag{2.15}$$

By plotting (2.15) in Fig. 2.8, one can distinguish two regions of operation separated by the border case of $m = 1$. For $m < 1$, closed loop operation actually causes an increase in IM3 distortion as m is reduced. This is expected since the RF-to-IF gain of out-of-channel interferers is inversely proportional to m as given by (2.6), which means that the feedback path needs to handle an amplified version of the interferers present at the input of the receiver, causing its distortion to dominate over that of the LNA. On the other hand, when increasing m beyond unity, the change in IM3 distortion approaches zero since now the feedback path needs to handle an attenuated version of the interferers and the distortion of the LNA determines the linearity performance. Increasing m also corresponds to a higher loop gain which improves the linearity of the IF part of the receiver as discussed earlier. Thus, although Fig. 2.8 only considers $g_{m3,\mathrm{lna}}$ and $g_{m3,\mathrm{fb}}$, the region for $m > 1$ also shows that the non-linearity of the LNA, which is outside the loop, sets an upper limit on the linearity of the whole receiver chain as expected. Note that this insight into the

operation of the loop is in agreement with the general discussion at the beginning of this section.

However, Fig. 2.8 shows that this limitation can be overcome by setting m equal to unity, i.e. by matching the LNA and feedback transconductances. Under this condition, the distortion of the LNA can be canceled because an inverted replica of input interferers is forced at the output via the feedback action, causing the feedback transconductance to perfectly sink the distortion currents sourced by the LNA. In other words, with the aid of negative feedback, the LNA and the feedback transconductor form a voltage mirror for out-of-channel interferers (where the HPF is a short circuit). This arrangement has several advantages:

1. It cancels LNA distortion caused by out-of-channel interferers without placing the LNA inside the loop, thus avoiding injecting noise and mixer harmonics at the antenna, which significantly decouples the noise-linearity-harmonic radiation trade-off that typically exists in passive mixer filters implemented directly at the antenna (section 1.3.6).

2. As opposed to having the LNA inside the loop, filtering at the output of the LNA eliminates at least one extra pole from the loop, which results in a higher loop BW for the same phase margin.

3. It is a large signal linearization based on matching a non-linear V-to-I operation with a similar non-linear I-to-V operation.

4. It is based on feedback and matching transconductances, which makes it robust to process spread.

5. The non-linearity of the feedback path is not a limitation.

In case 1, our simplified analysis predicts that such cancellation is not possible due to the presence of the HPF between the two transconductors which prevent the in-channel IM3 product from flowing between the two transconductors. However, full circuit simulations of the receiver configured in case 1 show that partial cancellation is still possible. The cancellation in this case still exhibits the same dependence on the ratio of transconductors (i.e. maximum partial cancellation for equal transconductors), but, due to the frequency translation between the inputs of two transconductors, only holds when the BW of the LNA is higher than the loop bandwidth plus LO frequency. Further overview of the different tests carried out to understand the origin of this linearity improvement is given in Appendix B. An explanation that encompasses all listed observations has not been reached and further investigation is still required.

	Case 1	
Non-linearity	**IM3 product due to in-channel interferers**	**IM3 product due to out-of-channel interferers**
$g_{m3,\mathrm{lna}}$	$-\frac{3}{4}g_{m3,\mathrm{lna}}R_f A_{\mathrm{mix}}A^3$	$-\frac{3}{4}g_{m3,\mathrm{lna}}R_f A_{\mathrm{mix}}A^3$
$g_{o3,\mathrm{lna}}$	$-\frac{3}{4}g_{o3,\mathrm{lna}}R_f A_{\mathrm{mix}}A^3$ $\times G_{\mathrm{lna}}^3(R_{\mathrm{SW}}+\frac{R_f}{A_{vo}})^3$	$-\frac{3}{4}g_{o3,\mathrm{lna}}R_f A_{\mathrm{mix}}A^3$ $\times(\frac{G_{\mathrm{lna}}}{G_{\mathrm{fb}}})^3(\frac{1}{A_{\mathrm{mix}}^2 A_{vo}})^3$
$\alpha_{i3,\mathrm{A}}$	$+\frac{3}{4}\alpha_{i3,\mathrm{A}}A^3$ $\times(G_{\mathrm{lna}}\frac{R_f}{A_{vo}}A_{\mathrm{mix}})^3$	$+\frac{3}{4}\alpha_{i3,\mathrm{A}}A^3$ $\times(\frac{G_{\mathrm{lna}}}{G_{\mathrm{fb}}})^3(\frac{1}{A_{\mathrm{mix}}A_{vo}})^3$
$\alpha_{o3,\mathrm{A}}$	$-\frac{3}{4}\alpha_{o3,\mathrm{A}}A^3$ $\times(G_{\mathrm{lna}}R_f A_{\mathrm{mix}})^3$	$-\frac{3}{4}\alpha_{o3,\mathrm{A}}A^3$ $\times(\frac{G_{\mathrm{lna}}}{G_{\mathrm{fb}}})^3(\frac{1}{A_{\mathrm{mix}}})^3$
$g_{m3,\mathrm{fb}}$	0	0
$g_{o3,\mathrm{fb}}$	0	0

Table 2.1: Calculated third order intermodulation distortion products falling in-channel in an active feedback receiver.

	Case 2	
Non-linearity	**IM3 product due to in-channel interferers**	**IM3 product due to out-of-channel interferers**
$g_{m3,\mathrm{lna}}$	$-\frac{3}{4}g_{m3,\mathrm{lna}}R_f A_{\mathrm{mix}}A^3$	$-\frac{3}{4}g_{m3,\mathrm{lna}}R_f A_{\mathrm{mix}}A^3$
$g_{o3,\mathrm{lna}}$	$-\frac{3}{4}g_{o3,\mathrm{lna}}R_f A_{\mathrm{mix}}A^3$ $\times G_{\mathrm{lna}}^3(R_{\mathrm{SW}}+\frac{R_f}{A_{vo}})^3$	$-\frac{3}{4}g_{o3,\mathrm{lna}}R_f A_{\mathrm{mix}}A^3$ $\times(\frac{G_{\mathrm{lna}}}{G_{\mathrm{fb}}})^3(\frac{1}{A_{\mathrm{mix}}^2 A_{vo}})^3$
$\alpha_{i3,\mathrm{A}}$	$+\frac{3}{4}\alpha_{i3,\mathrm{A}}A^3$ $\times(G_{\mathrm{lna}}\frac{R_f}{A_{vo}}A_{\mathrm{mix}})^3$	$+\frac{3}{4}\alpha_{i3,\mathrm{A}}A^3$ $\times(\frac{G_{\mathrm{lna}}}{G_{\mathrm{fb}}})^3(\frac{1}{A_{\mathrm{mix}}A_{vo}})^3$
$\alpha_{o3,\mathrm{A}}$	$-\frac{3}{4}\alpha_{o3,\mathrm{A}}A^3$ $\times(G_{\mathrm{lna}}R_f A_{\mathrm{mix}})^3$	$-\frac{3}{4}\alpha_{o3,\mathrm{A}}A^3$ $\times(\frac{G_{\mathrm{lna}}}{G_{\mathrm{fb}}})^3(\frac{1}{A_{\mathrm{mix}}})^3$
$g_{m3,\mathrm{fb}}$	0	$+\frac{3}{4}g_{m3,\mathrm{fb}}A^3$ $\times R_f A_{\mathrm{mix}}(\frac{G_{\mathrm{lna}}}{G_{\mathrm{fb}}})^3$
$g_{o3,\mathrm{fb}}$	$-\frac{3}{4}g_{o3,\mathrm{fb}}R_f A_{\mathrm{mix}}A^3$ $\times G_{\mathrm{lna}}^3(R_{\mathrm{SW}}+\frac{R_f}{A_{vo}})^3$	$-\frac{3}{4}g_{o3,\mathrm{fb}}R_f A_{\mathrm{mix}}A^3$ $\times(\frac{G_{\mathrm{lna}}}{G_{\mathrm{fb}}})^3(\frac{1}{A_{\mathrm{mix}}^2 A_{vo}})^3$

Table 2.2: Calculated third order intermodulation distortion products falling in-channel in an active feedback receiver.

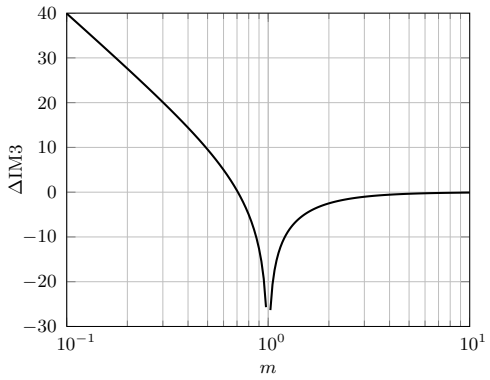

Figure 2.8: Change in out-of-channel IM3 due to $g_{m3,lna}$ and $g_{m3,fb}$ as a function of the ratio of feedback and LNA transconductances m (Table 2.2).

2.5 Conclusions

In this chapter, active feedback for RF channel selection has been presented. Filtering is achieved by employing a frequency translation loop with a high loop gain to convert an IF HPF to an RF channel-select filter. The large value of on-chip capacitance typically needed in passive mixer filters is reduced in the active feedback receiver by a factor proportional to the available loop gain, which results in a highly compact design. In a modern high speed CMOS process, the RF filter characteristics are primarily determined by the IF part of the loop and, thus, the filter maintains tunability through changing the clock frequency. In addition, due to the active nature of the feedback path, the maximum rejection achievable in the stop-band of the filter is not limited by the switch resistance of the mixers. This allows for using significantly smaller switches and consequently translates to lower power consumption in the LO buffers. However, the filter rejection is now limited by the amount of loop gain that can be achieved for given phase and gain margins. With the continued scaling of CMOS technology, it is expected that increasingly higher speed will be available to allow for increasingly higher loop gain values. Furthermore, the feedback loop offers the possibility of utilizing a voltage mirror for canceling the IM3 distortion products caused by out-of-channel interferers in the LNA. This eliminates the limitation set by the LNA on the linearity of the receiver chain without filtering prior to the LNA, therefore avoiding noise and harmonics injection at the antenna.

Chapter 3

Detailed Analysis of Frequency Translation Loops

In this chapter detailed analysis of frequency translation loops employing passive mixers is developed.

Several other works have used frequency translation loops, mostly with passive mixers [43–45], although active mixers have also been used [46]. In [43] and [46] filtering is carried out via a separate negative feedback loop (i.e. independent of the receiver's down-conversion path) to provide an RF notch and an RF pass-band filter, respectively. In [44], the forward down-conversion path of the receiver is incorporated into the loop to provide RF filtering at the antenna interface, but unlike [34], the loop is in positive feedback configuration. In a different context, [45] uses a frequency translation loop to achieve low noise 50Ω matching at the input of a multi-band receiver.

In literature, thorough analysis has been provided for open loop passive mixer circuits operating in both current [25] and voltage [47] domains. However, despite their wide use as discussed above, no similarly detailed analysis is available for frequency translation loops with passive mixers. Rather, only basic system level analysis is available, mainly to provide a qualitative description for the operation of the loop [43, 44, 48], or investigate general receiver non-idealities like I/Q mismatch [49].

The difficulty of analyzing these loops essentially arises from the presence of harmonic components inside the loop, as well as the lack of isolation between the input and output of a passive mixer. This paper provides a detailed circuit analysis of frequency translation loops employing passive mixers by solving the frequency domain equations of the system in an iterative manner to obtain an accurate closed form solution. The analysis developed here is based on the negative feedback receiver architecture presented in [50], i.e. it assumes a frequency translation loop that incor-

porates the IF part of the receiver chain. However, the analysis holds equally well for: (1) a separate feedback loop that is independent of the receiver's down-conversion path, (2) an LNA inside the loop, and (3) positive feedback operation. Furthermore, the analysis is valid for a general N-path system with a single balanced (SB) or double balanced (DB) architecture.

The solution obtained for the RF/IF filtering provided by the loop is shown to fit circuit simulations within 0.5 to 1.5 dB over the span of several LO harmonics. Consequently, the analysis accurately predicts main performance parameters of the system such as stop-band rejection, in-band loss and loop stability, and can thus be used for both system design and optimization. In contrast, the idealized analysis [50], although much simpler and can serve as a preliminary design guide, is shown to be quite inadequate in predicting such performance parameters.

This chapter is organized as follows: First, Section 3.1 presents a generic N-path frequency translation loop in the context of a front-end receiver, and a from which single path schematic is extracted for analysis. Section 3.2 starts with idealized system analysis, followed by a detailed analysis in Section 3.3, which is the focus of this chapter. In Section 3.4 analyses results are verified against circuit simulations. Section 3.5 addresses the stability of the system taking into account harmonic folding effects in the loop. In Section 3.6, normalized design curves are developed to discuss the different trade-offs in the system, which further demonstrates the need for the accuracy provided by the detailed analysis. Finally, Section 2.3, applies the developed analysis procedure to examine the noise behavior of the system, and Section 3.8 concludes this chapter.

3.1 Generic N-path Active Feedback Receiver

Fig. 3.1 shows the schematic of an N-path direct conversion receiver with frequency translation loop. The paths are operated with non-overlapping clocks, thus the duty cycle of the LO signal is 1/N. Each pair of paths (one differential path) operating with two 180° out-of-phase LO signals (one differential LO signal) comprise a forward path and a feedback path. In the forward path, one set of switches arranged in a double balanced fashion down-converts the differential RF signal to a differential IF signal, while a similar set of switches in the feedback path performs the reverse operation. Note that by removing the grayed connections, the circuit is transformed from a DB architecture to an SB architecture.

By using the concept of half circuit [4], the detailed circuit diagram of one SB path can be drawn as shown in Fig. 3.2. This serves as the basis for both the idealized and detailed analyses carried out in this section. In the forward path, the LNA is a V-to-I converter g_{m1} that supplies RF current to the down-conversion switches followed

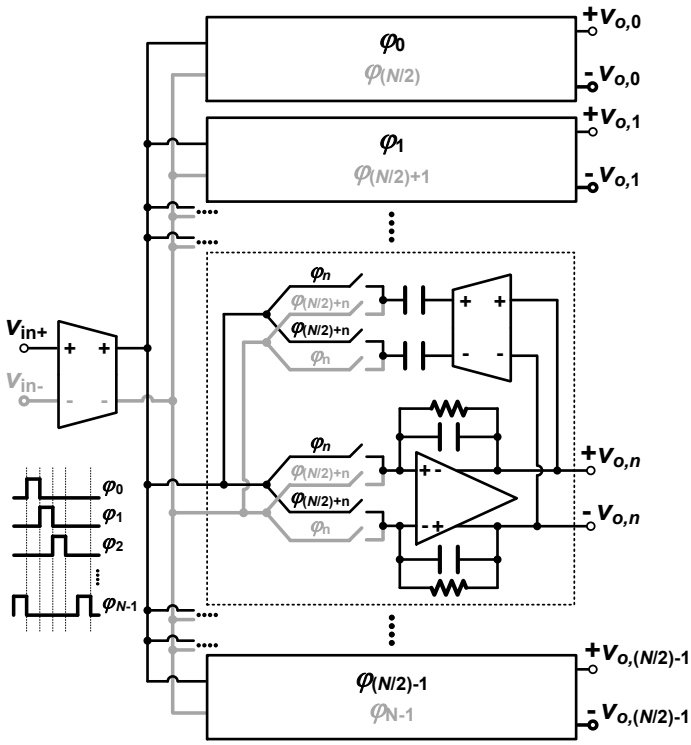

Figure 3.1: N-path active feedback receiver.

by an IF transimpedance amplifier with a frequency dependent voltage gain $A_v(\omega)$. Down-conversion with such a current commutating arrangement is known to improve the linearity of a receiver [24]. The capacitor C_f across the trans-impedance amplifier is a Miller capacitor needed for loop stability. In the feedback path, a first order HPF with capacitor C_{hpf} is used. For simplicity, the output impedance of the feedback transconductor driving the up-conversion mixer is included into the transfer function of the HPF. Thus, the corner frequency of the HPF is determined by C_{hpf} together with the output impedance of the feedback transconductor and the load seen through the up-conversion mixer by C_{hpf} (which, from the IF side of C_{hpf}, is given by the total resistance at the RF node plus the switch resistance divided by the duty cycle [47]). In contrast, the output impedance of the LNA transconductance is explicitly taken into account in order to accurately model the RF part of the frequency translation loop. With all the essential node impedances defined, the parasitic capacitances of the switches can always be absorbed in one or more of these impedances.

Although the circuit diagram in Fig. 3.2 depicts a single path, including the LO phase $e^{j\frac{2\pi}{N}n}$ allows for a generic N-path receiver analysis by summing over all values

of n. Furthermore, the analysis carried out for the SB circuit is also valid for its DB counterpart by using the Fourier series coefficients of a differential LO signal and twice the switch resistance R_{SW}.

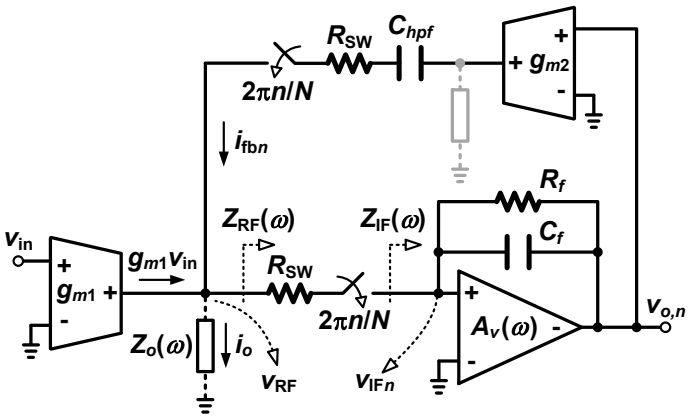

Figure 3.2: Single path active feedback receiver for analysis.

The analysis for ideal circuit operation is first carried out, followed by detailed analysis of actual circuit operation, which is the main focus of this paper.

3.2 Idealized Circuit Analysis

The idealized analysis presented here is essentially a generalization of the analysis in Section 2.2 that would apply equally well to both frequency translation loops and active feedback receivers, and would allow for direct comparison with detailed analysis results.

Due to passivity of the down-conversion mixer, the input impedance of the trans-impedance amplifier $Z_{\mathrm{IF}}(\omega)$ is up-converted to RF to appear in series with the switch ON resistance R_{SW}. As a result, the impedance seen through the down-conversion mixer from the RF side $Z_{\mathrm{RF}}(\omega_{\mathrm{LO}}+\Delta\omega)$ is given by $R_{\mathrm{SW}}+|a_1|^2 Z_{\mathrm{IF}}(\Delta\omega)$ [25], where a_1 is the Fourier series coefficient of the first harmonic of the LO (i.e. current conversion gain).

In open loop operation (i.e. up-conversion mixer OFF), $Z_{\mathrm{RF}}(\omega_{\mathrm{LO}}+\Delta\omega)$ appears in parallel with the output impedance of the LNA $Z_o(\omega_{\mathrm{LO}}+\Delta\omega)$, which determines the RF voltage due to the current $g_{m1}v_{\mathrm{in}}(\omega_{\mathrm{LO}}+\Delta\omega)$ supplied by the LNA. The current divider created between the same two impedances also determines the portion of the RF current going into the down-conversion mixer. In closed loop operation, this current, and consequently the impedance at the output of the LNA, are modified by the loop gain $T_{\mathrm{ideal}}(\omega)$. As such, the RF and IF voltages on either side of the

down-conversion mixer can be expressed as

$$v_{\mathrm{IF}n,\mathrm{ideal}}(\Delta\omega) = g_{m1}\frac{Z_o(\omega_{\mathrm{LO}}+\Delta\omega)}{Z_o(\omega_{\mathrm{LO}}+\Delta\omega)+R_{\mathrm{SW}}+|a_1|^2 Z_{\mathrm{IF}}(\Delta\omega)} \times a_{-1}e^{j\frac{2\pi}{N}n}\frac{Z_{\mathrm{IF}}(\Delta\omega)}{1+T_{\mathrm{ideal}}(\Delta\omega)}v_{\mathrm{in}}(\omega_{\mathrm{LO}}+\Delta\omega) \tag{3.1}$$

$$V_{\mathrm{RF,ideal}}(\Delta\omega) = g_{m1}\frac{Z_o(\omega_{\mathrm{LO}}+\Delta\omega)\big(R_{\mathrm{SW}}+|a_1|^2 Z_{\mathrm{IF}}(\Delta\omega)\big)}{Z_o(\omega_{\mathrm{LO}}+\Delta\omega)+R_{\mathrm{SW}}+|a_1|^2 Z_{\mathrm{IF}}(\Delta\omega)} \times \frac{1}{1+T_{\mathrm{ideal}}(\Delta\omega)}V_{\mathrm{in}}(\omega_{\mathrm{LO}}+\Delta\omega) \tag{3.2}$$

$$T_{\mathrm{ideal}}(\Delta\omega) = g_{m2}\frac{Z_o(\omega_{\mathrm{LO}}+\Delta\omega)}{Z_o(\omega_{\mathrm{LO}}+\Delta\omega)+\big(R_{\mathrm{SW}}+|a_1|^2 Z_{\mathrm{IF}}(\Delta\omega)\big)} \times |a_1|^2 Z_{\mathrm{IF}}(\Delta\omega)A_v(\Delta\omega)H_{\mathrm{hpf}}(\Delta\omega) \tag{3.3}$$

where $\Delta\omega$ is the frequency offset from LO, and the term $e^{j\frac{2\pi}{N}n}$ represents the phase shift of the down-converted signal due to the phase of the LO in an N-path system ($n = 0, 1, 2, \ldots N-1$).

To find the bandwidth of the RF channel filter created by the frequency translation loop, the parameters $A_v(\omega)$, $H_{\mathrm{hpf}}(\omega)$ and $Z_{\mathrm{IF}}(\omega)$ are first expressed as

$$A_v(\omega) = \frac{A_{vo}}{(1+j\omega/\omega_{\mathrm{IF1}})} \tag{3.4}$$

$$H_{\mathrm{hpf}}(\omega) = \frac{j\omega/\omega_{\mathrm{hpf}}}{(1+j\omega/\omega_{\mathrm{hpf}})} \tag{3.5}$$

$$Z_{\mathrm{IF}}(\omega) = \frac{R_f}{(1+j\omega/\omega_{\mathrm{IF2}})}\cdot\frac{1}{1+A_v(\omega)} \tag{3.6}$$

where ω_{IF1} is the dominant pole of the IF amplifier, $\omega_{\mathrm{IF2}} = 1/(R_f C_f)$, and ω_{hpf} is the corner frequency of the first order HPF. By substituting (3.4) – (3.6) into (3.2), it can be shown that the RF channel filter bandwidth is [50]

$$BW_{\mathrm{ch}} = \frac{\omega_{\mathrm{hpf}}}{1+T_o} \tag{3.7}$$

where $T_o = g_{m2}R_f A_{\mathrm{mix}}^2 A_{vo}$ is the maximum available loop gain (i.e. at $\Delta\omega = 0$ with no HPF present). Thus, for a fixed resistive part of the HPF, the capacitance needed to achieve a given channel bandwidth is reduced by a factor equal to the $(1 + T_o)$. With the major part of the loop being at IF, a high loop gain is relatively easy to achieve, and consequently, a significant reduction in the amount of die area required for capacitance is possible.

The expressions in (3.1) – (3.3) are ideal because two simplifying assumptions are made:

1. Only the first LO harmonic is considered for the down-/up-conversion gain of the mixers.

2. The version of the signal up-converted by the first LO harmonic of the down-conversion mixer is discarded (i.e. assumed to be completely filtered out by the loop before being down-converted by the the first LO harmonic of the up-conversion mixer).

Although the above two assumptions allow for a simple analysis that captures the basic operation of the circuit, they cause the resulting expressions in (3.1)–(3.3) to fail in giving an accurate prediction for crucial performance parameters such as stop-band rejection, in-band loss and loop gain (Section 3.6).

In principle, an accurate solution can be obtained by applying LPTV system theory [51, 52]. However, in this paper, an alternative approach is adopted to obtain closed form expressions for the IF and RF voltages, as well as the loop gain, by solving the frequency domain equations of the system in an iterative manner. This approach has the advantage that it offers intuition into the operation of the circuit and requires no knowledge other than basic Fourier analysis.

The key idea behind the iterative approach relies on the fact that every time the signal traverses the loop, or goes through the down-conversion mixer and "reflects back on itself", it is multiplied with two sets of Fourier series coefficients (representing the LO harmonics of the mixers). Since these coefficients have a magnitude of less than one for all LO harmonics, starting with an initial solution and recursively feeding the outcome into the equations of the system adds increasingly smaller contributions, and the result quickly converges towards a solution. In contrast to the inherently narrow-band expressions in (3.1)–(3.3), the iterative solution fits the results from full circuit simulations within 1dB over a frequency range that spans several LO harmonics, thus providing accurate prediction of key system parameters for optimum design (Section 3.6).

3.3 Detailed Circuit Analysis

The n-th path IF voltage (that is, the voltage at the IF side of the down-conversion mixer) is determined by the sum of currents going through the down-conversion mixer and the IF impulse response $z_{\mathrm{IF}}(t)$

$$v_{\mathrm{IF}n}(t) = \left\{ \left[g_{m1} v_{\mathrm{in}}(t) + i_{\mathrm{fb}n}(t) - i_o(t) \right] \cdot S_{\mathrm{DC}n}(t) \right\} * z_{\mathrm{IF}}(t) \tag{3.8}$$

where $*$ indicates the convolution operation and $S_{\mathrm{DC}n}(t)$ is the periodic square wave driving the n-th path down-conversion mixer, given by its Fourier series expansion

as [53]

$$S_{\mathrm{DC}n}(t) = \sum_{k=-\infty}^{\infty} a_k e^{jk\omega_{\mathrm{LO}}(t-\frac{n}{N}T_{\mathrm{LO}})} \tag{3.9}$$

$$a_k = \begin{cases} \frac{1}{N}e^{-jk\frac{\pi}{N}}\mathrm{sinc}(\frac{k\pi}{N}) & \text{SB design} \\ \frac{1}{N}e^{-jk\frac{\pi}{N}}\mathrm{sinc}(\frac{k\pi}{N})(1-e^{-jk\pi}) & \text{DB design} \end{cases} \tag{3.10}$$

where $T_{\mathrm{LO}} = 2\pi/\omega_{\mathrm{LO}}$ and, similar to Section 3.2, $n = 0, 1, 2, \ldots N-1$.

In addition, the current supplied by the n-th feedback path can be expressed as a function of the n-th IF voltage

$$i_{\mathrm{fb}n}(t) = -g_{m2}\Big[\big[-a_v(t) * v_{\mathrm{IF}n}(t)\big] * h_{\mathrm{hpf}}(t)\Big] \cdot S_{\mathrm{UC}n}(t) \tag{3.11}$$

where $S_{\mathrm{UC}n}(t)$ is the n-th path periodic square wave driving the up-conversion mixer similarly given by (3.9) and (3.10), and $-a_v(t)$ and $h_{\mathrm{hpf}}(t)$ represent the impulse response of the inverting IF amplifier and the HPF, respectively. By substituting (3.11) in (3.8) and taking the Fourier transform

$$\begin{aligned} V_{\mathrm{IF}n}(\omega) \;=\; & g_{m1}Z_{\mathrm{IF}}(\omega)\sum_{k=-\infty}^{\infty} a_k e^{-jk\frac{2\pi}{N}n} V_{\mathrm{in}}(\omega - k\omega_{\mathrm{LO}}) \\ - \; & g_{m2}Z_{\mathrm{IF}}(\omega)\sum_{m=-\infty}^{\infty}\sum_{k=-\infty}^{\infty} a_m a_k e^{-j(m+k)\frac{2\pi}{N}n} \\ & \times A_v\big(\omega-(m+k)\omega_{\mathrm{LO}}\big) H_{\mathrm{hpf}}\big(\omega-(m+k)\omega_{\mathrm{LO}}\big) \\ & \times V_{\mathrm{IF}n}\big(\omega-(m+k)\omega_{\mathrm{LO}}\big) \\ - \; & Z_{\mathrm{IF}}(\omega)\sum_{k=-\infty}^{\infty} a_k e^{-jk\frac{2\pi}{N}n}\frac{V_{\mathrm{RF}}(\omega-k\omega_{\mathrm{LO}})}{Z_o(\omega-k\omega_{\mathrm{LO}})} \end{aligned} \tag{3.12}$$

where $I_o(\omega)$ has been expressed as $V_{\mathrm{RF}}(\omega)/Z_o(\omega)$, and $A_v(\omega)$, $H_{\mathrm{hpf}}(\omega)$ and $Z_{\mathrm{IF}}(\omega)$ are still given by (3.4), (3.5), and (3.6), respectively.

Furthermore, since the different down/up-conversion paths are operated with non-overlapping clocks, the RF voltage (that is, the voltage at the RF side of the down-conversion mixer) can be expressed as the sum of the voltage drop across the switch resistance R_{SW} and the IF voltage contributions from all paths up-converted via the down-conversion mixer

$$v_{\mathrm{RF}}(t) = \big[g_{m1}v_{\mathrm{in}}(t) + \sum_{n=0}^{N-1} i_{\mathrm{fb}n}(t) - i_o(t)\big]R_{\mathrm{SW}} + \sum_{n=0}^{N-1} v_{\mathrm{IF}n}(t)\cdot S_{\mathrm{DC}n}(t) \tag{3.13}$$

And by taking the Fourier transform and collecting terms

$$\begin{aligned} V_{\mathrm{RF}}(\omega) &= g_{m1}\frac{R_{\mathrm{SW}}Z_o(\omega)}{R_{\mathrm{SW}}+Z_o(\omega)}V_{\mathrm{in}}(\omega) \\ &+ \frac{Z_o(\omega)}{R_{\mathrm{SW}}+Z_o(\omega)}\sum_{n=0}^{N-1}\sum_{k=-\infty}^{\infty} a_k e^{-jk\frac{2\pi}{N}n} \\ &\quad\times\left[1-g_{m2}R_{\mathrm{SW}}A_v(\omega-k\omega_{\mathrm{LO}})H_{\mathrm{hpf}}(\omega-k\omega_{\mathrm{LO}})\right] \\ &\quad\times V_{\mathrm{IF}n}(\omega-k\omega_{\mathrm{LO}}) \end{aligned} \tag{3.14}$$

Although (3.12) and (3.14) involve only two unknowns, namely $V_{\mathrm{IF}n}(\omega)$ and $V_{\mathrm{RF}}(\omega)$, the frequency shifted replicas introduced by the mixers do not allow for a straightforward solution. However, the IF voltage can be obtained by solving (3.12) iteratively, and substituting the result in (3.14) to find the RF voltage.

Carrying out this iterative procedure (Appendices C and D) results in a closed form solution for the IF and RF voltages for all harmonic mixing components. By substituting with $k=-1$ and $k=0$ in (D.3) and (D.12), respectively, the IF and RF responses due to the first LO harmonic can be found as

$$V_{\mathrm{IF}n}(\Delta\omega) = M'_{\mathrm{IF}_{-1}}(\Delta\omega)\mathcal{E}_{\mathrm{IF}_{-1}}(\Delta\omega)V_{\mathrm{in}}(\omega_{\mathrm{LO}}+\Delta\omega) \tag{3.15}$$

$$V_{\mathrm{RF}}(\omega_{\mathrm{LO}}+\Delta\omega) = \left[M'_{\mathrm{RF,SW0}}(\Delta\omega)+M'_{\mathrm{RF0}}(\Delta\omega)\right]\mathcal{E}_{\mathrm{RF0}}(\Delta\omega)V_{\mathrm{in}}\left(\Delta\omega+\omega_{\mathrm{LO}}\right) \tag{3.16}$$

where the mixing functions $M'_{\mathrm{IF}_{-1}}(\Delta\omega)$, $M'_{\mathrm{RF,SW0}}(\Delta\omega)$, $M'_{\mathrm{RF0}}(\Delta\omega)$ and the corresponding error terms $\mathcal{E}_{\mathrm{IF}_{-1}}(\Delta\omega)$ and $\mathcal{E}_{\mathrm{RF0}}(\Delta\omega)$ are as given by (3.17) – (3.21).

$$M'_{\mathrm{IF}_{-1}}(\Delta\omega) = g_{m1}e^{j\frac{2\pi}{N}n}Z_{\mathrm{CL}}(\Delta\omega)\frac{Z_o(\Delta\omega-k\omega_{\mathrm{LO}})}{R_{\mathrm{SW}}+Z_o(\Delta\omega-k\omega_{\mathrm{LO}})} \tag{3.17}$$

$$\mathcal{E}_{\mathrm{IF}_{-1}}(\Delta\omega) = a_k - g_{m2}\sum_{\substack{p=\infty\\ p\neq 0}}^{\infty}\sum_{m=-\infty}^{\infty} a_m a_{p-m}a_{-(1+p)}A_{\mathrm{IF}}(\omega-p\omega_{\mathrm{LO}})Z_{\mathrm{CL}}(\Delta\omega-p\omega_{\mathrm{LO}}) \tag{3.18}$$

$$\begin{aligned} M'_{\mathrm{RF,SW0}}(\Delta\omega) &= g_{m1}R_{\mathrm{SW}}\left[\frac{Z_o(\omega_{\mathrm{LO}}+\Delta\omega)}{R_{\mathrm{SW}}+Z_o(\omega_{\mathrm{LO}}+\Delta\omega)}\right]^2 \\ &\quad\times\left[1-g_{m2}N\sum_{m=-\infty}^{\infty}a_m A_{\mathrm{IF}}\left(\Delta\omega+(1-m)\omega_{\mathrm{LO}}\right)Z_{\mathrm{CL}}\left(\Delta\omega+(1-m)\omega_{\mathrm{LO}}\right)\right] \end{aligned} \tag{3.19}$$

$$M'_{\mathrm{RF0}}(\Delta\omega) = g_{m1}\Big[\frac{Z_o(\omega_{\mathrm{LO}}+\Delta\omega)}{R_{\mathrm{SW}}+Z_o(\omega_{\mathrm{LO}}+\Delta\omega)}\Big]^2 N \sum_{m=-\infty}^{\infty} a_m Z_{\mathrm{CL}}\big(\Delta\omega+(1-m)\omega_{\mathrm{LO}}\big) \tag{3.20}$$

$$\varepsilon_{\mathrm{RF0}}(\Delta\omega) = a_{Nm} - g_{m2}\sum_{l=-\infty}^{\infty}\sum_{\substack{p=\infty\\ p\neq 0}}^{\infty} a_l a_{p-l} a_{-(p+m)} Z_{\mathrm{CL}}\big(\Delta\omega+(1-p-m)\omega_{\mathrm{LO}}\big) \times A_{\mathrm{IF}}\big(\Delta\omega+(1-p-m)\omega_{\mathrm{LO}}\big) \tag{3.21}$$

The term $\varepsilon_{\mathrm{IF}_{-1}}$ represents the effect of undesirable harmonic components that alter the shape of the IF LPF created by the frequency translation loop. Similarly, the term $\varepsilon_{\mathrm{RF0}}$ represents the effect of harmonic mixing on the corresponding band-pass filter at RF. At the same time however, the term $\varepsilon_{\mathrm{RF0}}$ advantageously reduces the effect of the switch resistance on the maximum achievable stop-band rejection at RF as will be shown in Section 3.4.

Note that the bandwidth of the IF/RF channel filter created by the frequency translation loop can be obtained from the expressions in (3.15) and (3.16), respectively, using a narrow-band approximation. Under such approximation, $\varepsilon_{\mathrm{IF}_{-1}}(\Delta\omega) \approx \varepsilon_{\mathrm{RF0}}(\Delta\omega) \approx M'_{\mathrm{RF,SW0}}(\Delta\omega) \approx 0$, and the filter bandwidth is still given by (3.7), albeit the value of T_o is now significantly different as will be explained in Section 3.5.

3.4 Verification of Results

To verify the results of Sections 3.2 and 3.3, the derived IF and RF voltages are first normalized with respect to the open loop voltages at the first LO harmonic (i.e. $g_{m2} = 0$ and $\Delta\omega = 0$) to obtain the IF and RF filter transfer functions, respectively. That is

$$H_{\mathrm{IF}}(\Delta\omega) = \frac{V_{\mathrm{IF}n}(\Delta\omega)}{V_{\mathrm{IF}n}(0)|_{g_{m2}=0}} \tag{3.22}$$

$$H_{\mathrm{RF}}(\omega_{\mathrm{LO}}+\Delta\omega) = \frac{V_{\mathrm{RF}}(\omega_{\mathrm{LO}}+\Delta\omega)}{V_{\mathrm{RF}}(\omega_{\mathrm{LO}})|_{g_{m2}=0}} \tag{3.23}$$

where the expressions in (3.22) and (3.23) are valid for both the idealized and detailed analyses, and can now be verified against Spectre circuit simulations (PSS + PAC) for different design criteria.

Starting with a SB design, Fig. 3.3 shows the RF and IF filter transfer functions in open and closed loop operation for the case of an ideal switch with zero resistance and a high loop phase margin of approximately 90° (Section 3.5). As a first observation, comparison with circuit simulation results shows that the idealized analysis provides a poor prediction of the filtering response, and only around the first harmonic of the LO. This is a direct, and expected, consequence of neglecting higher harmonics in

the analysis. In contrast, the detailed analysis is capable of predicting the response of the system with a maximum error of < 0.5dB at LO harmonics and < 1.5dB in-between, maintained across a range of several LO harmonics. Furthermore, the operation of the frequency translation loop is evident from comparing the open and closed loop operation of the circuit. As expected, filtering is provided, both at RF and IF, around all LO harmonics. The filtering suppression predicted by idealized analysis is underestimated mainly due to the error in prediction of the available loop gain as will be explained in Section 3.5. Also note that, in general, the RF filtering achieved is not symmetric for positive and negative frequency offsets from LO because the spectrum of the (real) RF signal is naturally centered around DC instead.

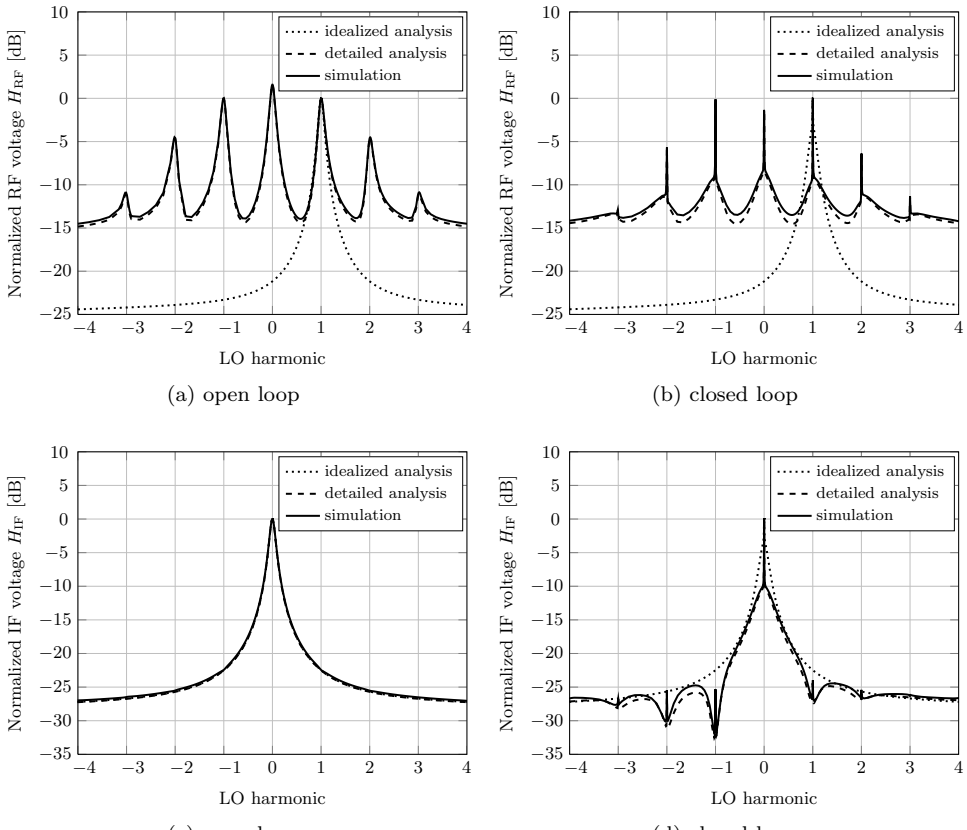

(a) open loop (b) closed loop

(c) open loop (d) closed loop

Figure 3.3: Filtering in a 4-path single balanced design with $R_{\mathrm{SW}} = 0$. Simulation/calculation parameters: $g_{m2}/g_{m1} = 1$, $g_{m1}R_f = 10$, $A_{vo} = 20$dB, $R_o = R_f$, target phase margin $\approx 90°$ ($\omega_{\mathrm{IF1}}/\omega_{\mathrm{LO}} = 3$ and $\omega_{\mathrm{IF2}}/\omega_{\mathrm{LO}} = 0.0625$), $\omega_{\mathrm{hpf}}/\omega_{\mathrm{LO}} = 0.0067$, $\omega_{\mathrm{RF}}/\omega_{\mathrm{LO}} = 2$. (a) RF response in open loop operation. (b) RF response in closed loop operation. (c) IF response in open loop operation. (d) IF response in closed loop operation.

Fig. 3.4 shows the results of a DB design using the same set of design parameters of the SB design in Fig. 3.3. The accuracy of the detailed analysis is similarly evident. The operation of the frequency translation loop is as expected, with the response at even harmonics suppressed in a DB design. Compared to its SB counterpart (Fig. 3.3), a DB design achieves higher suppression ($\approx$ 5dB) because the higher conversion gain of double balanced switches results in a higher loop gain (Section 3.5). Finally, note that the results of the detailed analysis show an even better fit between prediction and simulation ($<$ 0.5dB over the entire frequency range displayed) due to the suppression of even harmonics which improves the accuracy of the solution. This is because the neglected terms (mainly due to the limited number of iterations) contain less harmonic content, and, therefore, have a smaller effect on the final solution.

Likewise, Fig. 3.5 shows the accuracy of the prediction provided by detailed analysis for a DB design with low Z_{IF} (equivalently high A_{vo}) and finite switch resistance ($R_{\text{SW}} = 0.01 \times Rf$). In open loop operation, the switch resistance severely degrades the maximum achievable suppression at the RF side, which is a fundamental drawback in many voltage mixer filters [28, 31]. In contrast, closed loop operation is essentially unaffected by the switch resistance and remains capable of achieving similar RF suppression (only about 2dB lower) to that obtained in an equivalent design with the same loop gain but $R_{\text{SW}} = 0$ (3.4). This is expected, since the loop sinks current through a transconductor (g_{m2}) whose output impedance is significantly larger than, and therefore highly independent of, the switch resistance. In that respect, filtering via a feedback loop is advantageous since it allows for using smaller switches which directly translates to lower power in the driving LO buffers.

Finally, Fig. 3.6 shows the verification results for a DB design with a target phase margin $< 60°$. The accuracy of the detailed analysis, as well as the operation of the frequency translation loop, remain evident. The significantly different response of the circuit compared to the designs in Fig. 3.3 – 3.5 is due to the difference in targeted phase margin. The placement of poles in the loop to achieve stability will be discussed in Section 3.5

3.5 Loop Stability

An accurate approximation for the loop gain is found from the derivation in Appendix C as

$$T_{\text{IF-IF}}(\omega) = g_{m2} Z_{\text{IF}}(\omega) A_v(\omega) H_{\text{hpf}}(\omega) \sum_{m=-\infty}^{\infty} |a_m|^2 \tag{3.24}$$

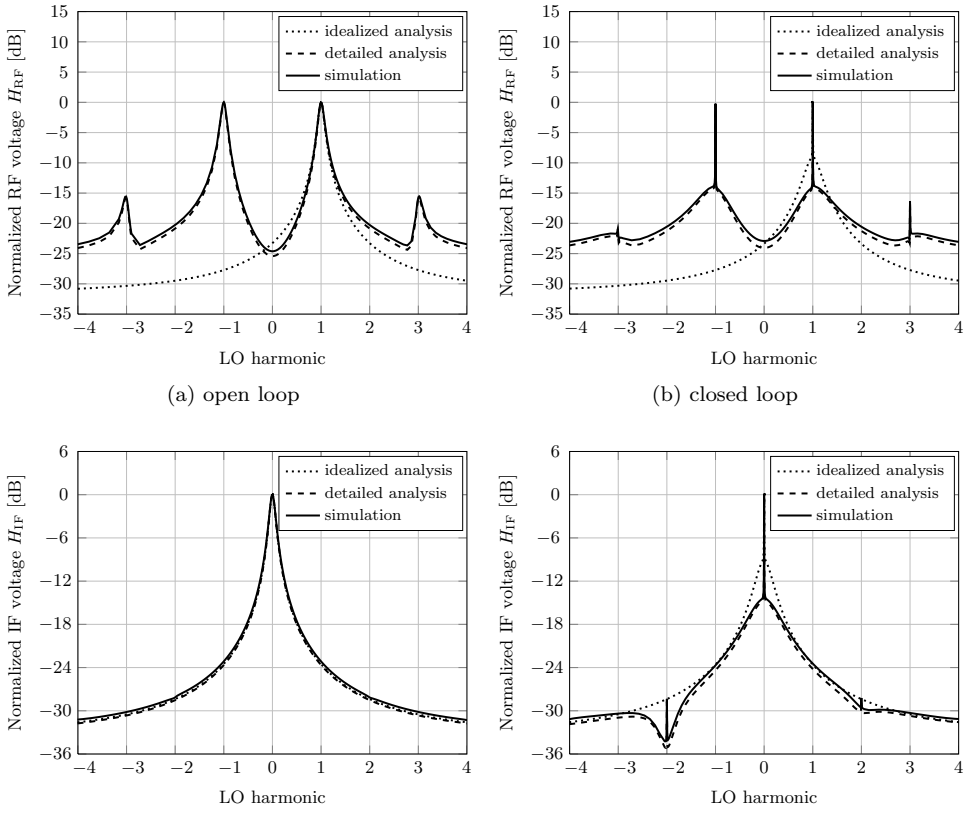

(a) open loop (b) closed loop

(c) open loop (d) closed loop

Figure 3.4: Filtering in a 4-path double balanced design with $R_{\mathrm{SW}} = 0$. Simulation/calculation parameters: $g_{m2}/g_{m1} = 1$, $g_{m1}R_f = 10$, $A_{vo} = 20\mathrm{dB}$, $R_o = R_f$, target phase margin $\approx 90^\circ$ ($\omega_{\mathrm{IF1}}/\omega_{\mathrm{LO}} = 3$ and $\omega_{\mathrm{IF2}}/\omega_{\mathrm{LO}} = 0.0625$), $\omega_{\mathrm{hpf}}/\omega_{\mathrm{LO}} = 0.0067$, $\omega_{\mathrm{RF}}/\omega_{\mathrm{LO}} = 2$. (a) RF response in open loop operation. (b) RF response in closed loop operation. (c) IF response in open loop operation. (d) IF response in closed loop operation.

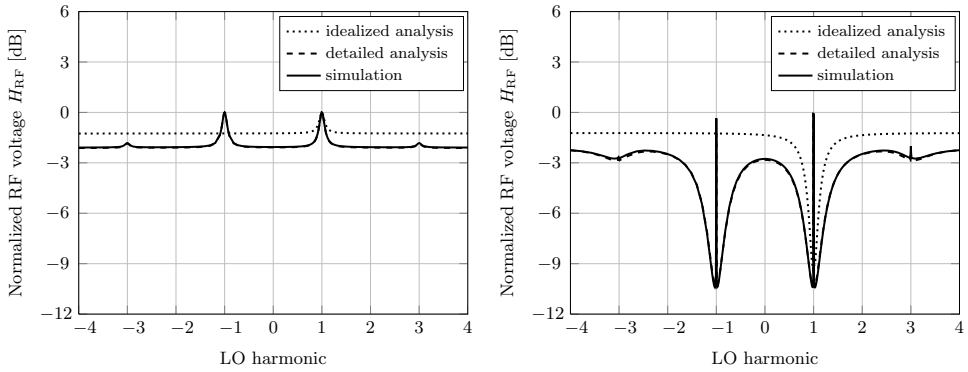

(a) open loop (b) closed loop

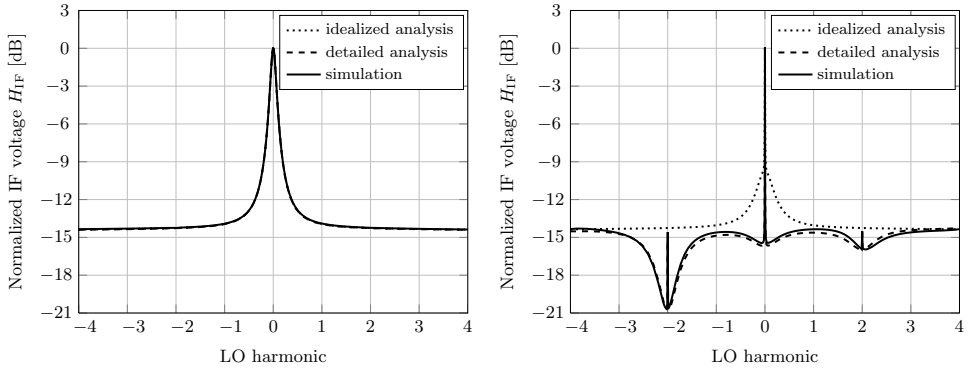

(c) open loop (d) closed loop

Figure 3.5: Filtering in a 4-path double balanced design with $R_{\mathrm{SW}} = 0.01R_f$. Simulation/calculation parameters: $g_{m2}/g_{m1} = 1$, $g_{m1}R_f = 10$, $A_{vo} = 40$dB, $R_o = R_f$, target phase margin $\approx 90^\circ$ ($\omega_{\mathrm{IF1}}/\omega_{\mathrm{LO}} = 3$ and $\omega_{\mathrm{IF2}}/\omega_{\mathrm{LO}} = 0.0625$), $\omega_{\mathrm{hpf}}/\omega_{\mathrm{LO}} = 0.0067$, $\omega_{\mathrm{RF}}/\omega_{\mathrm{LO}} = 2$. (a) RF response in open loop operation. (b) RF response in closed loop operation. (c) IF response in open loop operation. (d) IF response in closed loop operation.

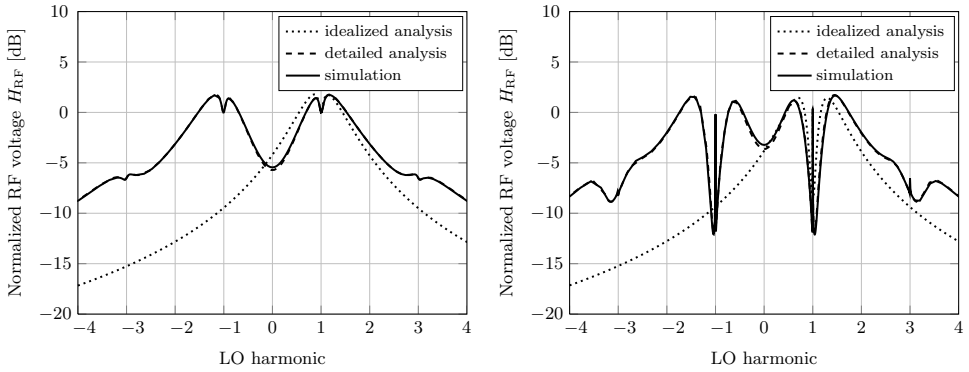

(a) open loop (b) closed loop

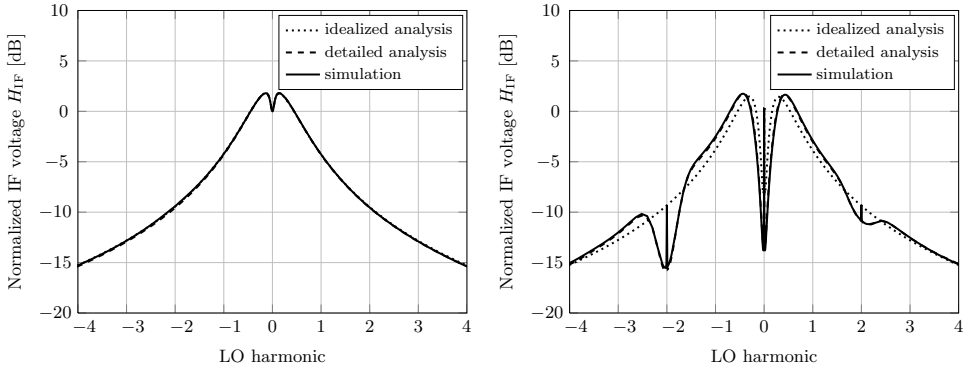

(c) open loop (d) closed loop

Figure 3.6: Filtering in a 4-path double balanced design with $R_{\mathrm{SW}} = 0$. Simulation/calculation parameters: $g_{m2}/g_{m1} = 1$, $g_{m1}R_f = 10$, $A_{vo} = 20$dB, $R_o = R_f$, target phase margin $\approx 90^\circ$ ($\omega_{\mathrm{IF1}}/\omega_{\mathrm{LO}} = 0.0472$ and $\omega_{\mathrm{IF2}}/\omega_{\mathrm{LO}} = 0.0625$), $\omega_{\mathrm{hpf}}/\omega_{\mathrm{LO}} = 0.0067$, $\omega_{\mathrm{RF}}/\omega_{\mathrm{LO}} = 2$. (a) RF response in open loop operation. (b) RF response in closed loop operation. (c) IF response in open loop operation. (d) IF response in closed loop operation.

By subtituting with (3.4) – (3.6) in (3.24)

$$T_{\text{IF-IF}}(\Delta\omega) = \frac{T_o}{\left(1 + j\frac{\Delta\omega}{\omega_{\text{IF1}}(1+A_{vo})}\right)\left(1 + j\frac{\Delta\omega}{\omega_{\text{IF2}}}\right)} \frac{j\frac{\Delta\omega}{\omega_{\text{hpf}}}}{\left(1 + j\frac{\Delta\omega}{\omega_{\text{hpf}}}\right)} \tag{3.25}$$

where T_o is the maximum loop bandwidth given by

$$T_o = g_{m2}\frac{R_f}{1 + A_{vo}} A_{vo} \sum_{m=-\infty}^{\infty} |a_m|^2 \tag{3.26}$$

Fig. 3.7 shows the idealized bode plot of the loop gain based on (3.25). The loop gain exhibits a low frequency offset cross-over point ω_{hpf}/T_o (due to the HPF), and a high frequency offset cross-over point ω_t (due to limited loop bandwidth). Since a first order HPF is used, the low cross-over is always stable. For the high cross-over point, the HPF is almost a short circuit, and the system can be treated as a two pole system. Thus, the phase margin ϕ can be determined by the traditional approximation [12]

$$\omega_{\text{IF1}}(1 + A_{vo}) \approx \omega_{\text{IF2}} T_o \tan(\phi) \tag{3.27}$$

It is also beneficial to compare $T_{\text{IF-IF}}(\Delta\omega)$ in (3.24) to the loop gain of the idealized analysis, $T_{\text{ideal}}(\Delta\omega)$ in (3.3). Under the same approximations used above, the main difference in the loop gain expressions lies in the contribution of the mixers to the total loop gain. While idealized analysis predicts that only the first LO harmonic ($|a_1|^2$) affects the loop gain, detailed analysis shows that in fact the whole energy of the LO signal ($\sum_{m=-\infty}^{\infty} |a_m|^2$) contributes to the loop gain. Intuitively, this can be understood by considering a signal of a given frequency offset $\Delta\omega$ traversing the loop: the signal will experience one frequency translation $\pm k\omega_{\text{LO}}$ through the down-conversion mixer, and an opposite frequency translation $\mp k\omega_{\text{LO}}$ through the up-conversion mixer. Thus, all LO harmonics contribute to the propagation of the signal around the loop. This is an advantage since the contribution of all LO harmonics to the loop gain directly translates to higher suppression of interferers.

Comparing $T_{\text{IF-IF}}(\Delta\omega)$ and $T_{\text{ideal}}(\Delta\omega)$ against circuit simulations for a 4-path DB design (Fig. 3.8) shows that indeed the idealized analysis underestimates the available loop gain. The difference in prediction of the maximum loop gain is roughly 8dB which, as expected, corresponds to the ratio $(2/N)/|a_1|^2$ for a 4-path DB design, where $(2/N)$ is the energy of the signal equivalent to the summation of Fourier series coefficients in (3.26).

It should finally be noted that an accurate prediction of the loop gain consequently allows for a correct prediction of channel filter bandwidth according to (3.7). In the example of Fig. 3.8 for instance, idealized analysis would result in a filter bandwidth estimate of about twice the actual value.

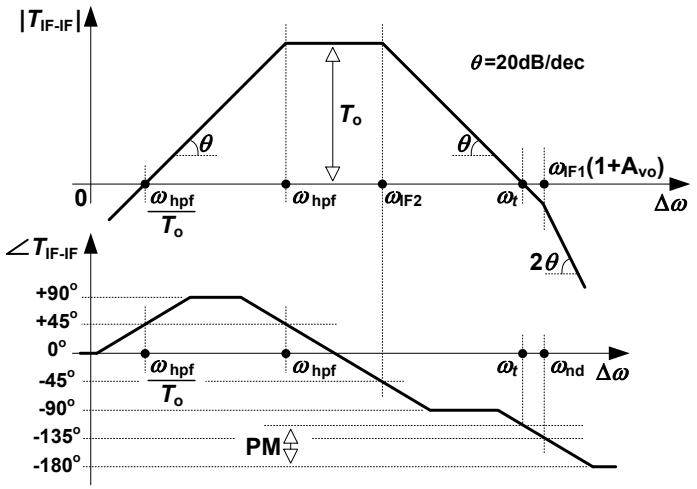

Figure 3.7: Idealized bode plot of loop gain

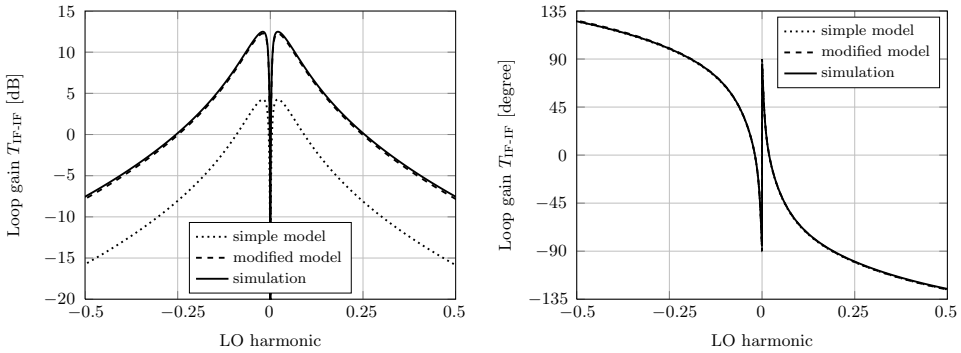

Figure 3.8: Comparison between the loop gain prediction of idealized and detailed models for a 4-path double balanced design in closed loop operation with a target phase margin of 60°. Simulation/calculation parameters: $g_{m2}/g_{m1} = 1$, $g_{m1}R_f = 10$, $A_{vo} = 20$dB, $R_{\text{SW}} = 0$, $R_o = R_f$, $\omega_{\text{hpf}}/\omega_{\text{LO}} = 0.0067$, $\omega_{\text{RF}}/\omega_{\text{LO}} = 2$. (a) Magnitude. (b) Phase.

3.6 System Trade-offs and Optimization

Having defined the IF and RF filter transfer functions in Section 3.4, the performance of the system can further be examined by defining conventional filter parameters that characterize the operation of the system. For our purposes in this paper, three key parameters are defined for RF filtering as shown in Fig. 3.9 (but corresponding parameters can be defined for IF filtering as well): maximum Stop-Band Rejection (SBR), in-channel loss/gain (L_{ch}) and the stop-bandwidth of the filter ($\Delta\omega_{\text{SB}}$).

The maximum RF stop-band rejection is the maximum suppression provided by the loop around the first harmonic of the LO, and is found as the difference between the open loop[1] and closed loop responses, corrected for in-band loss/gain

$$\mathrm{SBR} = \max\left[\frac{H_{\mathrm{RF}}(\omega_{\mathrm{LO}}+\Delta\omega)\big|_{g_{m2}=0,r_{o2}\to\infty}}{H_{\mathrm{RF}}(\omega_{\mathrm{LO}}+\Delta\omega)} - L_{\mathrm{ch}}\right] \tag{3.28}$$

where L_{ch} is the in-channel loss/gain given by

$$L_{\mathrm{ch}} = \frac{H_{\mathrm{RF}}(\omega_{\mathrm{LO}})|_{g_{m2}=0,r_{o2}\to\infty}}{H_{\mathrm{RF}}(\omega_{\mathrm{LO}})} \tag{3.29}$$

Furthermore, the stop-bandwidth $\Delta\omega_{\mathrm{SBW}}$ is the frequency offset from LO at which the SBR provided by the frequency translation loop drops to 3dB

$$\Delta\omega_{\mathrm{SBW}} \to \left|\frac{H_{\mathrm{RF}}(\omega_{\mathrm{LO}}+\Delta\omega_{\mathrm{SBW}})\big|_{g_{m2}=0,r_{o2}\to\infty}}{H_{\mathrm{RF}}(\omega_{\mathrm{LO}}+\Delta\omega_{\mathrm{SBW}})} - L_{\mathrm{ch}}\right| = \frac{1}{\sqrt{2}} \tag{3.30}$$

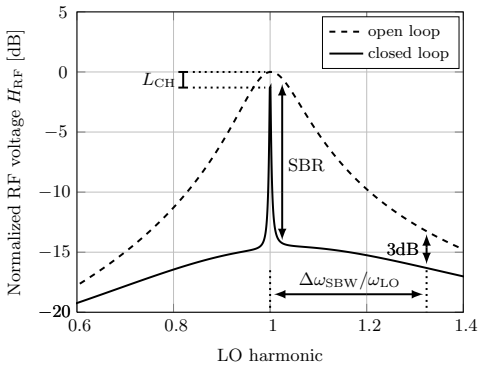

Figure 3.9: Definition of filter parameters

The predicted and simulated parameters in (3.28) – (3.30) are plotted in Fig. 3.10 and 3.11 versus the normalized loop bandwidth ($\omega_{\mathrm{IF2}}/\omega_{\mathrm{LO}}$) for two DB designs with a target phase margin of 90° and 60°, respectively. In both cases, performing as low as one iteration significantly improves the accuracy of the solution, especially for SBR and L_{ch}. In contrast to the idealized system solution, detailed analysis accurately predicts the performance of the system over the entire range of loop bandwidths examined. The discrepancy at high loop bandwidths mainly arises due to harmonic

[1]In open loop operation, the upconversion mixer is disabled. In all the expressions derived in this chapter, this is equivalent to setting $g_{m2} = 0$. As such, the HPF, including the output impedance of the feedback transconductor, drops out from all equations since H_{hpf} always appears multiplied by g_{m2}.

mixing components becoming more pronounced with less filtering in the loop, which, in turn, affects the accuracy of a solution with limited number of iterations.

The different trade-offs in the system can also be examined using the results in Fig. 3.10 and 3.11 (similar observations can be made regarding the IF response unless explicitly stated).

As a first observation, the curves in Fig. 3.10a and 3.11a show an optimum loop bandwidth beyond which the maximum RF SBR starts to drop (an effect not predicted by idealized analysis). For low loop bandwidths, the increase in SBR with increasing the loop bandwidth is due to the increased separation between the dominant pole of the loop ω_{IF2} and ω_{hpf}, which allows the loop bandwidth to increase towards its maximum value T_o (Fig. 3.7). For higher loop bandwidths, harmonic mixing components come into play. This is because in contrast to an idealized system, the filter response in an actual system is translated IF to RF around all harmonics of the LO (Fig. 3.3b and 3.4b). As such, an excessively higher loop bandwidth results in more overlap between the different harmonic responses, "filling up" the stop-band of the filter around the first harmonic and adversely affecting the maximum rejection achieved. This is a crucial observation since the loop bandwidth is directly related to the power consumption in the loop. That, in combination with the results in 3.10c and 3.11c, reveals a trade-off between rejection, stop-bandwidth and power consumption. Finally, it should be noted that the effect of harmonic responses at IF is minor, thus, a higher loop bandwidth rather causes the maximum SBR at IF to saturate towards a value determined by the maximum loop gain T_o.

Furthermore, harmonic mixing products cause in-channel loss (negative change in magnitude, Fig. 3.10b) or gain (positive change in magnitude, Fig. 3.11b), which increases with increasing loop bandwidth. While in-channel loss translates to higher NF, in-channel gain results in higher distortion due to larger signal swing.

Thus, a detailed analysis is necessary for both system design and optimization. Based on available design parameters (N, SB/DB, $g_{m1}R_f$, A_{vo}, R_{SW}/R_f, R_o/R_f, and target phase margin), normalized design curves similar to the ones in Fig. 3.10 and 3.11 can be generated to aid in accurate circuit design and achieve an optimized performance (SBR, L_{ch}, and $\Delta\omega_{\mathrm{SBW}}$) within the available power budget (g_{m2}/g_{m1}).

3.7 Noise

The developed iterative procedure can also be utilized to analyze the noise behavior of the system taking into account noise folding effects.

The main noise sources in the system are shown in Fig. 3.12. In Appendix E, the iterative procedure is carried out for each of these sources to find its transfer function to output. By summing the uncorrelated noise contributions from all sources, the

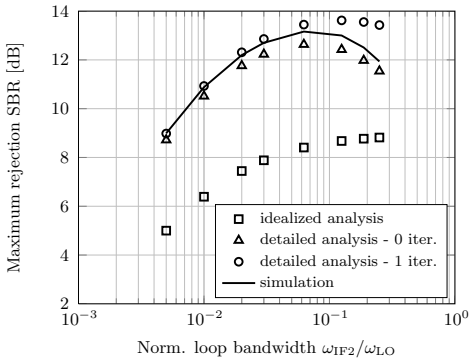

(a)

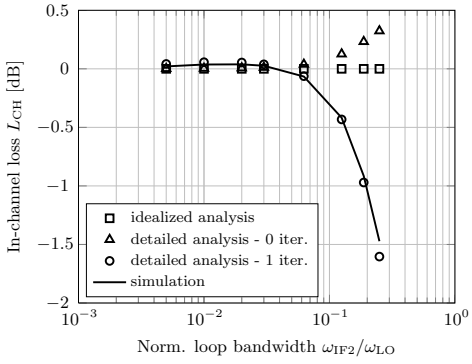

(b)

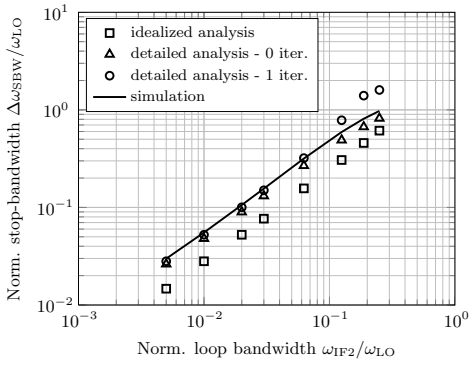

(c)

Figure 3.10: Comparison between the RF performance prediction of idealized and detailed analyses versus normalized loop bandwidth (ω_{IF2}/ω_{LO}) for a 4-path double balanced design in closed loop operation and a target phase margin = 90°. Simulation/calculation parameters: $g_{m2}/g_{m1} = 1$, $g_{m1}R_f = 10$, $A_{vo} = 20$dB, $R_{SW} = 0$, $R_o = R_f$, $\omega_{hpf}/\omega_{LO} = 0.0067$, $\omega_{RF}/\omega_{LO} = 2$. (a) Maximum RF stop-band rejection. (b) RF In-channel loss. (c) RF stop-bandwidth.

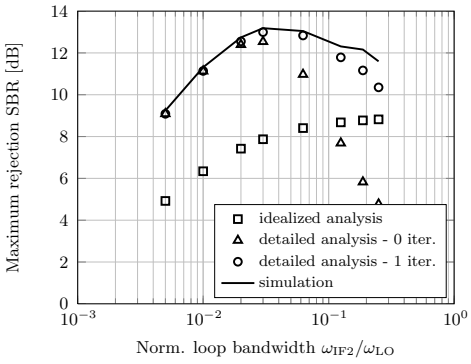

(a)

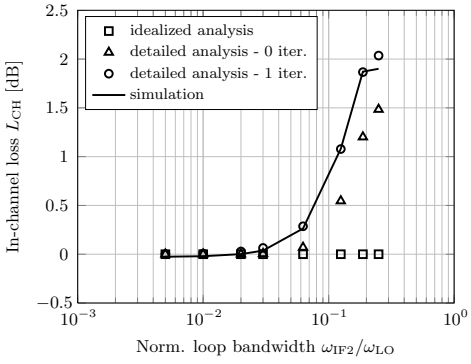

(b)

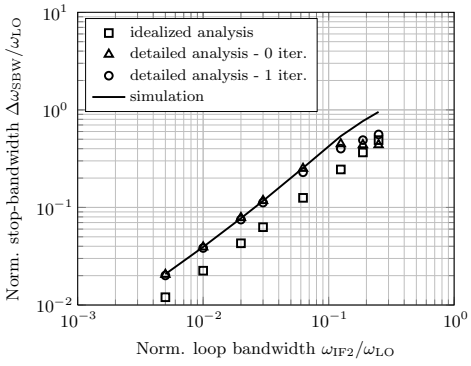

(c)

Figure 3.11: Comparison between the RF performance prediction of idealized and detailed analyses versus normalized loop bandwidth (ω_{IF2}/ω_{LO}) for a 4-path double balanced design in closed loop operation and a target phase margin = 60°. Simulation/calculation parameters: $g_{m2}/g_{m1} = 1$, $g_{m1}R_f = 10$, $A_{vo} = 20$dB, $R_{SW} = 0$, $R_o = R_f$, $\omega_{hpf}/\omega_{LO} = 0.0067$, $\omega_{RF}/\omega_{LO} = 2$. (a) Maximum RF stop-band rejection. (b) RF In-channel loss. (c) RF stop-bandwidth.

noise factor F can be expressed as $F = 1 + \mathrm{EF}$ where, EF is the excess noise factor quantifying the different noise contributions in the system. For an RF output

$$\mathrm{EF}_{\mathrm{RF}} = \frac{\sum\limits_{\text{all sources}} \overline{v_n}^2_{,\mathrm{RF}}(\omega_{\mathrm{LO}} + \Delta\omega)}{4KTR_s \sum\limits_{k=-\infty}^{\infty} \left[M_{\mathrm{RF,SW}k}(\Delta\omega) + M_{\mathrm{RF}k}(\Delta\omega)\right]} \tag{3.31}$$

where the summation in the numerator of (3.31) is for all output noise contributions given by (E.4), (E.11), (E.17), (E.24), and (E.30), and R_s is the source resistance.

To verify the expression in (3.31), several designs with different parameters (architecture, number of paths, transconductance values .. etc.) have been tested against Spectre circuit simulations (PSS+PNOISE). Fig. 3.13 shows one such test of a 4-path DB design. The results show that NF predictions match circuit simulations within roughly 0.9dB across the entire range of loop bandwidths examined (other test cases examined exhibit similar accuracy).

Comparing open and closed results shows that the frequency translation loop does not cause a deterioration in NF. This is expected since the HPF in the feedback path filters out most of the noise before being up-converted to the band of interest. However, an increased loop bandwidth causes more noise components to fold into the filter bandwidth and, thus, causes an increase in NF, which is consistent with the discussion in Section 3.6.

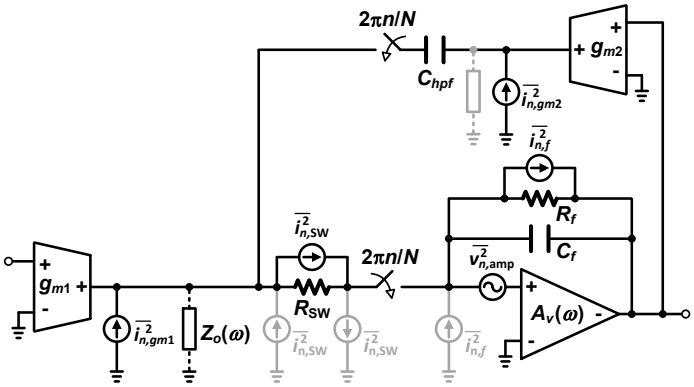

Figure 3.12: Noise sources in a frequency translation loop

3.8 Conclusion

An iterative procedure for analyzing frequency translation loops employing passive mixers has been presented. The resulting closed form expressions are capable of accurately predicting the filtering action of the loop, as well as its noise behavior. Using

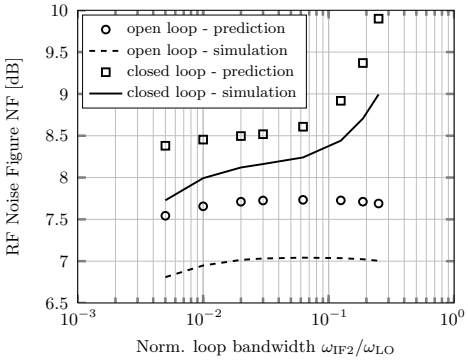

Figure 3.13: Comparison between NF prediction of detailed analysis and Spectre PSS + PNOISE circuit simulations versus normalized loop bandwidth (ω_{IF2}/ω_{LO}) for a test case of a 4-path double balanced design. Simulation/calculation parameters: $g_{m1}R_s = 1$, $g_{m2}R_s = 1$, $R_f/Rs = 20$, $A_{vo} =$ 20dB, $R_{SW}/R_s = 0.4$, $R_o = R_f$, $\omega_{hpf}/\omega_{LO} = 0.0067$, $\omega_{RF}/\omega_{LO} = 2$, target phase margin = 90°.

these harmonic transfer functions, normalized design curves are generated to quantify the performance of the loop in terms of filter stop-band rejection, in-channel loss and stop-bandwidth. The curves can then be used for system design and optimization.

For RF filtering, results reveal an optimum loop bandwidth where stop-band rejection is maximum, and beyond which a trade-off exists between interferer suppression and the stop-bandwidth of the filter. For stability, analysis results show that the loop can indeed be made stable by conventional feedback compensation despite the presence of LO harmonics in the loop. Furthermore, the derived loop gain expression shows that the contribution of the mixers to the loop gain is significantly higher than expected. This is because the complete energy of the LO signal is involved in the down/up-conversion process and not just the first LO harmonic, which advantageously translates to higher stop-band rejection. Finally, the loop is found to have a minor effect on the noise performance of the system due to the presence of the HPF in the feedback path which heavily filters out the noise of the IF blocks before being up-converted to the band of interest.

Chapter 4

Chip Design

A prototype designed in a standard 65nm CMOS process occupies $< 0.06\text{mm}^2$ and utilizes an RF channel-select filter with a 1-to-2.5GHz tunable center frequency to achieve 48dB of stop-band rejection and a wideband IIP3 $> +12$dBm.

Section 4.1 presents the designed chip prototype and section 4.2 discusses simulation results. Section 4.3 presents measurement results, and Section 4.4 concludes this chapter.

4.1 Implementation

To verify the concept, an active feedback receiver front-end was designed and implemented in a 65nm low power (LP) standard CMOS process. The design shown in Fig. 4.1 is entirely based on self-biased inverters and switches, which, in addition to its simplicity, offers several advantages. These include a high Gain-Bandwidth product due to current re-use in inverters, eliminating the need for bias circuitry, lower second-order distortion [54], and a design that lends itself to easy porting from one technology to another. The first IF amplifier incorporates a 3pF Miller capacitance for frequency compensation of the loop, as well as a shunt feedback resistance for establishing a low input impedance. However, due to the limited gain available from a one stage inverter, the input impedance is not low enough to ensure a low swing at the output of the LNA transconductor. As a result, in-channel IIP3 is relatively low as shown in measurements discussed later in this Chapter (Fig. 4.6).

One set of switches arranged in a double balanced fashion down-converts the differential RF input (i.e. 2-phase real signal) into differential I/Q signals (i.e. 4-phase complex signal) at IF. A similar set of switches in the feedback path combines the I/Q signals to perform the reverse operation. As expected, the 25Ω switches are about 3-to-5 times smaller than what is typically seen in state-of-the-art designs using

passive mixers for filtering [28, 29]. The feedback transconductors are placed at IF and followed by the HPF to filter out flicker noise before being up-converted to the channel band. Furthermore, the LNA and feedback transconductors are matched to exploit partial IM3 cancellation as explained in section 2.4. Although placing the matched feedback transconductors at RF would, in general, offer better cancellation, the relatively high output impedance of the forward path in this design severely degrades the loop gain when driving the voltage mixers necessary for up-conversion. Therefore, partial IM3 cancellation is chosen as a compromise in this design. Finally, for sake of simplicity to demonstrate the feedback loop, our chip prototype uses a simple 50Ω termination to ground to provide input matching at the expense of 3dB degradation in NF.

An on-chip clock divider is included to generate the 4-phase LO signal necessary for differential I/Q operation. The input to the clock circuitry is an external sinusoidal signal of 4 times the desired LO. The external signal is first amplified and clipped through a series of inverters before being passed on to the divider. The divider is based on a ring counter with a reset, and implemented with 4 D-type transmission gate flip flops. Using a HPF and a $4:1$ voltage divider, The non-overlapping clock signals are raised to one quarter of the supply to drive the mixer switches with an LO signal that swings between 0.3V and 1.5V.

The measurement interface provides isolation to measure the output without disturbing the loop. Noise and full channel bandwidth can be measured via the inverter buffers, while actual in-band gain and linearity can be measured via large (15kΩ) output resistors. The feedback loop in the designed receiver has a gain of about 20dB ($\approx 10\times$ reduction in capacitance) and a unity gain frequency of > 500MHz on either side of the LO frequency. The total capacitance in this design is only 60pF (15pF $\times 4$ for differential I/Q operation) to achieve a 5MHz channel bandwidth. Compared to the amount of capacitance required by other state-of-the art receivers, the active feedback receiver requires less than 25% of the capacitance to achieve one-tenth of the channel bandwidth in a typical mixer-first receiver [21], and less than 20% of the capacitance to achieve about 12% of the channel bandwidth of an N-path filter [29]. The corresponding benefit in area reduction is evident from the small active area required ($< 0.06\text{mm}^2$) including the clock circuitry. The die photograph in Fig. 4.2 shows the implemented chip, which is pad limited due to the multiple outputs required for testing.

4.2 Simulation Results

Table 4.1 shows a comparison of simulated key receiver parameters for open (up-conversion mixer OFF) and closed loop operation. The closed loop in-band gain

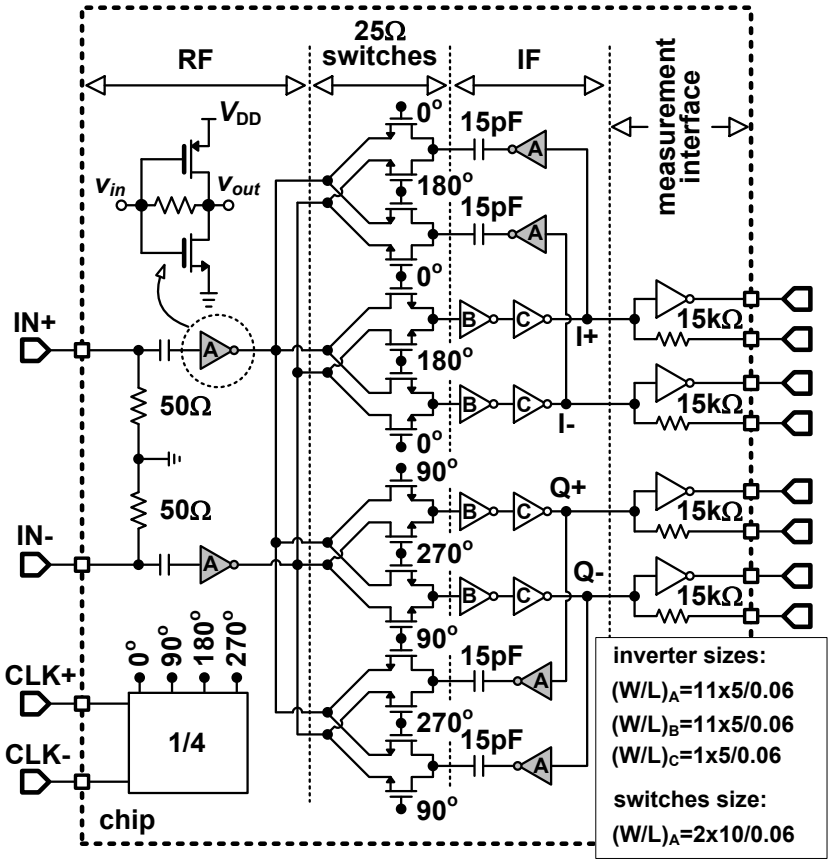

Figure 4.1: Schematic of implemented active feedback receiver.

drops by less than 4dB mainly due to the loading effect of the feedback path. As expected the NF degradation due to closed loop operation is minor (0.3dB) because the noise of the feedback path within the desired channel bandwidth is heavily filtered out by the HPF. At a relatively small frequency offset of 20MHz, the receiver rejection ratio is improved by almost 14dB, achieved at RF at the output of the LNA.

Consequently, as expected, two-tone simulations show an improvement in maximum wideband IIP3 of about 15dB, achieved at more than 3 times lower frequency offset compared to the open loop case. Similar improvement is simulated for the wideband blocking performance of the receiver, i.e. the blocker power level at which the small signal gain of the desired signal drops by 1dB (P-1dB). The current consumption in closed loop operation is higher by approximately 20mA mainly due to the four IF transconductors matched to the LNA.

Since filtering after the LNA would normally cause the LNA to set an upper

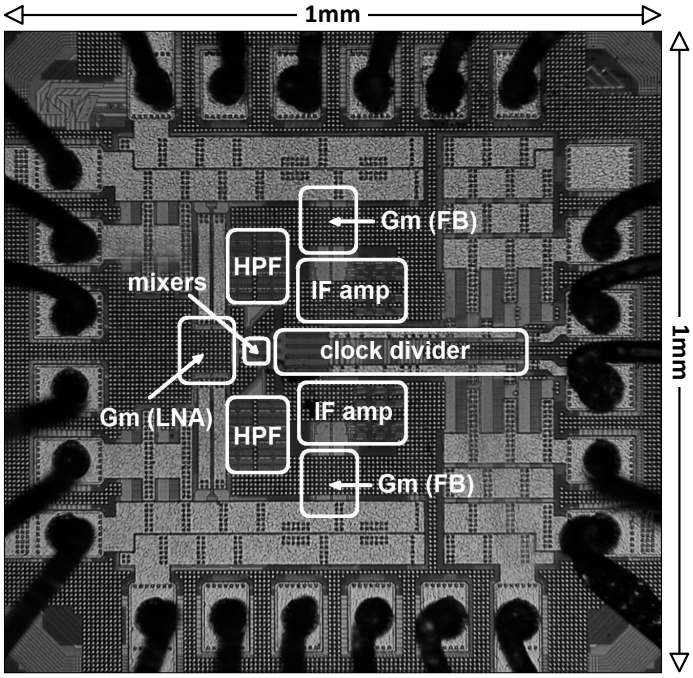

Figure 4.2: Die photograph (65nm).

limit on the overall linearity of the receiver (section 2.4), the improvement in IIP3 due to distortion canceling is examined by comparing the maximum IIP3 achieved by the active feedback receiver to the maximum IIP3 that can be achieved by the LNA. Simulations of the self-biased inverter LNA with 50Ω matching at its input and the same test tones listed in Table 4.1 show a maximum IIP3 of approximately 4dBm, achieved when the LNA output is presented with a perfect AC short circuit. Comparing this value to that listed in Table 4.1 indicates that the effect of distortion canceling is about 8-to-9dB improvement in IIP3.

4.3 Measurement Results

Figure 4.3(a) shows the measured RF-to-IF gain for positive and negative frequency offsets (Δf) for the case of a 2GHz LO frequency (f_{LO}). The receiver achieves a gain of 30dB (measurement buffers de-embedded), and a channel bandwidth of 5MHz (2.5MHz on either side of the LO). A maximum stop-band rejection of 48dB is achieved at 250MHz frequency offset. The rejection is mainly achieved by the loop gain (40dB in 2 decades). The extra 8dB measured in roll-off over 2 decades is due

	open loop	**closed loop**	
RF-to-IF gain ($\Delta f = 50$kHz)	34.8	31	dB
DSB NF ($\Delta f = 2$MHz)	7.2	7.5	dB
Receiver rejection ($\Delta f = 20$MHz)	1.9	15.5	dB
Maximum wideband IIP3	-2.3 $\Delta f = 500$MHz	12.1 $\Delta f = 160$MHz	dBm
Maximum wideband P-1dB	-16.2 $\Delta f = 500$MHz	-6 $\Delta f = 160$MHz	dBm
Current consumption	31.5	50.1	mA

Table 4.1: Simulated key parameters of implemented active feedback receiver for open and closed loop operation for $f_{\mathrm{LO}} = 2$GHz. For two-tone measurements, tones are located at $f_{\mathrm{LO}} + \Delta f$ and $f_{\mathrm{LO}} + 2\Delta f - 25$kHz. For blocking performance measurements, the desired signal and blocker are located at $f_{\mathrm{LO}} + 50$kHz and $f_{\mathrm{LO}} + \Delta f$, respectively.

to extra filtering in the forward path of the receiver, which means that the phase margin is somewhat lower than expected. This accounts for the discrepancy between measurement and simulation. Finally, the variation between positive and negative frequency offsets is ± 0.5dB across the entire range of measured frequency offsets.

The measured RF-to-IF gain for $\Delta f > 0$ and different values of f_{LO} is also shown in Fig. 4.3(b), with a similar variation range of ± 0.5dB. Similar results have been measured for $\Delta f < 0$. According to the analysis in section 2.2.2, such a symmetry of the measured RF-to-IF gain for positive and negative frequency offsets, as well as the tunability for different values of LO frequency, indicate that the operation of the loop is primarily determined by the IF blocks and that the bandwidth of the RF part of the loop is not a limitation.

The RF-to-IF gain has also been measured for 10 chip samples. The results for $f_{\mathrm{LO}} = 2$GHz and $\Delta f > 0$ are shown in Fig. 4.4. The average RF-to-IF gain is 30.8dB and the average maximum stop-band rejection is 48.2dB (Fig. 4.4(a)). The standard deviation of gain versus frequency offset is shown in Fig. 4.4(b), with a maximum in-band deviation of around 0.6dB at $\Delta f = 2.5$MHz, and a maximum stop-band rejection deviation of less than 1.6dB at $\Delta f = 300$MHz. The corresponding standard deviation of channel bandwidth for $\Delta f > 0$ is shown in Fig.4.4(c), with a mean channel bandwidth of 2.4MHz on either side of the LO. Similar results, with similar statistics, have been measured across the entire range of measurement ($-500\mathrm{MHz} \leq \Delta f \leq +500\mathrm{MHz}$ for $1\mathrm{GHz} \leq f_{\mathrm{LO}} \leq 2.5\mathrm{GHz}$).

Fig. 4.5 shows a measured DSB NF in the range of $7.25 - 8.9$dB for $f_{\mathrm{LO}} = 1 - 2.5$GHz, measured at a single differential output (I or Q) at a frequency offset of 2MHz (1/f noise corner frequency = 500kHz). As shown by the simulation results in Table 4.1, the relatively high NF of the receiver is not due to a fundamental

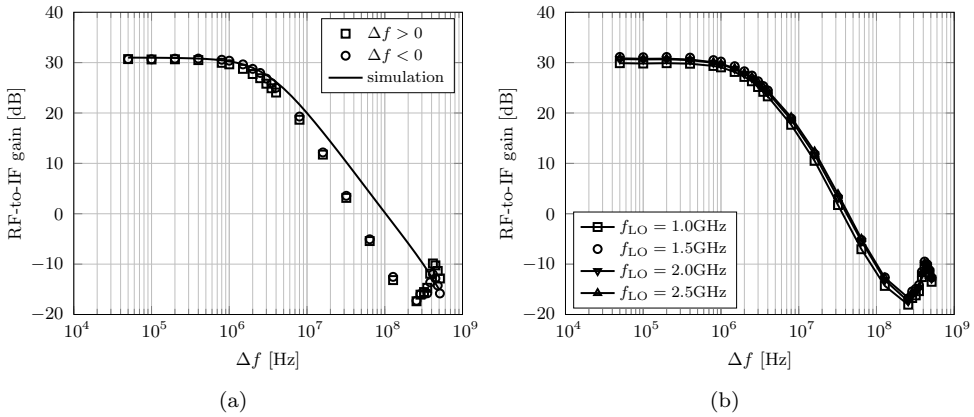

Figure 4.3: Measured RF-to-IF gain. (a) For positive and negative frequency offsets and $f_{\mathrm{LO}} = 2$GHz. Solid line indicates circuit simulation. Similar results have been measured (and simulated) for $f_{\mathrm{LO}} = 1, 1.5$ and 2.5GHz. (b) For $\Delta f > 0$ and different values of f_{LO}. Similar results have been measured for $\Delta f < 0$.

limitation of the active feedback architecture. Rather, there are two main reasons for this: (1) topology of amplifiers, and (2) input matching of the receiver.

The inverters used as amplifiers are self-biased at roughly half the supply voltage to maximize headroom and provide the same common mode level for cascading stages. Thus, they can only operate in strong inversion and a noise speed trade-off is not possible. Therefore, in this design, all inverters contribute roughly equally to the noise in the system and a lower NF is not possible without excessive power consumption. Alternatively, a self-biased inverter structure like the one presented in [55] can be used to provide the possibility of weak/moderate inversion operation, while retaining the benefits of a simple self-biased inverter. In addition, the "improved inverter" provides roughly twice the voltage gain and reduces flicker noise due to the presence of degeneration devices for self-bias. Indeed, circuit simulations that we have been carrying out lately in a standard 65nm CMOS process show that such an improved inverter is capable of achieving the same NF as that of a simple self-biased inverter, and lower than half its $1/f$ corner frequency, for less than one-fourth the current consumption, while still providing a gigahertz range of operation.

In addition, the simple 50Ω termination at the input of the receiver has a significant impact on NF. Alternative techniques such as inductive degeneration are widely used to achieve low noise 50Ω matching [37–39]. However, when aiming for a wide tuning range and a compact design, the use of such techniques is undesirable due to their inherent narrowband nature and the large die area required for on-chip inductors. As such, wideband matching techniques like resistive shunt feedback [13, 14] or noise

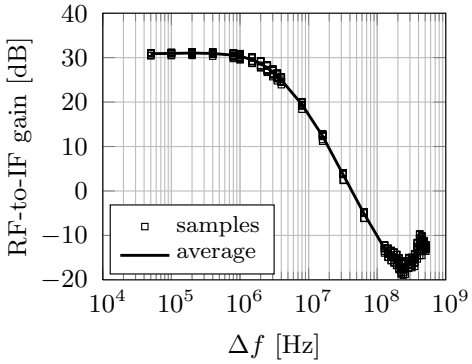

(a)

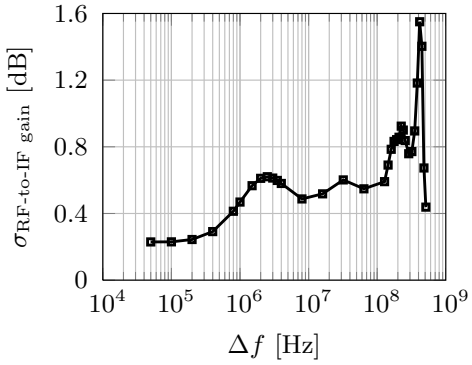

(b)

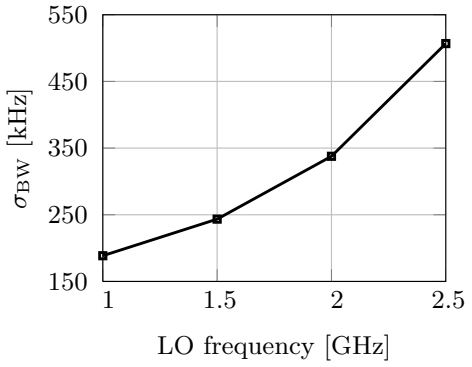

(c)

Figure 4.4: Measured RF-to-IF gain for 10 chip samples for $f_{\text{LO}} = 2\text{GHz}$ and $\Delta f > 0$. Similar results, with similar statistics, have been measured across the entire range of measurement ($-500\text{MHz} \leq \Delta f \leq +500\text{MHz}$ for $1\text{GHz} \leq f_{\text{LO}} \leq 2.5\text{GHz}$). (a) RF-to-IF gain. Solid line indicates the average. (b) Standard deviation of RF-to-IF gain. (c) Corresponding standard deviation of channel bandwidth around a mean value of 2.4MHz for $\Delta f > 0$.

canceling [40, 41] present a better alternative. In particular, it is estimated from circuit simulations that employing resistive shunt-feedback improves the NF by about 1.5 to 2dB for the same power consumption. Note, however, that in order to preserve the down-conversion operation of current commutating mixers, a two stage LNA would be required, in which the first stage provides a 50Ω match via resistive shunt-feedback, while the second stage provides a high impedance output (such an LNA can still be implemented with self-biased inverters). Alternatively, a separate matching device in shunt feedback configuration can be connected in parallel with the signal path. Another approach that preserves the current output of the LNA is a separate frequency translation loop for a shunt feedback matching [45] at the expense of 6dB degradation for out-of-channel IIP3.

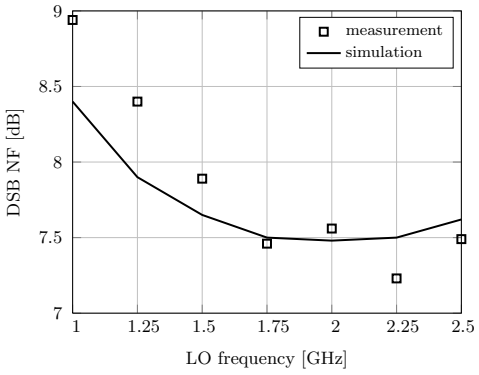

Figure 4.5: Measured DSB noise figure at $\Delta f = 2$MHz. Solid line indicates circuit simulation.

The linearity of the active feedback receiver is examined with two-tone measurements. Since we are only interested in intermodulation products that fall inside the channel bandwidth, measurement is carried out with the two tones located at frequency offsets of Δf and $2\Delta f - 25$kHz, such that the lower intermodulation product always falls in-channel at 25kHz. The measurement results shown in Fig. 4.6 show a wide-band IIP3 $> +12$dBm for interferers at > 60MHz offset. The difference between in-channel IIP3 (about -20dBm) and wideband IIP3 indicates an improvement of > 33dB thanks mainly to the feedback loop, with 7-to-9dB of that improvement due to partial IM3 cancellation as indicated from simulations. The discrepancy between measurement and simulation corresponds to that in Fig. 4.3(a) and is similarly due to higher than expected filtering in the forward path of the receiver.

In addition, IIP3 measurements for 10 chip samples are shown in Fig. 4.7 for $f_{\mathrm{LO}} = 2$GHz and $\Delta f > 0$, with the solid line indicating the average IIP3 (Fig.4.7(a)) and a maximum standard deviation of 1.6dB (Fig.4.7(b)). Similar results with similar statistics have been measured for negative frequency offsets and all values of LO.

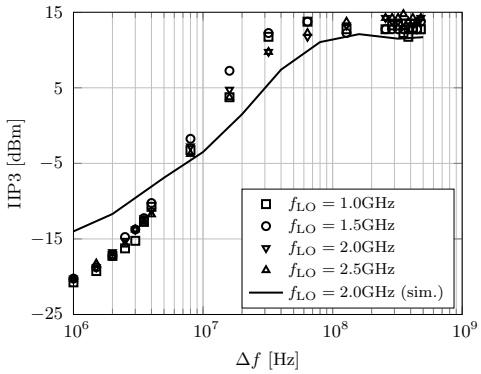

Figure 4.6: Measured IIP3 for $\Delta f > 0$. The two test tones are located at $f_{\mathrm{LO}} + \Delta f$ and $f_{\mathrm{LO}} + 2\Delta f - 25\mathrm{kHz}$. Solid line indicates circuit simulation for $f_{\mathrm{LO}} = 2\mathrm{GHz}$ and $\Delta f > 0$. Similar results have been measured (and simulated) for $\Delta f < 0$.

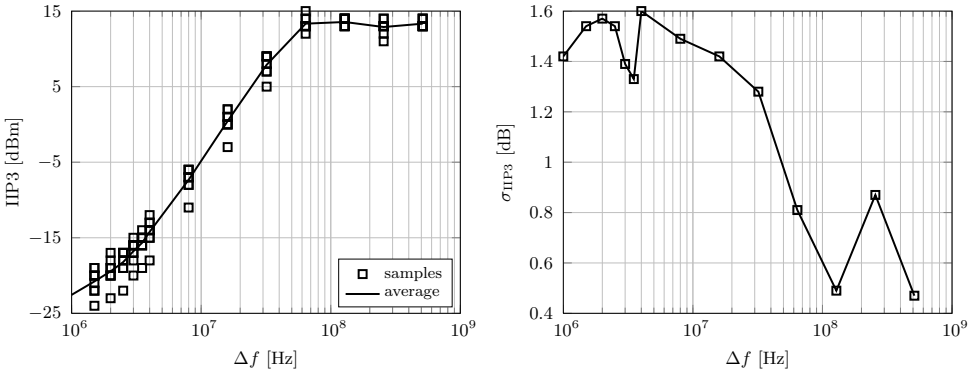

(a) (b)

Figure 4.7: Measured IIP3 for 10 chip samples for $f_{\mathrm{LO}} = 2\mathrm{GHz}$ and $\Delta f > 0$. The two test tones are located at $f_{\mathrm{LO}} + \Delta f$ and $f_{\mathrm{LO}} + 2\Delta f - 25\mathrm{kHz}$. Similar results, with similar statistics, have been measured across the entire range of measurement ($-500\mathrm{MHz} \leq \Delta f \leq +500\mathrm{MHz}$ for $1\mathrm{GHz} \leq f_{\mathrm{LO}} \leq 2.5\mathrm{GHz}$). (a) IIP3. Solid line indicates the average. (b) Corresponding standard deviation.

Fig. 4.8 shows the blocking performance of the receiver. Measured P-1dB exhibits a maximum of −3dBm for a blocker at 120MHz (> 19dB improvement). Similarly, P-1dB measurements for 10 chip samples are also shown in Fig. 4.9 for $f_{\mathrm{LO}} = 2\mathrm{GHz}$ and $\Delta f > 0$.

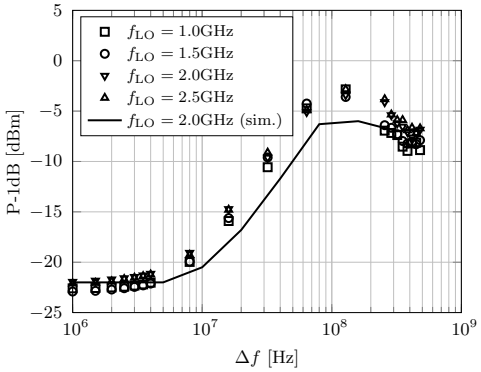

Figure 4.8: Measured blocking performance. The desired signal and the blocker are located at $f_{\mathrm{LO}} + 50\mathrm{kHz}$ and $f_{\mathrm{LO}} + \Delta f$, respectively. Solid line indicates circuit simulation for $f_{\mathrm{LO}} = 2\mathrm{GHz}$ and $\Delta f > 0$. Similar results have been measured (and simulated) for $\Delta f < 0$.

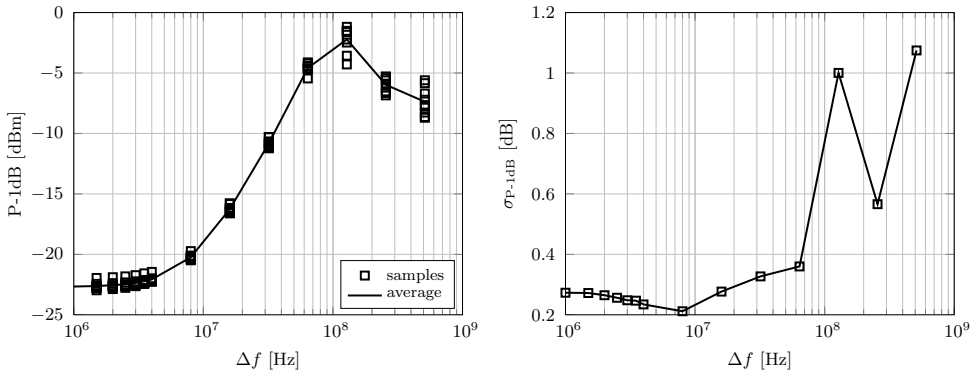

(a) (b)

Figure 4.9: Measured P-1dB for 10 chip samples for $f_{\mathrm{LO}} = 2\mathrm{GHz}$ and $\Delta f > 0$. The desired signal and the blocker are located at $f_{\mathrm{LO}} + 50\mathrm{kHz}$ and $f_{\mathrm{LO}} + \Delta f$, respectively. Similar results, with similar statistics, have been measured across the entire range of measurement ($-500\mathrm{MHz} \leq \Delta f \leq +500\mathrm{MHz}$ for $1\mathrm{GHz} \leq f_{\mathrm{LO}} \leq 2.5\mathrm{GHz}$). (a) P-1dB. Solid line indicates the average. (b) Corresponding standard deviation.

Excluding the clock divider and measurement buffers, the circuit core consumes 62mW from a 1.2V supply.

Tables 4.2 and 4.3 give a summary of measured parameters and compares performance to other state-of-the-art receivers. The presented design occupies about 80 to 97% less die area, while achieving comparable or better performance. The bandwidth of 5MHz is suitable for most applications in the 1 to 2.5GHz range and increasing it would further reduce the die size. Compared to the highest stop-band rejection ($\approx$ 50dB) reported by the superheterodyne architecture in [31], the direct conversion receiver presented in this work achieves a comparable rejection of (48dB) at about 5 times the frequency offset while occupying $< 8\%$ of the die area. Better or comparable wideband IIP3 of $> +12$dBm is measured at 2.5 to 13 times lower frequency offset (60MHz) compared to most reported values [24, 46]. Moreover, this design significantly outperforms previously reported feedback-based receivers [43, 46] in terms of gain, frequency range, stop-band rejection and wideband IIP3 while maintaining a competitive performance for other receiver parameters.

	This work	**[46]**	**[43]**	**[45]**	
Technology	65nm	0.18µm	65nm	45nm	CMOS
Active Area	< 0.06	< 1.8	1.2	< 0.2	mm^2
RF frequency	1–2.5	1.9	1.9	1.9 & 1.75	GHz
Gain	30	22.7	22.5	37	dB
Channel BW	5	–	–	16	MHz
DSB NF	7.25–8.9	4.1	< 8	2.5	dB
Stop-band rejection	48 Δf=250MHz	27 Δf=180MHz	10.5 Δf=5MHz	–	dB
Wideband IIP3	$> +12$ Δf=60MHz	+7.5	–	+1 Δf=190MHz	dBm
Wideband IIP2	> 49 Δf>30MHz	$\Delta f \approx 150$MHz	–	> 60 Δf=190MHz	dBm
Wideband P-1dB	-3 Δf=120MHz	+1 $\Delta f \approx$150MHz	< -15 Δf=20MHz	–	dBm
Power consumption	62	< 63	375	9.5	mW
Supply voltage	1.2	1.8	2.5	1.3	V

Table 4.2: Summary of measurement results and comparison to other feedback-based receivers.

	This work	[31]	[24]	[22]	[46]	
Technique	active feedback	super-heterodyne	harmonic rejection	mixer-first	feedforward	
Technology	65nm	65nm	65nm	65nm	65nm	CMOS
Active Area	< 0.06	0.76	< 1	2	0.28	mm^2
RF frequency	1–2.5	1.8–2	< 1	0.1–2.4	1.9	GHz
Gain	30	55	34.4	40–70	20.9	dB
Channel BW	5	–	12	20	4.5	MHz
DSB NF	7.25–8.9	2.8	4	< 5	6.8	dB
Stop-band rejection	48 Δf=250MHz	$\approx$50 Δf=40MHz	–	–	> 21 $\Delta f\approx$50MHz	dB
Wideband IIP3	$> +12$ Δf=60MHz	–	$+18$ Δf=800MHz	-8 to $+27$ Δf=20MHz	–	dBm
Wideband IIP2	> 49 Δf>30MHz	–	51 $\Delta f\approx$1.2GHz	56 –	–	dBm
Wideband P-1dB	-3 Δf=120MHz	–	-5 Δf=465MHz	-26 to $+5$ Δf=40MHz	> 0 Δf=80MHz	dBm
Power consumption	62	–	39.6	< 70	72	mW
Supply voltage	1.2	–	1.2	1.2/2.5	1.2/2.5	V

Table 4.3: Summary of measurement results and comparison to other state-of-the-art receivers.

4.4 Conclusions

In this chapter, a prototype of a direct conversion receiver employing an active feedback loop has been designed and implemented in a 65nm standard CMOS process. The design occupies 80 to 97% less die area compared to other state-of-the-art receivers and is tunable over a range of 1 to 2.5GHz. The receiver achieves a measured maximum stop-band rejection of 48dB and a measured wideband IIP3 $> +12$dBm, while maintaining a competitive performance for other receiver parameters.

Chapter 5

Conclusions and Future Work

This final chapter gives a summary of the work described in Chapters 1 to 4, as well as a discussion for possible future work on integrated RF filtering. Section 5.1 presents the summary and conclusions of this thesis and section 5.2 suggests future work.

5.1 Summary and Conclusions

Chapter 1 started with highlighting the demand for higher data rates and the associated multitude of available wireless standards that enable mobile access. For a wireless receiver front-ends, the increasingly crowded radio spectrum brings to the forefront co-existence problems such as distortion, harmonic mixing and reciprocal mixing. This is especially the case in a multi-mode receiver where many radios exist either on the same die or in the same package. As a result, one finds a variety of approaches reported in literature in recent years to mitigate many of these problems. These range from re-discovered concepts such as N-path filters and negative feedback employed for RF design, to novel receiver architectures like interference cancellation, mixer first receivers, and harmonic rejection receivers.

In particular, this work is concerned with improving the dynamic range of wideband receiver by improving its linearity. Towards this end, the discussion in Chapter 1 outlines three main architectural alternatives: (1) A receiver possesses a bandwidth high enough to cover all possible frequency bands, (2) A receiver in fact comprises several receivers in parallel connected to one or more antennas, and each receiver would then be dedicated, and in turn optimized, for one or more of the frequency bands of interest, and (3) a single programmable receiver chain would be tunable in such a way as to cover the necessary range of frequencies.

With the high power consumption and/or large die area associated with the first two alternatives, the third approach is found to be the most attractive, especially

when considering the advances in CMOS technology scaling. The programmability of such a receiver essentially corresponds to a high-Q RF channel select filter at the antenna with a tunable center frequency. Such narrow-band flexibility, if feasible, would be an ultimate solution for distortion caused by interferers.

Traditionally, high-Q filtering has been implemented by using off-chip components such as SAW filters [14]. In addition to being bulky and expensive, SAW filters are only suitable for selecting a fixed range of frequencies due to their lack of tunability. Therefore, they can only be used for selecting a complete application band at RF and/or IF channel selection where the desired channel is always down-converted to the same frequency.

In chapter 2, active feedback for RF channel selection has been presented as a means to improve the distortion performance of a wireless receiver front-end. This is achieved by providing channel selectivity as early as possible in the receiver chain, namely at RF, by employing a frequency translation loop with a high loop gain to convert an IF HPF to an RF channel-select filter. The fact that the characteristics of the loop are mainly determined by the IF part has a two-fold benefit: (1) Compared to an "all RF" loop, it is relatively easier to achieve a higher loop gain at IF, and consequently provide a higher stop-band rejection of the RF filter, and (2) In a modern high speed CMOS process, the RF filter characteristics are primarily determined by the IF part of the loop and, thus, the filter maintains tunability through changing the clock frequency.

Through a simple and intuitive analysis, the basic operation and benefits of such technique are examined. The large value of on-chip capacitance typically needed in passive mixer filters is reduced in the active feedback receiver by a factor proportional to the available loop gain, which results in a highly compact design.

In addition, due to the active nature of the feedback path, the maximum rejection achievable in the stop-band of the filter is not limited by the switch resistance of the mixers. This allows for using significantly smaller switches and consequently translates to lower power consumption in the LO buffers.

Furthermore, the feedback loop offers the possibility of utilizing a voltage mirror for canceling the IM3 distortion products caused by out-of-channel interferers in the LNA. However, the case of the HPF placed after the feedback amplifier, although seems to provide some degree of distortion canceling, is not yet fully understood and requires further investigation to account for the observed results of the different tests carried out.

In chapter 3, an iterative procedure for analyzing frequency translation loops employing passive mixers has been presented. In literature, thorough analysis has been provided for open loop passive mixer circuits. However, despite their use in several contexts such as feedforward interference cancellation or low noise 50Ω matching, no similarly detailed analysis is available for frequency translation loops with passive

mixers. The difficulty of analyzing these loops essentially arises from the presence of harmonic components inside the loop, as well as the lack of isolation between the input and output of a passive mixer.

The detailed analysis developed in this Chapter relies on solving the frequency domain equations of the system in an iterative manner to obtain an accurate closed form solution. The analysis is based on the negative feedback receiver architecture proposed in Chapter 2, but holds equally well for: (1) a separate feedback loop that is independent of the receiver's down-conversion path, (2) an LNA inside the loop, and (3) positive feedback operation. Furthermore, the analysis is valid for a general N-path single or double balanced architecture.

The solution obtained for the RF/IF filtering provided by the loop is shown to fit full circuit simulations within 0.5 to 1.5 dB over the span of several LO harmonics. Consequently, the analysis accurately predicts main performance parameters of the system such as stop-band rejection, in-band loss and loop stability, and can thus be used for both system design and optimization. In contrast, the idealized analysis in Chapter 2, although much simpler and can serve as a preliminary design guide, is shown to be quite inadequate in predicting such performance parameters.

Based on the results of analysis, two significantly important conclusions are made: (1) for RF filtering, results reveal an optimum loop bandwidth where stop-band rejection is maximum, and beyond which a trade-off exists between interferer suppression and the stop-bandwidth of the filter, which directly translates to a an optimized design in terms of power consumption, and (2) for stability, analysis results show that the loop can indeed be made stable by conventional feedback compensation despite the presence of LO harmonics in the loop. Furthermore, the derived loop gain expression shows that the contribution of the mixers to the loop gain is significantly higher than expected. This is because the complete energy of the LO signal is involved in the down/up-conversion process and not just the first LO harmonic, which advantageously translates to higher stop-band rejection.

In chapter 4, a prototype of a direct conversion receiver employing an active feedback loop has been designed and implemented in a 65nm standard CMOS process. The entire chip is based on self-biased inverters and switches, which, in addition to its simplicity, offers a high Gain-Bandwidth product due to current re-use in inverters, eliminates the need for bias circuitry, lowers second-order distortion and provides a design that lends itself to easy porting from one technology to another. For sake of simplicity to demonstrate the feedback loop, our chip prototype uses a simple 50Ω termination to provide input matching at the expense of 3dB degradation in NF.

The presented design occupies about 80 to 97% less die area ($< 0.06\text{mm}^2$) compared to other state-of-the-art receivers with a total capacitance of only 60pF (15pF$\times$4 for differential I/Q operation) to achieve a 5MHz channel bandwidth suitable for most applications in the 1 to 2.5GHz range, and increasing it would further reduce the die

size. Compared to the highest stop-band rejection ($\approx$ 50dB) reported by the super-heterodyne architecture, the direct conversion receiver presented in this work achieves a comparable rejection of (48dB) at about 5 times the frequency offset while occupying $< 8\%$ of the die area. The average measured NF over the operational LO range is about 8dB, which is relatively high due to matching with a simple 50Ω termination to ground at the input of the receiver, as well as the lack of noise-speed trade-off in the simple self-biased inverters used. Better or comparable wideband IIP3 of $> +12$dBm is measured at 2.5 to 13 times lower frequency offset (60MHz) compared to other state-of-the-art receivers. Moreover, this design significantly outperforms previously reported feedback-based receivers in terms of gain, frequency range, stop-band rejection and wideband IIP3 while maintaining a competitive performance for other receiver parameters. Finally, the performance reliability of the design is demonstrated by multiple samples measurements.

5.2 Future Work

The work carried out in this thesis can continued and extended in three main directions: (1) Determining the origin of partial IM3 distortion canceling when the HPF is present between the LNA and feedback transconductors, (2) improving the current implementation, and (3) providing high order RF filtering.

The simulated and measured observations discussed in Chapters 2 and 4, together with the simulation test cases in Appendix B provide a reliable documentation for further investigation of partial IM3 cancellation.

In terms of improving the current implementation, noise performance is one obvious issue. On one hand, given the value of supply voltage used, inverter amplifiers biased at roughly mid-rail (to maximize headroom and provide the same common mode level for cascading stages) can only operate in strong inversion. Thus, a trade-off between noise and speed is not exploited in this design. A conventional op-amp design for the forward path of the receiver is one option to provide the possibility of weak/moderate inversion operation to enable a noise-speed trade-off. Alternatively, improved self-biased inverter structures like the one proposed in [55] can enable a similar trade-off, while retaining the benefits of a simple self-biased inverter, as well as providing twice the voltage gain and lower flicker noise due to source degeneration.

In addition, providing low noise 50Ω matching at the input of the receiver is crucial. Instead of a simple resistive termination as currently implemented in the receiver, a significant improvement in NF can be achieved by employing resistive shunt-feedback to provide compact low noise wide-band matching. However, to preserve the down-conversion operation of current commutating mixers, a two stage LNA would be required, in which the first stage provides a 50Ω match via resistive shunt-feedback,

while the second stage provides a high impedance output (such an LNA can still be implemented with self-biased inverters). Another alternative is to replace the 50Ω resistor at the input of the receiver with a separate matching self-biased inverter connected in shunt with the signal path. This matching device would not contribute to the signal's path, but, similar to a matching device in the signal's path, its noise contribution can still be reduced by increasing its current consumption.

In terms of extending the viability of the system, the need for higher order RF filtering is definitely most needed, especially when it is intended for channel selection. This has been partially investigated during the course of this work and we find it interesting to give a brief overview of the results obtained thus far.

The functionality of the HPF $H_{\mathrm{HPF}}(s)$ can be implemented as $1 - H_{\mathrm{LPF}}(s)$ (Fig. 5.1), where $H_{\mathrm{LPF}}(s)$ is an LPF. As such, the frequency translation loop in the receiver now comprises two paths: a high bandwidth negative feedback path that (ideally) suppresses all signals at the feedback point (shown in Fig. 5.1 at the output of the LNA, but can be placed at the antenna as well), and a positive feedback path that regenerates the desired signal and, as such, is only required to have a bandwidth in the same order of the desired channel BW. The order of the resulting RF channel select filter of the receiver is now determined by the order of the IF LPF.

Assuming a second order LPF, $H_{\mathrm{HPF}}(s)$ can be expressed as

$$\begin{aligned} H_{\mathrm{HPF}}(s) &= 1 - H_{\mathrm{LPF}}(s) \\ &= 1 - \frac{\omega_o^2}{s^2 + \frac{\omega_o}{Q}s + \omega_o^2} \\ &= \frac{s^2 + 2\zeta\omega_o s}{s^2 + \frac{\omega_o}{Q}s + \omega_o^2} \end{aligned} \tag{5.1}$$

where $H_{\mathrm{LPF}}(s)$ has been expressed in a standard form in terms of its natural frequency ω_o and quality factor Q. Consequently, the closed loop transfer function representing the RF filter $H_{\mathrm{RF}}(s)$ at the output of LNA can then be found

$$H_{\mathrm{RF}}(s) = \frac{1}{1 + T_o\big(1 - H_{\mathrm{LPF}}(s)\big)} \tag{5.2}$$

where T_o is the DC loop gain. Note that for our purposes here, the bandwidth of the negative feedback path of the loop is considered to be infinite, i.e. all frequency dependence in the system results from $H_{\mathrm{LPF}}(s)$. Thus, only the stability at low frequency offsets (low cross-over point due to the HPF) is examined. Since at high frequency offsets, the output of the LPF is highly attenuated, the positive feedback path does not contribute to the loop gain and stability is determined solely by the negative feedback path in a manner similar to that discussed in Chapter 3.

The filtering effect in (5.2) can first be examined by inspection. For instance, assuming $T_o = 10$ and $H_{\mathrm{LPF}}(s) \approx 0.7$ (i.e. at the 3-dB frequency of the LPF),

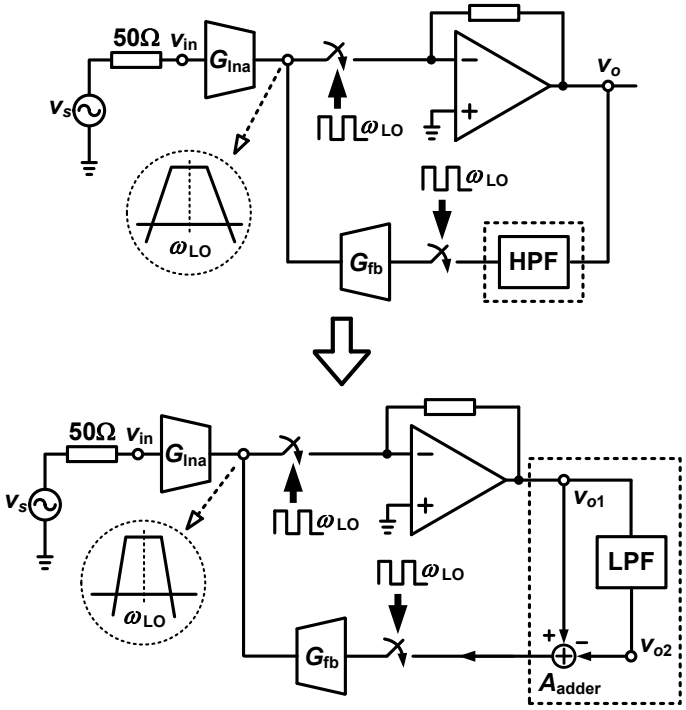

Figure 5.1: Proposed high order RF filtering architecture. The passive HPF is implemented as a $1 - \text{LPF}$ function, where LPF is a second order Low Pass Filter.

we find that $H_{\text{RF}}(s)$ has already dropped by more than 12dB. That is, because of the subtraction operation involved in synthesizing $H_{\text{HPF}}(s)$, the roll-off of the RF channel select filter created by the feedback loop will be mainly determined by the characteristics of the LPF below its 3-dB frequency. This suggests that the LPF is required to be a high Q filter. Since the positive feedback part is narrowband as previously discussed, the LPF can be a highly linear opamp-based active filter.

The most interesting observation, however, stems from examining the effect of the quality factor of the LPF on the RF filter characteristics. Figure 5.2a shows MATLAB simulations of (5.2) for different values of Q. It can be seen that, although $H_{\text{LPF}}(s)$ is a second order filter, the roll-off of $H_{\text{RF}}(s)$ can be made increasingly steeper than 40dB/dec by increasing Q. However, the peaking in the closed loop transfer function for excessively high Q values indicates reduced stability. This is indeed the case as shown from the corresponding loop gain plot in Fig. 5.2b and the marked phase at low frequency gain cross-over points in Fig. 5.2c indicating phase margin. Thus, stability requirements set an upper limit on the achievable RF filter roll-off. The results in Fig. 5.2a show that for a second order LPF of $Q = 4$, an RF filter roll-off higher

than 65dB/dec can be obtained at a phase margin better than 45° and less than 2dB peaking.

The actual limiting factor in the system, however, stems from the fixed DR of the feedback path. This is because the noise of the LPF is referred to 50Ω multiplied by a factor of $A_{\text{adder}}G_{\text{fb}}/G_{\text{lna}}$, while the gain for out-of-channel interferers from the input of G_{lna} to the negative feedback input of the adder as dictated by the feedback action is equal to $G_{\text{lna}}/(G_{\text{fb}}A_{\text{adder}})$, the reciprocal of the noise factor. As such, the problem boils down to a tight trade-off between noise and linearity. To examine this point, we consider the case of distortion canceling, i.e. $G_{\text{fb}} = G_{\text{lna}}$. Under this condition, the noise and linearity of the system for a given loop gain would essentially be determined by the gain of the adder. For $A_{\text{adder}} >> 1$, the system would exhibit high linearity because the distortion in the adder is low since interferers appear at its input reduced in amplitude by a factor equal to A_{adder}, while, on the other hand, the noise contribution of the LPF appears at the antenna multiplied by the same factor A_{adder} and excessive power consumption in the LPF would be required to obtain a reasonable NF. Conversely, for $A_{\text{adder}} << 1$, the noise contribution of the LPF would be minimized but the linearity of the system would be determined by that of the adder. Note that, although the adder operates at IF, it is part of the negative feedback path and employing negative feedback to improve its linearity would severely degrade the loop bandwidth, and, consequently, the stop-bandwidth of the channel select RF filter.

To overcome such limitation, two proposals require further investigation:

1. From a circuit level perspective, the noise problem stems from removing the physical HPF capacitor in the feedback path and implementing it as $1 - \text{LPF}$. Knowing the target function, implementations that contain a series capacitor can be sought.

2. From a system level perspective, the noise up-converted to the received channel band can be avoided by employing the frequency translation loop to handle self-blockers in a FDD system. As such, the up-conversion mixers would be operated with the LO of the transmitter and noise would be up-converted to the transmission band instead.

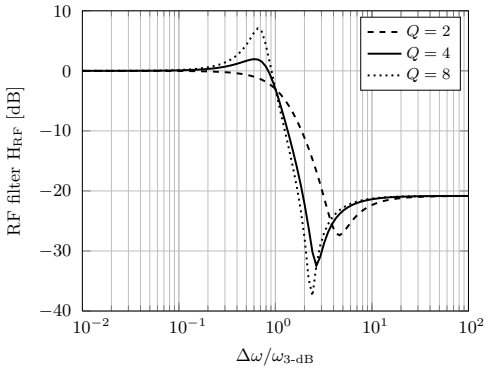

(a) RF filter

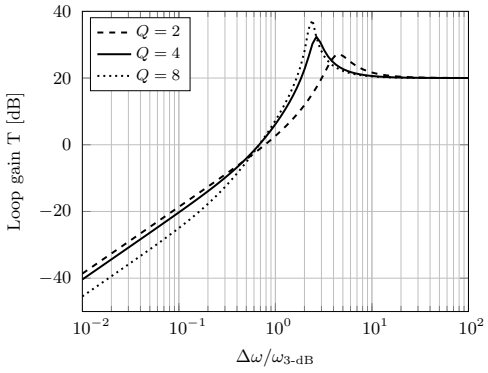

(b) Loop gain

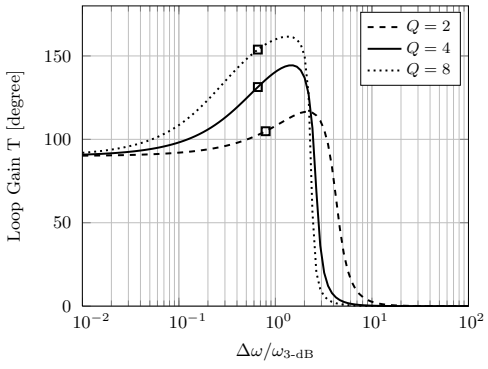

(c) Loop gain

Figure 5.2: MATLAB simulation results of high order filtering for a loop gain $T_o = 20$dB. (a) High order RF filter transfer function as given by (5.2) for different values of LPF Q. (b) Loop gain magnitude. (c) Loop gain phase and corresponding low frequency gain cross-over points marked for indicating phase margin.

Appendix A

Non-linear System Response

In this section, a general procedure for deriving the response of a non-linear amplifier with feedback is given and applied for the active feedback receiver.

The procedure is outlined in Fig. A.1 and is as follows:

(a) Given a small signal excitation v_s, the first order (linear) response of the system is first obtained. The first order response is the set of all node voltages (or, equivalently, branch currents).

(b) The excitation source is then de-activated and the first order voltages are used as inputs to find the second order response of the system.

(c) In a similar manner, the third order response can be obtained by considering the sum of first and second order voltages as inputs to a third order system.

(d) The procedure is repeated for higher order responses.

Strictly speaking, the above procedure is an approximation because it ignores further interactions between the resulting distortion components. For instance, the third order distortion products obtained in step 3 mix with first and second order voltages via the second order term a_2. However, such secondary effects render the procedure quite cumbersome for hand calculations while providing no insight and marginal accuracy benefits.

The aforementioned procedure can now be applied to the active feedback system shown in Fig. 2.7 where only third order non-linearities are considered. The aim is to find the IM3 response of the system in response to two-tone excitation.

By first examining the transfer function of the system derived in section 2.2.1, the first order node voltages of the forward path can be written as

$$v_{o1} = -G_{\text{lna}} Z_{\text{CL1}} A_{\text{mix}} A_{v1} v_{\text{in1}} \tag{A.1}$$

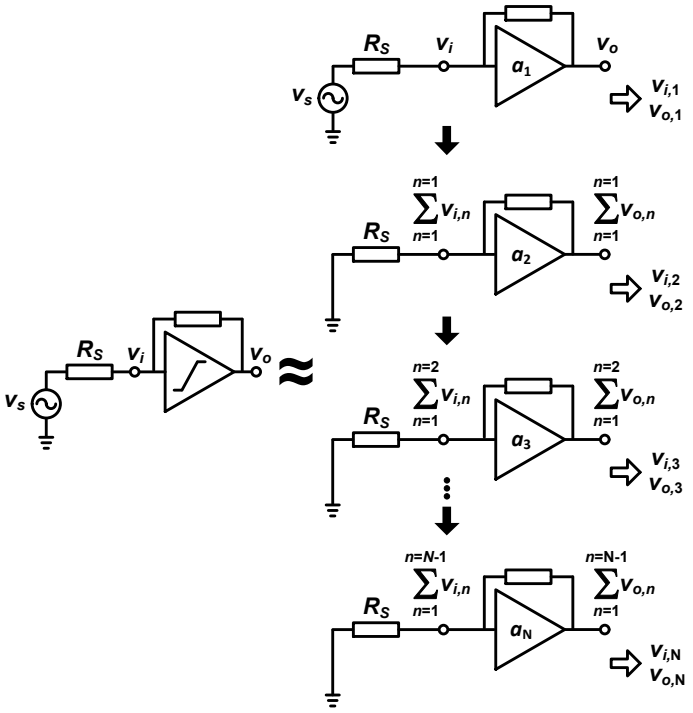

Figure A.1: Non-linear analysis procedure.

$$v_{e,\mathrm{if1}} = G_{\mathrm{lna}} Z_{\mathrm{OL1}} A_{\mathrm{mix}} v_{\mathrm{in1}} + G_{\mathrm{fb}} Z_{\mathrm{OL1}} A_{\mathrm{mix}}^2 H_{\mathrm{hpf1}} v_{o1} \tag{A.2}$$

$$v_{e,\mathrm{rf1}} = (A_{\mathrm{mix}} + \frac{R_{\mathrm{SW}}}{A_{\mathrm{mix}} Z_{\mathrm{if1}}}) v_{e,\mathrm{if1}} \tag{A.3}$$

where the shorthand subscript notation is used to indicate the frequency of interest, i.e. $X_1 = X(\Delta\omega_1)$ for IF quantities and $X_1 = X(\omega_{\mathrm{LO}} + \Delta\omega_1)$ for RF quantities, where X is any circuit quantity with frequency dependence.

In addition, approximating the HPF as a reciprocal block, the first order node voltages of the feedback path can be found

$$v_{x,\mathrm{if1}} = A_{\mathrm{mix}} H_{\mathrm{hpf1}} v_{e,\mathrm{rf1}} \tag{A.4}$$

$$v_{x,\mathrm{rf1}} = A_{\mathrm{mix}} H_{\mathrm{hpf1}} v_{o1} \tag{A.5}$$

Having determined the first order response, we can now proceed with finding the desired third order response.

A.1 IM3 Distortion due to the Forward Path

In the forward path, the following non-linear contributions are considered:

(a) Third order LNA non-linearity due to input excitation ($g_{m3,\mathrm{lna}}$ [I/V^3]).

(b) Third order LNA non-linearity due to output excitation ($g_{o3,\mathrm{lna}}$ [I/V^3]).

(c) Third order opamp non-linearity due to input excitation ($\alpha_{i3,\mathrm{A}}$ [V/V^3]).

(d) Third order opamp non-linearity due to output excitation ($\alpha_{o3,\mathrm{A}}$) [V/V^3].

Based on an input two-tone excitation of amplitude A and the first order voltages in (A.1)-(A.3), the IM3 output voltage for each of the non-linear coefficients listed above can be written as

$$v_{o3a} = -\frac{3}{4} g_{m3,\mathrm{lna}} Z_{\mathrm{OL3}} A_{\mathrm{mix}} A_{v3} A^3 - T_3 v_{o3a} \tag{A.6}$$

$$v_{o3b} = -\frac{3}{4} g_{o3,\mathrm{lna}} Z_{\mathrm{OL3}} A_{\mathrm{mix}} A_{v3} v_{e,\mathrm{rf1}}^3 - T_3 v_{o3b} \tag{A.7}$$

$$v_{o3c} = -\frac{3}{4} \alpha_{i3,\mathrm{A}} v_{e,\mathrm{if1}}^3 - T_3 v_{o3c} \tag{A.8}$$

$$v_{o3d} = -\frac{3}{4} \alpha_{o3,\mathrm{A}} v_{o1}^3 - T_3 v_{o3d} \tag{A.9}$$

where again the shorthand subscript notation is used for the IM3 response i.e. $X_3 = X(\Delta\omega_{\mathrm{IM3}})$ for IF quantities and $X_3 = X(\omega_{\mathrm{LO}} + \Delta\omega_{\mathrm{IM3}})$ for RF quantities, where X is any circuit quantity with frequency dependence and $\Delta\omega_{\mathrm{IM3}}$ is the frequency offset of the IM3 product.

The first term on the right-hand side of (A.6)-(A.9) represents the third order intermodulation distortion product generated by the LNA, while the second term in each of the equations represents the linear feedback of the IM3 product through the active feedback loop. Substituting with (A.1)-(A.3) in (A.6)-(A.9) and collecting terms yields the required IM3 distortion products

$$v_{o3a} = -\frac{3}{4} g_{m3,\mathrm{lna}} Z_{\mathrm{CL3}} A_{\mathrm{mix}} A_{v3} A^3 \tag{A.10}$$

$$v_{o3b} = -\frac{3}{4} g_{o3,\mathrm{lna}} Z_{\mathrm{CL3}} A_{\mathrm{mix}} A_{v3} (G_{\mathrm{lna}} \frac{Z_{o1} \parallel Z_{\mathrm{rf1}}}{1+T_1})^3 A^3 \tag{A.11}$$

$$v_{o3c} = -\frac{3}{4} \alpha_{i3,\mathrm{A}} \frac{1}{1+T_3} (G_{\mathrm{lna}} Z_{\mathrm{CL1}} A_{\mathrm{mix}})^3 A^3 \tag{A.12}$$

$$v_{o3d} = -\frac{3}{4} \alpha_{o3,\mathrm{A}} \frac{1}{1+T_3} (G_{\mathrm{lna}} Z_{\mathrm{CL1}} A_{\mathrm{mix}} A_{v1})^3 A^3 \tag{A.13}$$

A.2 Distortion due to the Feedback Path

In the feedback path, the following non-linear contributions are considered for each of the cases shown in Fig. 2.7:

(a) Case 1: Third order non-linearity of the IF feedback transconductance due to input excitation ($g_{m3,\mathrm{fb}}$ [I/V^3]).

(b) Case 1: Third order non-linearity of the IF feedback transconductance due to output excitation ($g_{o3,\mathrm{fb}}$ [I/V^3])

(c) Case 2: Third order non-linearity of the RF feedback transconductance due to input excitation ($g_{m3,\mathrm{fb}}$ [I/V^3]).

(d) Case 2: Third order non-linearity of the RF feedback transconductance due to output excitation ($g_{o3,\mathrm{fb}}$ [I/V^3]).

In a similar manner, the IM3 output voltage for each of the cases listed above can be written

$$v_{o3a} = -\frac{3}{4} g_{m3,\mathrm{fb}} Z_{\mathrm{OL3}} A_{\mathrm{mix}} A_{v3} H_{\mathrm{hpf3}} v_{o1}^3 - T_3 v_{o3a} \tag{A.14}$$

$$v_{o3b} = -\frac{3}{4} g_{o3,\mathrm{fb}} Z_{\mathrm{OL3}} A_{\mathrm{mix}} A_{v3} v_{x,\mathrm{if}}^3 - T_3 v_{o3b} \tag{A.15}$$

$$v_{o3c} = -\frac{3}{4} g_{m3,\mathrm{fb}} Z_{\mathrm{OL3}} A_{\mathrm{mix}} A_{v3} v_{x,\mathrm{rf}}^3 - T_3 v_{o3c} \tag{A.16}$$

$$v_{o3d} = -\frac{3}{4} g_{o3,\mathrm{fb}} Z_{\mathrm{OL3}} A_{\mathrm{mix}} A_{v3} v_{e,\mathrm{rf1}}^3 - T_3 v_{o3d} \tag{A.17}$$

Substituting with (A.1)-(A.5) in (A.14)-(A.17) and collecting terms yields the required IM3 distortion products

$$v_{o3a} = \frac{3}{4} g_{m3,\mathrm{fb}} Z_{\mathrm{CL3}} A_{\mathrm{mix}} A_{v3} H_{\mathrm{hpf3}} (G_{\mathrm{lna}} Z_{\mathrm{CL1}} A_{\mathrm{mix}} A_{v1})^3 A^3 \tag{A.18}$$

$$v_{o3b} = -\frac{3}{4} g_{o3,\mathrm{fb}} Z_{\mathrm{CL3}} A_{\mathrm{mix}} A_{v3} H_{\mathrm{hpf3}} (G_{\mathrm{lna}} \frac{Z_{o1} \parallel Z_{\mathrm{rf1}}}{1+T_1} A_{\mathrm{mix}} H_{\mathrm{hpf1}})^3 A^3 \tag{A.19}$$

$$v_{o3c} = \frac{3}{4} g_{m3,\mathrm{fb}} Z_{\mathrm{CL3}} A_{v3} A_{\mathrm{mix}}^4 H_{\mathrm{hpf1}}^3 (G_{\mathrm{lna}} Z_{\mathrm{CL1}} A_{\mathrm{mix}} A_{v1})^3 A^3 \tag{A.20}$$

$$v_{o3d} = -\frac{3}{4} g_{o3,\mathrm{fb}} Z_{\mathrm{CL3}} A_{\mathrm{mix}} A_{v3} (G_{\mathrm{lna}} \frac{Z_{o1} \parallel Z_{\mathrm{rf1}}}{1+T_1})^3 A^3 \tag{A.21}$$

Appendix B

Investigation of Distortion Canceling

This appendix gives an overview of the investigation carried out in an attempt to understand the source of extra improvement in IIP3 with the HPF present at the output of the feedback transconductor. Although a final conclusion regarding this improvement could not be reached, this overview aims to provide a reliable documentation of results for future investigation, as well as give an idea of the difficulty in tracing the problem.

A simplified block diagram of the feedback receiver and the test bench used is reproduced in Fig. B.1 for convenience. In addition, using the extracted small signal parameters of the inverter amplifiers (g_m, r_o, C_{gs}, C_{gd} and C_{db}), a linear model of the inverter amplifiers is constructed for test purposes. The simulated linear gain of the model fits that of the actual inverter within 0.5 dB in magnitude and 10° in phase, up to 10GHz.

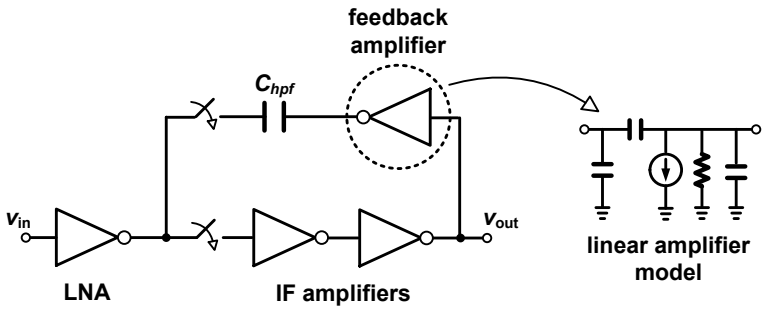

Figure B.1: simplified block diagram of the feedback receiver and the test bench used for investigating distortion canceling.

Since, in case of no distortion canceling, one expects the LNA to be the linearity bottleneck in the receiver, our reference IIP3 is that of the LNA with a shorted output. This is the best achievable IIP3 of the LNA since the swing at its output is zero. By starting with the case of all linear amplifiers, several test cases are simulated and a summary is given in Table B.1. The linearity change is ΔIIP3 is relative to our reference case. The results shows that the improvement in IIP3 beyond that of the reference case is happening due to the combination of the LNA and the feedback amplifier.

	LNA	**IF amplifier**	**Feedback amplifier**	ΔIIP_3 [dB]	
				65nm	28nm
1	linear model	linear model	linear model	+20	+17
2	actual amplifier	linear model	linear model	−1	−2
3	actual amplifier	actual amplifier	linear model	−1	−2
4	actual amplifier	actual amplifier	actual amplifier	+6	+4
5	actual amplifier	linear model	actual amplifier	+6	+4

Table B.1: Simulation results for testing the effect of different blocks on distortion canceling.

Next, further examination was carried out for case (5) in Table B.1 in 65nm technology. Third order non-linearity terms (g_{m3}, g_{o3}, g_{m2o1} and g_{m1o2}) were extracted for the inverters and progressively added to the linear model in a step-by-step fashion in order to examine which possible combinations might be resulting in the observed IIP3 improvement. A summary of the results is given in Table B.2. None of the likely combinations tested account for the observed improvement in IIP3.

	LNA	**Feedback amplifier**	ΔIIP_3 [dB]
1	linear model	linear model	+20
1	g_{m3}	g_{m3}	0
2	g_{m3} and g_{o3}	g_{m3} and g_{d3}	0
3	g_{m3}, g_{o3} and g_{m2o1}	g_{m3}, g_{o3} and g_{m2o1}	0
4	g_{m3}, g_{o3}, g_{m2o1} and g_{m1o2}	g_{m3}, g_{o3}, g_{m2o1} and g_{m1o2}	0

Table B.2: Simulation results for testing the effect of different non-linearity terms in the LNA and feedback amplifier on distortion canceling.

Appendix C

Iterative Calculation Method

In this Appendix, the iterative calculation method qualitatively described in Section 3.3 is developed in detail.

Starting with the IF voltage, by first substituting (3.14) in (3.12) and collecting terms

$$\begin{aligned}
V_{\mathrm{IF}n}(\omega) = {} & g_{m1} Z_{\mathrm{IF}}(\omega) \sum_{k=-\infty}^{\infty} a_k e^{-jk\frac{2\pi}{N}n} \\
& \times \frac{Z_o(\omega - k\omega_{\mathrm{LO}})}{R_{\mathrm{SW}} + Z_o(\omega - k\omega_{\mathrm{LO}})} V_{\mathrm{in}}(\omega - k\omega_{\mathrm{LO}}) \\
& - g_{m2} Z_{\mathrm{IF}}(\omega) \sum_{m=-\infty}^{\infty} \sum_{k=-\infty}^{\infty} a_m a_k e^{-j(m+k)\frac{2\pi}{N}n} \\
& \times A_{\mathrm{IF}}\big(\omega - (m+k)\omega_{\mathrm{LO}}\big) V_{\mathrm{IF}n}\big(\omega - (m+k)\omega_{\mathrm{LO}}\big) \\
& - Z_{\mathrm{IF}}(\omega) N \sum_{m=-\infty}^{\infty} \sum_{k=-\infty}^{\infty} a_m a_{Nk} e^{-jm\frac{2\pi}{N}n} \\
& \times \big[1 - g_{m2} R_{\mathrm{SW}} A_{\mathrm{IF}}\big(\omega - (m+k)\omega_{\mathrm{LO}}\big)\big] \\
& \times \frac{V_{\mathrm{IF}n}\big(\omega - (m+k)\omega_{\mathrm{LO}}\big)}{R_{\mathrm{SW}} + Z_o(\omega - m\omega_{\mathrm{LO}})}
\end{aligned} \tag{C.1}$$

where $A_{\mathrm{IF}}(\omega) = A_v(\omega) H_{\mathrm{hpf}}(\omega)$ is the transfer function for the cascade comprising the inverter amplifier and the HPF. Note that for the third term on the RHS of (C.1), a_{Nk} is non-zero only for $k = 0$ in a SB design. That, together with the fact that $Z_o(\omega)$ is typically $\gg Z_{\mathrm{IF}}(\omega)$, allows for discarding the third term in (C.1) while introducing negligible error to the overall solution. By defining $p = m + k$, the "no frequency translation" component (i.e. $p = 0$) can be further separated out of the second term

of (C.1)

$$V_{\mathrm{IF}n}(\omega) = g_{m1} Z_{\mathrm{IF}}(\omega) \sum_{k=-\infty}^{\infty} a_k e^{-jk\frac{2\pi}{N}n} \frac{Z_o(\omega - k\omega_{\mathrm{LO}})}{R_{\mathrm{SW}} + Z_o(\omega - k\omega_{\mathrm{LO}})} V_{\mathrm{in}}(\omega - k\omega_{\mathrm{LO}})$$
$$- g_{m2} Z_{\mathrm{IF}}(\omega) \sum_{\substack{p=-\infty \\ p\neq 0}}^{\infty} \sum_{m=-\infty}^{\infty} a_m a_{p-m} e^{-jp\frac{2\pi}{N}n} A_{\mathrm{IF}}(\omega - p\omega_{\mathrm{LO}}) V_{\mathrm{IF}n}(\omega - p\omega_{\mathrm{LO}})$$
$$- g_{m2} Z_{\mathrm{IF}}(\omega) A_{\mathrm{IF}}(\omega) V_{\mathrm{IF}n}(\omega) \sum_{m=-\infty}^{\infty} |a_m|^2 \tag{C.2}$$

By collecting $V_{\mathrm{IF}n}(\omega)$ terms, the effect of the frequency translation loop on modifying the input impedance of the trans-impedance amplifier becomes apparent

$$V_{\mathrm{IF}n}(\omega) = g_{m1} Z_{\mathrm{CL}}(\omega) \sum_{k=-\infty}^{\infty} a_k e^{-jk\frac{2\pi}{N}n} \frac{Z_o(\omega - k\omega_{\mathrm{LO}})}{R_{\mathrm{SW}} + Z_o(\omega - k\omega_{\mathrm{LO}})} V_{\mathrm{in}}(\omega - k\omega_{\mathrm{LO}})$$
$$- g_{m2} Z_{\mathrm{CL}}(\omega) \sum_{\substack{p=-\infty \\ p\neq 0}}^{\infty} \sum_{m=-\infty}^{\infty} a_m a_{p-m} e^{-jp\frac{2\pi}{N}n} A_{\mathrm{IF}}(\omega - p\omega_{\mathrm{LO}}) V_{\mathrm{IF}n}(\omega - p\omega_{\mathrm{LO}}) \tag{C.3}$$

where the closed loop impedance $Z_{\mathrm{CL}}(\omega)$ is related to the IF impedance $Z_{\mathrm{IF}}(\omega)$ by the "no frequency translation" loop gain $T_{\text{IF-IF}}(\omega)$ as expected in a shunt feedback system

$$Z_{\mathrm{CL}}(\omega) = \frac{Z_{\mathrm{IF}}(\omega)}{1 + T_{\text{IF-IF}}(\omega)} \tag{C.4}$$

$$T_{\text{IF-IF}}(\omega) = g_{m2} Z_{\mathrm{IF}}(\omega) A_{\mathrm{IF}}(\omega) \sum_{m=-\infty}^{\infty} |a_m|^2 \tag{C.5}$$

The expression in (C.2) can then be re-written as

$$V_{\mathrm{IF}n}(\omega) = V_{\mathrm{IF}n0}(\omega) - H_{\mathrm{FB}}\{V_{\mathrm{IF}n}(\omega)\} \tag{C.6}$$

where $V_{\mathrm{IF}n0}(\omega)$ represents the dependence of the IF voltage on input excitation

$$V_{\mathrm{IF}n0}(\omega) = g_{m1} Z_{\mathrm{CL}}(\omega) \sum_{k=-\infty}^{\infty} a_k e^{-jk\frac{2\pi}{N}n} \frac{Z_o(\omega - k\omega_{\mathrm{LO}})}{R_{\mathrm{SW}} + Z_o(\omega - k\omega_{\mathrm{LO}})} V_{\mathrm{in}}(\omega - k\omega_{\mathrm{LO}}) \tag{C.7}$$

and the frequency domain operator H_{FB} captures the effect of the feedback frequency translation loop, and is defined for a voltage $V_{\mathrm{x}}(\omega)$

$$H_{\mathrm{FB}}\{V_{\mathrm{x}}(\omega)\} = g_{m2} Z_{\mathrm{CL}}(\omega) \sum_{\substack{p=-\infty \\ p\neq 0}}^{\infty} \sum_{m=-\infty}^{\infty} a_m a_{p-m} e^{-jp\frac{2\pi}{N}n} A_{\mathrm{IF}}(\omega - p\omega_{\mathrm{LO}}) V_{\mathrm{x}}(\omega - p\omega_{\mathrm{LO}}) \tag{C.8}$$

Equation (C.6) is the key relation that serves as the basis for finding the harmonic and noise transfer functions of the system.

A solution for (C.6) can be found in an iterative manner by recursively applying the relation

$$V_{\mathrm{IF}ni}(\omega) = V_{\mathrm{IF}n0}(\omega) + H_{\mathrm{FB}}\{V_{\mathrm{IF}ni-1}(\omega)\} \tag{C.9}$$

where i denotes the i-th iteration. As such, $V_{\mathrm{IF}n0}(\omega)$ can also be viewed as the solution for the IF voltage when zero iterations are carried out (hence the 0 in the subscript). According to (C.8), each iteration multiplies the preceding result with two Fourier series coefficients as given by (3.10). Thus, successive iterations are expected to quickly converge towards a solution for $V_{\mathrm{IF}n}(\omega)$.

Appendix D

Harmonic Transfer Functions

D.1 IF Response

Utilizing (C.9) to perform one iteration

$$V_{\mathrm{IF}n1}(\omega) = V_{\mathrm{IF}n0}(\omega) - H_{\mathrm{FB}}\{V_{\mathrm{IF}0}(\omega)\} \tag{D.1}$$

The second term in the RHS of (D.1) can now be evaluated with the aid of (C.7) and (C.8). After simplifying and collecting terms

$$\begin{aligned} H_{\mathrm{FB}}\{V_{\mathrm{IF}n0}(\omega)\} = g_{m1}g_{m2}Z_{\mathrm{CL}}(\omega)sum_{\substack{p=-\infty \\ p\neq 0}}^{\infty} \sum_{m=-\infty}^{\infty}\sum_{k=-\infty}^{\infty} a_m a_{p-m} a_{k-p} e^{-jk\frac{2\pi}{N}n} \\ \times A_{\mathrm{IF}}(\omega - p\omega_{\mathrm{LO}})Z_{\mathrm{CL}}(\omega - p\omega_{\mathrm{LO}}) \frac{Z_o(\omega - k\omega_{\mathrm{LO}})}{R_{\mathrm{SW}} + Z_o(\omega - k\omega_{\mathrm{LO}})} V_{\mathrm{in}}(\omega - k\omega_{\mathrm{LO}}) \end{aligned} \tag{D.2}$$

By combining (C.7) and (D.2) in (D.1) and using the substitution $V_{\mathrm{IF}n}(\omega) \rightarrow V_{\mathrm{IF}n}(\Delta\omega)$, a solution for the down-converted IF voltage is found

$$V_{\mathrm{IF}n}(\Delta\omega) = \sum_{k=-\infty}^{\infty} M_{\mathrm{IF}k}(\Delta\omega) V_{\mathrm{in}}(\Delta\omega - k\omega_{\mathrm{LO}}) \tag{D.3}$$

where $M_{\mathrm{IF}k}(\Delta\omega)$ is the k-th LO harmonic transfer function, and is the product of two terms: a desired response $H_{\mathrm{IF}k}(\Delta\omega)$ and an error term $\varepsilon_{\mathrm{IF}k}(\Delta\omega)$

$$M_{\mathrm{IF}k}(\Delta\omega) = M'_{\mathrm{IF}k}(\Delta\omega)\, \varepsilon_{\mathrm{IF}k}(\Delta\omega) \tag{D.4}$$

$$M'_{\mathrm{IF}k}(\Delta\omega) = g_{m1}Z_{\mathrm{CL}}(\Delta\omega)e^{-jk\frac{2\pi}{N}n} \frac{Z_o(\Delta\omega - k\omega_{\mathrm{LO}})}{R_{\mathrm{SW}} + Z_o(\Delta\omega - k\omega_{\mathrm{LO}})} \tag{D.5}$$

$$\mathcal{E}_{\mathrm{IF}k}(\Delta\omega) = a_k - g_{m2} \sum_{\substack{p=\infty \\ p\neq 0}}^{\infty} \sum_{m=-\infty}^{\infty} a_m a_{p-m} a_{k-p} A_{\mathrm{IF}}(\omega - p\omega_{\mathrm{LO}}) Z_{\mathrm{CL}}(\Delta\omega - p\omega_{\mathrm{LO}}) \tag{D.6}$$

The general expression in (D.3) captures all harmonic mixing contributions to the down-converted IF voltage. The desired IF voltage down-converted due to the first LO harmonic corresponds to $k = -1$.

D.2 RF Response

To keep track of the different terms, (3.14) is first re-written as

$$V_{\mathrm{RF}}(\omega) = g_{m1} \frac{R_{\mathrm{SW}} Z_o(\omega)}{R_{\mathrm{SW}} + Z_o(\omega)} V_{\mathrm{in}}(\omega) + H_{\text{IF-RF}}\{V_{\mathrm{IF}n}(\omega)\} \tag{D.7}$$

where the frequency domain operator $H_{\text{IF-RF}}$ captures the effect of the IF voltage on the voltage generated at the RF side of the mixers due to their passivity, and is defined for a voltage parameter $V_{\mathrm{x}}(\omega)$ as

$$\begin{aligned} H_{\text{IF-RF}}\{V_{\mathrm{x}}(\omega)\} = \frac{Z_o(\omega)}{R_{\mathrm{SW}} + Z_o(\omega)} \sum_{n=0}^{N-1} \sum_{k=-\infty}^{\infty} a_k e^{-jk\frac{2\pi}{N}n} \\ \times \left[1 - g_{m2} R_{\mathrm{SW}} A_{\mathrm{IF}}(\omega - k\omega_{\mathrm{LO}})\right] \\ \times V_{\mathrm{x}}(\omega - k\omega_{\mathrm{LO}}) \end{aligned} \tag{D.8}$$

The RF response corresponding to one iteration can be found by substituting (D.1) in (D.7)

$$\begin{aligned} V_{\mathrm{RF1}}(\omega) &= g_{m1} \frac{R_{\mathrm{SW}} Z_o(\omega)}{R_{\mathrm{SW}} + Z_o(\omega)} V_{\mathrm{in}}(\omega) + H_{\text{IF-RF}}\{V_{\mathrm{IF}n1}(\omega)\} \\ &= g_{m1} \frac{R_{\mathrm{SW}} Z_o(\omega)}{R_{\mathrm{SW}} + Z_o(\omega)} V_{\mathrm{in}}(\omega) + H_{\text{IF-RF}}\{V_{\mathrm{IF}n0}(\omega)\} - H_{\text{IF-RF}}\big\{H_{\mathrm{FB}}\{V_{\mathrm{IF}n0}(\omega)\}\big\} \end{aligned} \tag{D.9}$$

and the two terms involving H operators on the RHS of (D.9) can be evaluated with the aid of (C.7), (C.8) and (D.8)

$$\begin{aligned} H_{\text{IF-RF}}\{V_{\mathrm{IF}n0}(\omega)\} = g_{m1} \frac{Z_o(\omega)}{R_{\mathrm{SW}} + Z_o(\omega)} N \sum_{m=-\infty}^{\infty} \sum_{k=-\infty}^{\infty} a_m a_{Nk-m} Z_{\mathrm{CL}}(\omega - m\omega_{\mathrm{LO}}) \\ \times \left[1 - g_{m2} R_{\mathrm{SW}} A_{\mathrm{IF}}(\omega - m\omega_{\mathrm{LO}})\right] \frac{Z_o(\omega - Nk\omega_{\mathrm{LO}})}{R_{\mathrm{SW}} + Z_o(\omega - Nk\omega_{\mathrm{LO}})} \\ \times V_{\mathrm{in}}(\omega - Nk\omega_{\mathrm{LO}}) \end{aligned} \tag{D.10}$$

$$
\begin{aligned}
H_{\text{IF-RF}}\big\{H_{\text{FB}}\{V_{\text{IF}n0}(\omega)\}\big\} = g_{m1}g_{m2}\frac{Z_o(\omega)}{R_{\text{SW}}+Z_o(\omega)} \\
&\times N\sum_{l=-\infty}^{\infty}\sum_{\substack{p=-\infty\\p\neq 0}}^{\infty}\sum_{m=-\infty}^{\infty}\sum_{k=-\infty}^{\infty} a_l a_{p-l} a_m a_{Nk-p-m} \\
&\times Z_{\text{CL}}\big(\omega-(p+m)\omega_{\text{LO}}\big)H_{\text{IF}}\big(\omega-(p+m)\omega_{\text{LO}}\big) \\
&\times Z_{\text{CL}}(\omega-m\omega_{\text{LO}})\big[1-g_{m2}R_{\text{SW}}A_{\text{IF}}(\omega-m\omega_{\text{LO}})\big] \\
&\times \frac{Z_o(\omega-Nk\omega_{\text{LO}})}{R_{\text{SW}}+Z_o(\omega-Nk\omega_{\text{LO}})}V_{\text{in}}(\omega-Nk\omega_{\text{LO}})
\end{aligned}
\tag{D.11}
$$

By combining (D.10) and (D.11) in (D.9), re-arranging terms, and finally using the substitution $V_{\text{RF}}(\omega)\rightarrow V_{\text{RF}}(\omega_{\text{LO}}+\Delta\omega)$, a solution for the RF voltage is found

$$
V_{\text{RF}}(\omega_{\text{LO}}+\Delta\omega)=\sum_{k=-\infty}^{\infty}\big[M_{\text{RF,SW}k}(\Delta\omega)+M_{\text{RF}k}(\Delta\omega)\big]V_{\text{in}}\big(\Delta\omega+(1-Nk)\omega_{\text{LO}}\big)
\tag{D.12}
$$

where $M_{\text{RF,SW}k}(\Delta\omega)$ and $M_{\text{RF}k}(\Delta\omega)$ are the k-th LO harmonic functions. The function $M_{\text{RF,SW}k}(\Delta\omega)$ arises due to the finite switch resistance (i.e. $M_{\text{RF,SW}k}(\Delta\omega)=0$ for $R_{\text{SW}}=0$), and is the product of two terms

$$
M_{\text{RF,SW}k}(\Delta\omega)=M'_{\text{RF,SW}k}(\Delta\omega)\,\mathcal{E}_{\text{RF}k}(\Delta\omega)
\tag{D.13}
$$

$$
\begin{aligned}
M'_{\text{RF,SW}k}(\Delta\omega) = g_{m1}\frac{R_{\text{SW}}Z_o(\omega_{\text{LO}}+\Delta\omega)}{R_{\text{SW}}+Z_o(\omega_{\text{LO}}+\Delta\omega)} \\
&\times\Big[\delta(k)-g_{m2}N\sum_{m=-\infty}^{\infty}a_m Z_{\text{CL}}\big(\Delta\omega+(1-m)\omega_{\text{LO}}\big) \\
&\qquad\times A_{\text{IF}}\big(\Delta\omega+(1-m)\omega_{\text{LO}}\big) \\
&\qquad\times\frac{Z_o\big(\Delta\omega+(1-Nk)\omega_{\text{LO}}\big)}{R_{\text{SW}}+Z_o\big(\Delta\omega+(1-Nk)\omega_{\text{LO}}\big)}\Big]
\end{aligned}
\tag{D.14}
$$

$$
\begin{aligned}
\mathcal{E}_{\text{RF}k}(\Delta\omega)=a_{Nm-k}-g_{m2}\sum_{l=-\infty}^{\infty}\sum_{\substack{p=\infty\\p\neq 0}}^{\infty}a_l a_{p-l}a_{Nk-p-m} \\
&\times Z_{\text{CL}}\big(\Delta\omega+(1-p-m)\omega_{\text{LO}}\big)A_{\text{IF}}\big(\Delta\omega+(1-p-m)\omega_{\text{LO}}\big)
\end{aligned}
\tag{D.15}
$$

where $\delta(k)$ is the Dirac delta function. Similarly, the function $M_{\text{RF}k}(\Delta\omega)$ is the product of two terms

$$
M_{\text{RF}k}(\Delta\omega)=M'_{\text{RF}k}(\Delta\omega)\,\mathcal{E}_{\text{RF}k}(\Delta\omega)
\tag{D.16}
$$

$$
\begin{aligned}
M'_{\mathrm{RF}k}(\Delta\omega) = g_{m1} &\frac{Z_o(\omega_{\mathrm{LO}}+\Delta\omega)}{R_{\mathrm{SW}} + Z_o(\omega_{\mathrm{LO}}+\Delta\omega)} \\
&\times N \sum_{m=-\infty}^{\infty} a_m Z_{\mathrm{CL}}\big(\Delta\omega+(1-m)\omega_{\mathrm{LO}}\big) \\
&\times \frac{Z_o\big(\Delta\omega + (1-Nk)\omega_{\mathrm{LO}}\big)}{R_{\mathrm{SW}} + Z_o\big(\Delta\omega + (1-Nk)\omega_{\mathrm{LO}}\big)}
\end{aligned}
\tag{D.17}
$$

The general expression in (D.12) captures all harmonic mixing contributions to the RF voltage. The desired RF voltage due to the first LO harmonic corresponds to $k = 0$.

Appendix E

Noise Transfer Functions

In this Appendix, the noise transfer functions for each of the noise sources in Fig. 3.12 are derived. The derivation is based on the same iterative procedure developed in Appendix C. Unless otherwise stated, the noise transfer functions obtained relate the output noise voltage to the noise source as follows

$$\overline{v_n}^2_{,\mathrm{IF}n}(\Delta\omega) = \sum_{k=\infty}^{\infty} \left|N_{\mathrm{IF}k}(\Delta\omega)\right|^2 \overline{x}_n^2(\Delta\omega - k\omega_{\mathrm{LO}}) \tag{E.1}$$

$$\overline{v_n}^2_{,\mathrm{RF}}(\Delta\omega) = \sum_{k=\infty}^{\infty} \left|N_{\mathrm{RF}k}(\Delta\omega)\right|^2 \overline{x}_n^2\big(\Delta\omega + (1-k)\omega_{\mathrm{LO}}\big) \tag{E.2}$$

where $N_{\mathrm{IF}k}(\Delta\omega)$ and $N_{\mathrm{RF}k}(\Delta\omega)$ are the noise transfer functions from the noise source $\overline{x}_n^2$ to the IF and RF outputs, respectively, where $\overline{x}_n^2$ is either a noise voltage or current.

E.1 Noise due to Input Transconductor

Noting that the noise current $\overline{i_n}^2_{,g_{m1}}(\omega)$ in Fig. 3.12 is injected into the loop at the same node as the input signal current $g_{m1}V_{in}(\omega)$ in Fig. 3.2, the IF and RF noise transfer functions become readily available from the results in Appendix D. Thus, by using the substitution $g_{m1}V_{\mathrm{in}}(\omega) \rightarrow i_{n,g_{m1}}(\omega)$, the IF and RF noise transfer functions can be found from (D.3) and (D.12), respectively

$$N_{\mathrm{IF}k,gm1}(\Delta\omega) = M_{\mathrm{IF}k}(\Delta\omega)/g_{m1} \tag{E.3}$$

$$N_{\mathrm{RF}k,gm1}(\Delta\omega) = \big[M_{\mathrm{RF,SW}k}(\Delta\omega) + M_{\mathrm{RF}k}(\Delta\omega)\big]/g_{m1} \tag{E.4}$$

E.2 Noise due to Feedback Transconductor

IF and RF time domain equations are

$$v_{n,\mathrm{IF}n}(t) = \Big[\big[i_{\mathrm{fb}n}(t) - i_o(t)\big] \cdot S_{\mathrm{DC}n}(t)\Big] * z_{\mathrm{IF}}(t) \tag{E.5}$$

$$v_{n,\mathrm{RF}}(t) = \big[i_{\mathrm{fb}n}(t) - i_o(t)\big] R_{\mathrm{SW}} + v_{n,\mathrm{IF}n}(t) S_{\mathrm{DC}n}(t) \tag{E.6}$$

and $i_{\mathrm{fb}n}(t)$ now contains a superimposed noise component

$$i_{\mathrm{fb}n}(t) = g_{m2}\Big[\big[-a_v(t) * v_{\mathrm{IF}n}(t) + i_{n,gm2}(t)\big] * h_{\mathrm{hpf}}(t)\Big] S_{\mathrm{UC}n}(t) \tag{E.7}$$

By substituting (E.7) in both of (E.5) and (E.6), taking the Fourier transform and assuming $Z_o(\omega) >> Z_{\mathrm{CL}}(\omega)$

$$\begin{aligned} v_{n,\mathrm{IF}n}(\omega) = {} & Z_{\mathrm{CL}}(\omega) \sum_{m=-\infty}^{\infty} \sum_{k=-\infty}^{\infty} a_m a_{m-k} e^{-jk\frac{2\pi}{N}n} H_{\mathrm{hpf}}(\omega - k\omega_{\mathrm{LO}}) i_{n,gm2}(\omega - k\omega_{\mathrm{LO}}) \\ & - g_{m2} Z_{\mathrm{CL}}(\omega) \sum_{m=-\infty}^{\infty} \sum_{\substack{k=\infty \\ k\neq 0}}^{\infty} a_m a_{k-m} e^{-jk\frac{2\pi}{N}n} A_{\mathrm{IF}}(\omega - k\omega_{\mathrm{LO}}) v_{n,\mathrm{IF}n}(\omega - k\omega_{\mathrm{LO}}) \end{aligned} \tag{E.8}$$

$$\begin{aligned} v_{n,\mathrm{RF}}(\omega) = {} & \frac{R_{\mathrm{SW}} Z_o(\omega)}{R_{\mathrm{SW}} + Z_o(\omega)} \sum_{k=-\infty}^{\infty} a_k e^{-jk\frac{2\pi}{N}n} H_{\mathrm{hpf}}(\omega - k\omega_{\mathrm{LO}}) i_{n,gm2}(\omega - k\omega_{\mathrm{LO}}) \\ & + \frac{Z_o(\omega)}{R_{\mathrm{SW}} + Z_o(\omega)} \sum_{k=-\infty}^{\infty} a_k e^{-jk\frac{2\pi}{N}n} \big[1 - g_{m2} R_{\mathrm{SW}} A_{\mathrm{IF}}(\omega - k\omega_{\mathrm{LO}})\big] \\ & \times v_{n,\mathrm{IF}n}(\omega - k\omega_{\mathrm{LO}}) \end{aligned} \tag{E.9}$$

Applying (C.9) to (E.8) for one iteration

$$N_{\mathrm{IF}k}(\Delta\omega) = Z_{\mathrm{CL}}(\Delta\omega) e^{-jk\frac{2\pi}{N}n} H_{\mathrm{hpf}}(\Delta\omega - k\omega_{\mathrm{LO}}) \sum_{m=-\infty}^{\infty} a_m a_{k-m} \tag{E.10}$$

and consequently, by using (E.1) and (E.10) in (E.9) and summing noise power from all N paths, the RF noise transfer function is obtained

$$\begin{aligned} N_{\mathrm{RF}k}(\Delta\omega) = {} & \sqrt{N} \frac{Z_o(\omega_{\mathrm{LO}} + \Delta\omega)}{R_{\mathrm{SW}} + Z_o(\omega_{\mathrm{LO}} + \Delta\omega)} e^{-jk\frac{2\pi}{N}n} H_{\mathrm{hpf}}\big(\Delta\omega + (1-k)\omega_{\mathrm{LO}}\big) \\ & \times \Big[a_k R_{\mathrm{SW}} - \sum_{p=\infty}^{\infty} \sum_{m=\infty}^{\infty} a_m a_{p-m} a_{k-p} Z_{\mathrm{CL}}\big(\Delta\omega + (1-k+p)\omega_{\mathrm{LO}}\big) \\ & \times \big[1 - g_{m2} R_{\mathrm{SW}} A_{\mathrm{IF}}\big(\Delta\omega + (1-k+p)\omega_{\mathrm{LO}}\big)\big]\Big] \end{aligned} \tag{E.11}$$

E.3 Noise due to Switch Resistance

Since the up-conversion switches are driven from the IF side by a transconductor with an output impedance significantly larger than R_{SW}, their noise contribution is minor and can be neglected. For the down-conversion switches, the switch resistances can be modeled with one resistor on the RF side because the different paths are operated with non-overlapping clocks. As such, the time domain equations are

$$v_{n,\mathrm{IF}n}(t) = \Big[\big[i_{\mathrm{fb}n}(t) - i_o(t)\big] \cdot S_{\mathrm{DC}n}(t)\Big] * z_{\mathrm{IF}}(t) \tag{E.12}$$

$$v_{n,\mathrm{RF}}(t) = \big[i_{n,\mathrm{SW}} + \sum_{n=0}^{N-1} i_{\mathrm{fb}n}(t) - i_o(t)\big] R_{\mathrm{SW}} + \sum_{n=0}^{N-1} v_{\mathrm{IF}n}(t) \cdot S_{\mathrm{DC}n}(t) \tag{E.13}$$

By substituting for $i_{\mathrm{fb}n}(t)$ with (3.11) in both of (E.12) and (E.13), taking the Fourier transform and assuming $Z_o(\omega) >> Z_{\mathrm{CL}}(\omega)$

$$\begin{aligned} v_{n,\mathrm{IF}n}(\omega) = &-Z_{\mathrm{CL}}(\omega) \sum_{k=-\infty}^{\infty} a_k e^{-jk\frac{2\pi}{N}n} \frac{R_{\mathrm{SW}}}{Z_o(\omega - k\omega_{\mathrm{LO}}) + R_{\mathrm{SW}}} i_{n,\mathrm{SW}}(\omega - k\omega_{\mathrm{LO}}) \\ &-g_{m2} Z_{\mathrm{CL}}(\omega) \sum_{m=-\infty}^{\infty} \sum_{\substack{k=-\infty \\ k\neq 0}}^{\infty} a_m a_{k-m} e^{-jk\frac{2\pi}{N}n} A_{\mathrm{IF}}(\omega - k\omega_{\mathrm{LO}}) v_{n,\mathrm{IF}n}(\omega - k\omega_{\mathrm{LO}}) \end{aligned} \tag{E.14}$$

$$\begin{aligned} v_{n,\mathrm{RF}}(\omega) = &\frac{R_{\mathrm{SW}} Z_o(\omega)}{R_{\mathrm{SW}} + Z_o(\omega)} i_{n,\mathrm{SW}}(\omega - k\omega_{\mathrm{LO}}) \\ &+ \frac{Z_o(\omega)}{R_{\mathrm{SW}} + Z_o(\omega)} \sum_{n=0}^{N-1} \sum_{k=-\infty}^{\infty} a_k e^{-jk\frac{2\pi}{N}n} \big[1 - g_{m2} R_{\mathrm{SW}} A_{\mathrm{IF}}(\omega - k\omega_{\mathrm{LO}})\big] \\ &\times v_{n,\mathrm{IF}n}(\omega - k\omega_{\mathrm{LO}}) \end{aligned} \tag{E.15}$$

Applying (C.9) to (E.14) for one iteration

$$\begin{aligned} N_{\mathrm{IF}k}(\Delta\omega) = &-Z_{\mathrm{CL}}(\Delta\omega) \frac{R_{\mathrm{SW}}}{R_{\mathrm{SW}} + Z_o(\Delta\omega - k\omega_{\mathrm{LO}})} e^{-jk\frac{2\pi}{N}n} \\ &\times \Big[a_m - g_{m2} \sum_{\substack{p=\infty \\ p\neq 0}}^{\infty} \sum_{m=\infty}^{\infty} a_k a_{p-k} a_{m-p} A_{\mathrm{IF}}(\Delta\omega - k\omega_{\mathrm{LO}}) Z_{\mathrm{CL}}(\Delta\omega - k\omega_{\mathrm{LO}})\Big] \end{aligned} \tag{E.16}$$

and consequently, by using (E.1) and (E.16) in (E.15), the RF noise transfer function

is obtained

$$
\begin{aligned}
N_{\mathrm{RF}k} = & \frac{R_{\mathrm{SW}} Z_o(\omega_{\mathrm{LO}}+\Delta\omega)}{R_{\mathrm{SW}} + Z_o(\omega_{\mathrm{LO}}+\Delta\omega)} \\
& \times\delta(k)\Big[1 - N\frac{R_{\mathrm{SW}} + Z_o\big(\Delta\omega+(1-Nk)\big)}{R_{\mathrm{SW}} + Z_o\big(\Delta\omega+(1-Nk)\big)} \sum_{m=\infty}^{\infty} |a_m|^2 \frac{Z_{\mathrm{CL}}\big(\Delta\omega + (1-m)\omega_{\mathrm{LO}}\big)}{R_{\mathrm{SW}} + Z_o(\omega_{\mathrm{LO}}+\Delta\omega)} \\
& \qquad \times\big[1 - g_{m2} R_{\mathrm{SW}} A_{\mathrm{IF}}\big(\Delta\omega+(1-m)\omega_{\mathrm{LO}}\big)\big] Z_{\mathrm{CL}}\big(\Delta\omega + (1-m)\omega_{\mathrm{LO}}\big)\Big] \\
& - \frac{R_{\mathrm{SW}} Z_o(\omega_{\mathrm{LO}}+\Delta\omega)}{R_{\mathrm{SW}} + Z_o(\omega_{\mathrm{LO}}+\Delta\omega)} \\
& \times\big[1 - \delta(k)\big] N\frac{R_{\mathrm{SW}} + Z_o\big(\Delta\omega+(1-Nk)\big)}{R_{\mathrm{SW}} + Z_o\big(\Delta\omega+(1-Nk)\big)} \sum_{m=\infty}^{\infty} |a_m|^2 \frac{Z_{\mathrm{CL}}\big(\Delta\omega + (1-m)\omega_{\mathrm{LO}}\big)}{R_{\mathrm{SW}} + Z_o(\omega_{\mathrm{LO}}+\Delta\omega)} \\
& \times\big[1 - g_{m2} R_{\mathrm{SW}} A_{\mathrm{IF}}\big(\Delta\omega+(1-m)\omega_{\mathrm{LO}}\big)\big] Z_{\mathrm{CL}}\big(\Delta\omega + (1-m)\omega_{\mathrm{LO}}\big)\Big] \qquad \text{(E.17)}
\end{aligned}
$$

E.4 Noise due to IF Amplifier

$$
v_{n,\mathrm{IF}n}(t) = \Big[\big[i_{\mathrm{fb}n}(t) - i_o(t)\big] \cdot S_{\mathrm{DC}n}(t)\Big] * z_{\mathrm{IF}}(t) - a_v(t) * \big[(v_{n,\mathrm{IF}n}(t) + v_{n,\mathrm{opamp}}(t)\big] \qquad \text{(E.18)}
$$

$$
v_{n,\mathrm{RF}}(t) = \big[i_{\mathrm{fb}n}(t) - i_o(t)\big] R_{\mathrm{SW}} + v_{\mathrm{IF}n}(t) \cdot S_{\mathrm{DC}n}(t) \qquad \text{(E.19)}
$$

and $i_{\mathrm{fb}n}(t)$ now contains a superimposed noise component

$$
i_{\mathrm{fb}n}(t) = g_{m2}\Big[\big[- a_v(t) * \big(v_{\mathrm{IF}n}(t) + v_{n,\mathrm{opamp}}(t)\big)\big] * h_{\mathrm{hpf}}(t)\Big] S_{\mathrm{UC}n}(t) \qquad \text{(E.20)}
$$

By substituting (E.20) in both of (E.18) and (E.19), taking the Fourier transform and assuming $Z_o(\omega) >> Z_{\mathrm{CL}}(\omega)$

$$
\begin{aligned}
v_{n,\mathrm{IF}n}(\Delta\omega) = & -\frac{A_v(\omega)}{1 + A_v(\omega)} v_{n,\mathrm{opamp}}(\omega) \\
& - g_{m2} Z_{\mathrm{CL}}(\omega) \sum_{m=-\infty}^{\infty} \sum_{\substack{k=-\infty \\ k\neq 0}}^{\infty} a_m a_{k-m} e^{-jk\frac{2\pi}{N}n} A_{\mathrm{IF}}(\omega - k\omega_{\mathrm{LO}}) \\
& \quad \times v_{n,\mathrm{opamp}}\big(\omega - k\omega_{\mathrm{LO}}\big) \\
& - g_{m2} Z_{\mathrm{CL}}(\omega) \sum_{m=-\infty}^{\infty} \sum_{\substack{k=-\infty \\ k\neq 0}}^{\infty} a_m a_{k-m} e^{-jk\frac{2\pi}{N}n} A_{\mathrm{IF}}(\omega - k\omega_{\mathrm{LO}}) \\
& \quad \times v_{n,\mathrm{IF}n}(\omega - k\omega_{\mathrm{LO}}) \qquad \text{(E.21)}
\end{aligned}
$$

$$
\begin{aligned}
v_{n,\mathrm{RF}}(\omega) = & \frac{Z_o(\omega)}{R_{\mathrm{SW}} + Z_o(\omega)} \sum_{k=-\infty}^{\infty} a_k e^{-jk\frac{2\pi}{N}n} \big[1 - g_{m2} R_{\mathrm{SW}} A_{\mathrm{IF}}(\omega - k\omega_{\mathrm{LO}})\big] \\
& \times v_{n,\mathrm{IF}n}(\omega - k\omega_{\mathrm{LO}}) \qquad \text{(E.22)}
\end{aligned}
$$

Applying (C.9) to (E.21) for one iteration

$$N_{\mathrm{IF}k}(\Delta\omega) = -\delta(k)\Big[\frac{A_v(\omega)}{1+A_v(\omega)} + g_{m2}Z_{\mathrm{CL}}(\Delta\omega)A_{\mathrm{IF}}(\Delta\omega)\sum_{m=\infty}^{\infty}|a_m|^2\Big] - \big[1-\delta(k)\big]g_{m2}Z_{\mathrm{CL}}(\Delta\omega)\sum_{m=\infty}^{\infty}a_m a_{k-m}e^{-jk\frac{2\pi}{N}n} \times A_{\mathrm{IF}}(\Delta\omega - k\omega_{\mathrm{LO}})\Big[1-\frac{A_v(\Delta\omega-k\omega_{\mathrm{LO}})}{1+A_v(\Delta\omega-k\omega_{\mathrm{LO}})}\Big] \tag{E.23}$$

and consequently, by using (E.1) and (E.23) in (E.22) and summing noise power from all N paths, the RF noise transfer function is obtained

$$H_{\mathrm{RF}k}(\Delta\omega) = -\sqrt{N}\frac{Z_o(\omega_{\mathrm{LO}}+\Delta\omega)}{R_{\mathrm{SW}}+Z_o(\omega_{\mathrm{LO}}+\Delta\omega)}e^{-jk\frac{2\pi}{N}n}a_k \times\big[1-g_{m2}R_{\mathrm{SW}}A_{\mathrm{IF}}\big(\Delta\omega+(1-k)\omega_{\mathrm{LO}}\big)\big] \times\Big[\frac{A_v\big(\Delta\omega+(1-k)\omega_{\mathrm{LO}}\big)}{1+A_v\big(\Delta\omega+(1-k)\omega_{\mathrm{LO}}\big)}+\frac{T_{\text{IF-IF}}\big(\Delta\omega+(1-k)\omega_{\mathrm{LO}}\big)}{1+T_{\text{IF-IF}}\big(\Delta\omega+(1-k)\omega_{\mathrm{LO}}\big)}\Big] \tag{E.24}$$

E.5 Noise due to Feedback Resistor

Since the different paths are operating with non-overlapping LO clocks, the circuit is solved for one noisy path to obtain the IF noise transfer function. By summing the (uncorrelated) noise contributions from all paths, the RF noise transfer function can then be found.

The IF and RF time domain equations are

$$v_{n,\mathrm{IF}n}(t) = \Big[\big[i_{\mathrm{fb}n}(t)-i_o(t)\big]\cdot S_{\mathrm{DC}n}(t)+i_{n,f}(t)\Big] * z_{\mathrm{IF}}(t) \tag{E.25}$$

$$v_{n,\mathrm{RF}}(t) = \big[i_{\mathrm{fb}n}(t)-i_o(t)\big]R_{\mathrm{SW}}+v_{n,\mathrm{IF}n}(t)S_{\mathrm{DC}n}(t) \tag{E.26}$$

By substituting for $i_{\mathrm{fb}n}(t)$ with (3.11) in both of (E.25) and (E.26), taking the Fourier transform and assuming $Z_o(\omega) >> Z_{\mathrm{CL}}(\omega)$

$$v_{n,\mathrm{IF}n}(\omega) = i_{n,f}(\omega)Z_{\mathrm{CL}}(\omega) - g_{m2}Z_{\mathrm{CL}}(\omega)\sum_{m=-\infty}^{\infty}\sum_{\substack{k=-\infty\\k\neq 0}}^{\infty}a_m a_{k-m}e^{-jk\frac{2\pi}{N}n}A_{\mathrm{IF}}(\omega-k\omega_{\mathrm{LO}})v_{n,\mathrm{IF}n}(\omega-k\omega_{\mathrm{LO}}) \tag{E.27}$$

$$v_{n,\mathrm{RF}}(\omega) = \frac{Z_o(\omega)}{R_{\mathrm{SW}}+Z_o(\omega)}\sum_{k=-\infty}^{\infty}a_k e^{-jk\frac{2\pi}{N}n}\big[1-g_{m2}R_{\mathrm{SW}}A_{\mathrm{IF}}(\omega-k\omega_{\mathrm{LO}})\big] \times v_{n,\mathrm{IF}n}(\omega-k\omega_{\mathrm{LO}}) \tag{E.28}$$

Applying (C.9) to (E.27) for one iteration

$$N_{\mathrm{IF}k}(\Delta\omega) = Z_{\mathrm{CL}}(\Delta\omega)\Big[\delta(k) - \big[1-\delta(k)\big] g_{m2} a_k e^{-jk\frac{2\pi}{N}n} \times Z_{\mathrm{CL}}(\Delta\omega - k\omega_{\mathrm{LO}}) \times A_{\mathrm{IF}}(\Delta\omega - k\omega_{\mathrm{LO}})\Big] \times \sum_{m=-\infty}^{\infty} a_{k-m}\Big] \tag{E.29}$$

and consequently, by using (E.1) and (E.29) in (E.28) and summing noise power from all N paths, the RF noise transfer function is obtained

$$N_{\mathrm{RF}k}(\Delta\omega) = \sqrt{N}\frac{Z_o(\omega_{\mathrm{LO}}+\Delta\omega)}{R_{\mathrm{SW}}+Z_o(\omega_{\mathrm{LO}}+\Delta\omega)} Z_{\mathrm{CL}}\big(\Delta\omega+(1-k)\omega_{\mathrm{LO}}\big) e^{-jk\frac{2\pi}{N}n} \times a_k\big[1 - g_{m2} R_{\mathrm{SW}} A_{\mathrm{IF}}\big(\Delta\omega+(1-k)\omega_{\mathrm{LO}}\big)\big] \tag{E.30}$$

Bibliography

[1] Cisco, "Visual networking index: Forecast and methodology, 20112016," *White Paper*, pp. 1–16, May 2012.

[2] N. Economides, *The Economics of the Internet Backbone - Handbook of Telecommunications Economics*. Elsevier, 2006.

[3] A. F. Molisch, *Wireless Communications*, 2nd ed. England: Wiley, 2010.

[4] B. Razavi, *RF Microelectronics*, 1st ed. New Jersey: Prentice Hall, 1998.

[5] S. Haykin, "Cognitive radio: brain-empowered wireless communications," *IEEE J. Sel. Areas Commun.*, vol. 23, pp. 201–220, Feb. 2005.

[6] D. H. Mahrof, E. A. M. Klumperink, J. Haartsen, and B. Nauta, "On the effect of spectral location of interferers on linearity requirements for wideband cognitive radio receivers," in *4th IEEE Symposium of New Frontiers in Dynamic Spectrum Access Networks (DySPAN)*, Singapore, Apr. 2010.

[7] P. Wambacq and W. Sansen, *Distortion Analysis of Analog Integrated Circuits*, 1st ed. Boston: Kluwer Academic Publishers, 1998.

[8] J. Crols and M. S. J. Steyaert, "Low-if topologies for high-performance analog front ends of fully integrated receivers," *IEEE Trans. Circuits Syst. II*, vol. 45, pp. 269–282, Mar. 1998.

[9] B. Razavi, "Design considerations for direct-conversion receivers," *IEEE Trans. Circuits Syst. II*, vol. 44, pp. 428–435, Jun. 1997.

[10] B. Gilbert, "A precise four-quadrant multiplier with subnanosecond response," *IEEE J. Solid-State Circuits*, vol. 3, pp. 365–373, Dec. 1968.

[11] D. R. Tayloe, "Product detector and method therefor," U.S. Patent 6 230 000, 2001.

[12] G. Palumbo and S. Pennis, *Feedback Amplifiers: Theory and Design*, 1st ed. New York: Kluwer Academic Publishers, 2003.

[13] B. G. Perumana, J. C. Zhan, S. S. Taylor, B. R. Carlton, and J. Laskar, "Resistive feedback CMOS low-noise amplifiers for multiband applications," *IEEE Trans. Microw. Theory Tech.*, pp. 1218–1225, May 2008.

[14] J. C. Zhan and S. S. Taylor, "A 5GHz resistive-feedback CMOS LNA for low-cost multi-standard applications," in *IEEE Int. Solid-State Circuits Conf. Dig. Tech. Papers*, Feb. 2006, pp. 721–730.

[15] D. R. Webster, D. G. Haigh, J. B. Scott, and A. E. Parker, "Derivative superposition a linearization technique for ultra broadband systems," in *IEE Wideband Circuits, Modeling, Technology Colloq.*, May 1996, pp. 1–14.

[16] D. Webster, J. Scott, and D. Haigh, "Control of circuit distortion by the derivative superposition method," *IEEE Microwave and Guided Wave Lett.*, vol. 40, pp. 123–125, Mar. 1996.

[17] V. Aparin, G. Brown, and L. E. Larson, "Linearization of CMOS LNA's via optimum gate biasing," in *Int. Symp. on Circuits and Systems ISCAS*, May 2004, pp. 748–751.

[18] V. Aparin and L. E. Larson, "Modied derivative superposition method for linearizing FET low-noise ampliers," *IEEE Trans. Microw. Theory Tech.*, vol. 53, pp. 571–581, Feb. 2005.

[19] H. Darabi, "A blocker filtering technique for SAW-less wireless receivers," *IEEE J. Solid-State Circuits*, vol. 42, pp. 2766–2773, Dec. 2007.

[20] B. W. Cook, A. Berny, A. Molnar, S. Lanzisera, and K. S. J. Pister, "Low-power 2.4-GHz transceiver with passive RX front-end and 400-mV supply," *IEEE J. Solid-State Circuits*, vol. 41, pp. 2757–2766, Dec. 2006.

[21] K. Koli, J. Jussila, P. Sivonen, S. Kallioinen, and A. Parssinen, "A 0.2-to-2.0GHz 65nm CMOS receiver without LNA achieving $>$ 11dBm IIP3 and $<$ 6.5dB NF," in *IEEE Int. Solid-State Circuits Conf. Dig. Tech. Papers*, Feb. 2009, pp. 222–223.

[22] C. Andrews and A. C. Molnar, "A passive mixer-first receiver with digitally controlled and widely tunable RF interface," *IEEE J. Solid-State Circuits*, vol. 45, pp. 2696–2708, Dec. 2010.

[23] J. Weldon, R. S. Narayanaswami, J. C. Rudell, L. Lin, M. Otsuka, S. Dedieu, L. Tee, K. Tsai, C. Lee, and P. Gray, "A 1.75-GHz highly integrated narrow-band CMOS transmitter with harmonic-rejection mixers," *IEEE J. Solid-State Circuits*, vol. 36, pp. 2003–2015, Dec. 2001.

[24] Z. Ru, N. A. Moseley, E. A. M. Klumperink, and B. Nauta, "Digitally enhanced software-defined radio receiver robust to out-of-band interference," *IEEE J. Solid-State Circuits*, pp. 3359–3375, Dec. 2009.

[25] A. Mirzaei, H. Darabi, J. C. Leete, and Y. Chang, "Analysis and optimization of direct-conversion receivers with 25% duty-cycle current-driven passive mixers," *IEEE J. Solid-State Circuits*, vol. 57, pp. 2353–2366, Sep. 2010.

[26] A. Ghaffari, E. A. M. Klumperink, and B. Nauta, "A differential 4-path highly linear widely tunable on-chip band-pass filter," in *Proc. IEEE Radio Frequency Integr. Circuits Symp.*, May 2010, pp. 299–301.

[27] L. E. Franks and I. W. Sandberg, "An alternative approach to the realization of network transfer functions: The N-path filter," *Bell Sys. Tech. J.*, vol. 39, pp. 1321–1350, Sep. 1960.

[28] A. Ghaffari, E. A. M. Klumperink, M. C. M. Soer, and B. Nauta, "Tunable high-Q N-path band-pass filters: Modeling and verification," *IEEE J. Solid-State Circuits*, vol. 45, pp. 998–1010, May 2011.

[29] M. Darvishi, R. van der Zee, E. Klumperink, and B. Nauta, "A 0.3GHz to 1.2GHz tunable 4th order switched gm-C band-pass filter with $>$ 55dB ultimate rejection and out-of-band IIP3 = +29dBm," in *IEEE Int. Solid-State Circuits Conf. Dig. Tech. Papers*, Feb. 2012, pp. 358–359.

[30] M. Darvishi, R. van der Zee, E. Klumperink, and B. Nauta, "A 0.1-to-1.2GHz tunable 6th-order n-path channel-select filter with 0.6dB passband ripple and +7dBm blocker tolerance," in *IEEE Int. Solid-State Circuits Conf. Dig. Tech. Papers*, Feb. 2013.

[31] A. Mirzaei, H. Darabi, and D. Murphy, "A low-power process-scalable super-heterodyne receiver with integrated high-Q filters," in *IEEE Int. Solid-State Circuits Conf. Dig. Tech. Papers*, Feb. 2011, pp. 60–61.

[32] S. Chehrazi, A. Mirzaei, and A. A. Abidi, "Second-order intermodulation in current-commutating passive FET mixers," *IEEE Trans. Circuits Syst. I*, vol. 56, pp. 2556–2568, Dec. 2009.

[33] S. Chehrazi, A. Mirzaei, and A. A. Abidi, "Noise in current-commutating passive FET mixers," *IEEE Trans. Circuits Syst. I*, vol. 57, pp. 332–344, Feb. 2010.

[34] S. Youssef, R. van der Zee, and B. Nauta, "Active feedback receiver with integrated tunable RF channel selectivity, distortion cancelling, 48dB stopband rejection and $> +12$dBm wideband IIP3, occupying $< 0.06\text{mm}^2$ in 65nm CMOS," in *IEEE Int. Solid-State Circuits Conf. Dig. Tech. Papers*, Feb. 2012, pp. 166–168.

[35] W. Sansen, *Analog Design Essentials*, 1st ed. The Netherlands: Springer, 2006.

[36] J. Shi, Y. Z. Xiong, K. Kang, L. Nan, and F. Lin, "RF noise of 65-nm MOSFETs in the weak-to-moderate-inversion region," *IEEE Electron Device Lett.*, pp. 185–188, Feb. 2009.

[37] A. N. Karanicolas, "A 2.7-V 900-MHz CMOS LNA and mixer," *IEEE J. Solid-State Circuits*, vol. 31, pp. 1939–1944, Dec. 1996.

[38] D. K. Shaeffer and T. H. Lee, "A 1.5-V 1.5-GHz CMOS low noise amplifier," *IEEE J. Solid-State Circuits*, vol. 32, pp. 745–759, May 1997.

[39] F. Gatta, E. Sacchi, F. Svelto, P. Vilmercati, and R. Castello, "A 2-dB noise figure 900-MHz differential CMOS LNA," *IEEE J. Solid-State Circuits*, vol. 36, pp. 1444–1452, Oct. 2001.

[40] F. Bruccoleri, E. A. M. Klumperink, and B. Nauta, "Wide-band CMOS low-noise amplifier exploiting thermal noise canceling," *IEEE J. Solid-State Circuits*, vol. 39, pp. 275–282, Feb. 2004.

[41] S. C. Blaakmeer, E. A. M. Klumperink, D. M. W. Leenaerts, and B. Nauta, "Wideband balun-LNA with simultaneous output balancing, noise-canceling and distortion-canceling," *IEEE J. Solid-State Circuits*, vol. 43, pp. 1341–1350, Jun. 2008.

[42] A. J. Annema, B. Nauta, R. Langevelde, and H. Tuinhout, "Analog circuits in ultra-deep-submicron CMOS," *IEEE J. Sel. Areas Commun.*, vol. 40, pp. 132–143, Jan. 2005.

[43] T. Werth, C. Schmits, R. Wunderlich, and S. Heinen, "An active feedback interference cancellation technique for blocker filtering in RF receiver front-ends," *IEEE J. Solid-State Circuits*, vol. 45, pp. 989–997, May 2010.

[44] C. Izquierdo, A. Kaiser, F. Montaudon, and P. Cathelin, "Reconfigurable wideband receiver with positive feed-back translational loop," in *Proc. IEEE Radio Frequency Integr. Circuits Symp.*, Jun. 2011, pp. 1–4.

[45] X. He and H. Kundur, "A compact SAW-less multiband WCDMA/GPS receiver front-end with translational loop for input matching," in *IEEE Int. Solid-State Circuits Conf. Dig. Tech. Papers*, Feb. 2011, pp. 372–374.

[46] A. Safarian, A. Shameli, A. Rofougaran, M. Rofougaran, and F. D. Flaviis, "Integrated blocker filtering RF front ends," in *Proc. IEEE Radio Frequency Integr. Circuits Symp.*, Jun. 2007, pp. 13–16.

[47] M. Soer, E. A. M. Klumperink, P. T. de Boer, F. E. van Fliet, and B. Nauta, "Unified frequency-domain analysis of switched-series-RC passive mixers and samplers," *IEEE Trans. Circuits Syst. I*, vol. 57, pp. 2618–2631, Oct. 2010.

[48] T. Werth, R. Wunderlich, and S. Heinen, "On I/Q-mismatch in active interference cancellation schemes," *52nd IEEE Int. Symp. on Circuits and Systems MWSCAS*, pp. 991–994, Aug. 2009.

[49] T. Werth, S. Kaehlert, and S. Heinen, "System design considerations for SAW-less front-ends at the example of GSM DCS1800," in *53rd IEEE Int. Symp. on Circuits and Systems MWSCAS*, Aug. 2010, pp. 648–651.

[50] S. Youssef, R. van der Zee, and B. Nauta, "Active feedback technique for RF channel selection in front-end receivers," *IEEE J. Solid-State Circuits*, vol. 47, pp. 1–15, Dec. 2012.

[51] T. Strom and S. Signell, "Analysis of periodically switched linear circuits," *IEEE Trans. Circuits Syst.*, vol. 24, pp. 531–541, Oct. 1977.

[52] C. C. Hull and R. G. Meyer, "A systematic approach to the analysis of noise in mixers," *IEEE Trans. Circuits Syst. I*, vol. 40, pp. 909–919, Dec. 1993.

[53] A. V. Oppenheim, A. S. Willsky, and S. H. Nawab, *Signals and Systems*, 2nd ed. NJ: Prentice Hall, 1997.

[54] B. Nauta, "Linear CMOS transconductance element for VHF filters," *Electron. Lett.*, vol. 25, pp. 448–450, Mar. 1989.

[55] M. Bazes, "Two novel fully complementary self-biased CMOS differential amplifiers," *IEEE J. Solid-State Circuits*, vol. 26, pp. 165–168, Feb. 1991.

List of Publications

S. Youssef, R. van der Zee, and B. Nauta, "Active feedback receiver with Integrated Tunable RF Channel Selectivity, Distortion Cancelling, 48dB Stopband Rejection and $> +12$dBm Wideband IIP3, Occupying $< 0.06\text{mm}^2$ in 65nm CMOS," *IEEE Int. Solid-State Circuits Conf. Dig. Tech. Papers*, Feb. 2012, pp. $166 - 168$.

S. Youssef, R. van der Zee, and B. Nauta, "Active Feedback Technique for RF Channel Selection in Front-End Receivers" *IEEE J. Solid-State Circuits*, vol. 47, pp. $3130 - 3144$, Dec. 2012.

S. Youssef, R. van der Zee, and B. Nauta, "Analysis of Frequency Translation Loops Employing Passive Mixers for RF Filtering in Receiver Front-Ends" *submitted to IEEE Trans. Circuits Syst. I (TCAS)*, 2013.

Acknowledgments

On some level, writing the last words in a book that contains four years worth of effort feels surreal. Today, I am 1563 days older and, hopefully, wiser, both on a technical and personal level. Several people have contributed towards this day, so a few words of gratitude are in order.

Moving from industry back to academia triggers mostly negative comments. Ranging from the purely pragmatic engineering perspective of "*What do you need a PhD for?*" and "*Such a waste of time*" to total indifference at best, the unasked for "advice" was quite annoying to say the least. In contrast, the enthusiasm and easy going manner of Bram Nauta, my promoter, made for a great impression during our first contact. One could say that he was only pursuing the best interest of his group by recruiting a new student (besides being a technical guru, he is a good marketeer, I have to admit), but this good first impression persisted during my stay in Twente. Despite his busy schedule, Bram's technical expertise and straight-to-the-point guidance continued throughout the entire duration of this project. For that, and for giving me the opportunity to begin with, I thank him.

My assistant-promoter, Ronan van der Zee, was no different. His open door policy and constant availability were essential. Our weekly meetings, in many cases, extended well beyond the one hour scheduled, sometimes chatting about completely unrelated topics, or even checking a YouTube video of a cool physics experiment. His expertise on feedback systems often raised insightful remarks and always forced me to find a better way to explain my point. His tireless feedback on versions upon versions of papers, as well as this thesis, was indispensable. His help extended right to the last minute when, during a weekend, I needed a Dutch translation for the abstract of this thesis. Thank you.

I would also like to thank Gerard Wienk for his prompt and continuous help with CAD issues, and for always taking the time to explain what he is doing (makes you feel less embarrassed when you are showing up regularly at his desk). Also thanks go to Henk de Vries for his persistent assistance in the laboratory, especially when things were getting tense around a submission deadline. Our group's management assistant, Gerdien Lammers, with her dedication and meticulous attention to detail, has been

a constant aid with all kinds of issues, making things run so seamlessly easy right to the very last minute. She literally saved my defense date. For that, and everything else, I thank her.

Thanks as well go to STW for funding this project, STMicroelectronics for Silicon donation and CMP for their assistance.

A few people encouraged me when I first decided to pursue doctoral studies. So, in no particular order, I wish to name them here: Arjan Leeuwenburgh my former manager at SiTel Semiconductor, and John Willms and Vojkan Vidojkovic my former colleagues at the same place; for your good natured character, I remain grateful.

I was also fortunate to have good office-mates during my stay in Twente. Xiang Gao (currently my from-a-distance work colleague as well), Fabian van Houwelingen and Niels Moseley welcomed me in their office room in Hogekamp when I first joined the group. Although, all three finished their studies shortly after I joined, I still remember the interesting technical discussions we had and the few jokes we shared. That contributed towards an easy transition in Twente. In Carre, late evening discussions with Milad Darvishi, became, more or less, something of a tradition. They usually started with some high level technical discussion that kept regressing back to basics (consequently, sometimes getting more confusing), and most often than not, ended in a completely different direction like politics or philosophy. From another office-mate, Saifullah Amir, I got to learn something about power converters, and a lot about life and politics in Pakistan.

Everything I managed to achieve rests upon the privileged start I was given in this life. For that, I can never thank my parents enough. Their care and teaching continue long after they are gone. My younger brother remains to be my link to home. His place has always been open for me and my wife whenever we needed to relax away from work for a while.

Finally, but foremost, I would like to thank Maggie, my wife, for her support throughout the long working hours and the associated ups and downs. She has always been interested in what I do, even though her curiosity, in many cases, was met with abruptly short replies from a tired person, frustrated from staring into a computer screen all day. Her kindness is always overwhelming and without her patience, many of the stumbling blocks along the way would not have been surpassed.

Shadi Youssef
Lausanne, 13 May, 2013

Biography

Shadi Youssef received the B.Sc. degree from Ain Shams University, Cairo, Egypt, in 2000, and the M.Sc. degree from Aalborg University, Denmark, in 2005. From 2006 to 2009 he was with SiTel Semiconductor (formerly National Semiconductor), The Netherlands, where he worked on the design of integrated CMOS power amplifiers. From 2009 to 2013 he worked towards his Ph.D. degree at the Integrated Circuits Design Group, University of Twente, Enschede, The Netherlands.

He is currently a Staff Design Engineer with Marvell Semiconductor, Switzerland. His interests include highly linear receiver front-ends and CMOS power amplifiers for wireless communications.